Analysis of Arches

by

Trupti Sonavane

B.Arch, Sir J.J College of Architecture, Mumbai, India, 2002

M.Arch, Virginia Tech, 2006

A thesis submitted to the

Faculty of the Graduate School of the

University of Colorado in partial fulfillment

of the requirements for the degree of

Master of Science

Department of Civil, Environmental and Architectural Engineering

2014

This thesis entitled:
Analysis of Arches
written by Trupti Sonavane
has been approved for the Department of Civil, Environmental and Architectural Engineering

Prof. Victor Saouma

Prof. George Hearn

Prof. Abbie Liel

Date

The final copy of this thesis has been examined by the signatories, and we find that both the content and the form meet acceptable presentation standards of scholarly work in the above mentioned discipline.

Sonavane, Trupti (M.S. Civil Engineering)

Analysis of Arches

Thesis directed by Prof. Victor Saouma

The purpose of this thesis is to develop a preliminary guide for the analysis and design of symmetrical circular arches.

In the context of the graduate curriculum that typically limits itself to rectilinear structures, this thesis makes an effort to apply basic principles (virtual work and the flexibility method) towards deriving analytic solutions for different types of elastic arches (reactions and internal forces). To the best of our knowledge, this is the most comprehensive repository of such closed formed solutions. To illustrate their application, the preliminary design of a concrete arch is reported. Furthermore, analytical results are assessed to assist engineers gain a feel for arch behavior.

The study broadly covers semicircular arches. The analysis includes different loading as well as support conditions that lead to statically determinate or indeterminate structural design cases. Effects of unsymmetrical loading conditions on these structures are also briefly covered in their analysis. The analytical solutions are derived with Mathematica, compared with reported analytical solutions (when available),validated with SAP 2000 models and used through Matlab for the design example.

Further,this design guide helps relate structural behavior of semicircular arches with their geometry. Influence of aspects like span to - rise ratio on horizontal thrust, support reactions, and forces across the span provides intuitive understanding of these structures. The study concludes with simplified analytical solutions and preliminary design recommendations.

Dedication

To all my teachers who had inspired, challenged and guided me in following the hardest paths in my life.

Acknowledgements

My deep gratitude goes to Dr. Victor Saouma for motivating me to follow my aspiration and for his diligent guidance and help in completing this thesis work.

I also want to recognize the valuable advice provided by Dr. Abbie Liel and Dr. George Hearn towards improving the work. I enjoyed working with my friend and fellow student Kyle Prusinski and I appreciate his input in the preliminary design of arches.

To my husband, Rahul Mhaskar, who inspired and encouraged me to study structural engineering and to my family and friends who provided their unconditional support, I am utmost thankful.

Contents

Chapter

Appendix

Tables

Table

Figures

Figure

Chapter 1

Introduction

1.1 Motivation

Arches have significant presence in architecture from pre-historic period to modern time. With its curvilinear form, an arch creates most intriguing connection with its surroundings. It is aesthetically appealing as well as structurally efficient and therefore its application is seen in some challenging projects.

As a student I was always fascinated by long spanned arch structures and I was interested in understanding their structural behavior. I found that, while structural engineering curriculum covered various methods of analysis and design, it primarily focused on their application towards rectilinear structures. Furthermore, no standard structural mechanics, analysis and design textbooks provided any guidance on how variations in arch geometry influence its structural behavior.

My curiosity to learn more about arches motivated me to apply the simple methods that I have learned, towards analysis and preliminary design of arches. With this thesis I made an effort to develop a set of analytical equations for different type of circular arches. Further, I used these equations to study behavior of arches under different loading conditions as well as to analyze effect of arch's geometry on its internal stresses. While this thesis work only covers some areas of the vast topic of arches, it provides the information needed to understand the primary structural behavior of arches.

1.2 Literature Study

The literature study involved scientific papers and books published on the topic of arches including development of their form from pre-historic time to modern period, their application in modern structures, advancement in their theory of analysis, common methods that are currently used for analysis, and their limited coverage in the most popular textbooks of civil engineering education. Following is the brief information on multiple resources used for this literature study.

Godoy (2007) claims that most popular textbooks have limited coverage considering the number of pages dedicated to arches. It also describes the significance of arches in modern structures and therefore emphasizes on the importance of including analysis of arches in civil engineering curricula. The Table 1.2 shown below is taken from the paper and it review 20 books on structural analysis.

The scientific paper by Clive L. Dym and Harry E. Williams (Dym and Williams, 2011) on the behavior exhibited by curved, arch like structures under radially directed and gravitational line loads provides estimates of the displacements and stress resultants in the arch. The paper also uses the results to offer insight into the assumptions underlying Robert Maillarts arch designs. The primary difference between this paper and the work presented in this thesis is that the paper provides estimates where as the thesis work provides exact solutions for internal stresses and deflection in the arch.

Huerta (2006) discusses method used by Antonio Gaudi to determine the parabolic shape of the arch that is commonly seen in the structure designed by him.

Acocella (2006) describes ancient and modern construction skills and the development of masonry arches from pre-historic time to modern period. It uses sketches and pictures to illustrate the various forms of the arch.

Salvadori and Heller (1986) focuses on the importance on structural engineering knowledge in architectural professional practice. It also briefly discuses different types of modern and historic arches and the rational behind their form and applications.

Title	**Author**	**Year**	**Pages**	**Publisher**	**Arches**	
					pp.	%
Fundamentals of Structural Analysis	Leet, Uang	2002	712	McGraw Hill	14	2.0%
Structures	Schodek	2001	576	Prentice	27	4.7%
Elementary theory of structures	Hsieh, Mau	1995	356	Prentice	0	0
Introduction to Structural Analysis and Design	Rajan	2001	639	Wiley	1	0.16%
Analysis of Structural Systems	Fleming	1997	546	Prentice	0	0
Analysis and Behavior of Structures	Rossow	1996	694	Prentice	0	0
Structural Analysis	Kassimali	1995	697	PSW	6	0.8%
Fundamentals of Structural Analysis	West, Geschwindner	2002	543	Wiley	4	0.7%
Structural Analysis and Behavior	Arbabi	1991	554	McGraw Hill	23	4.15%
Elementary Structures for Architects and Builders	Shaeffer	1998	388	Prentice	0	0
Structural Analysis	Chajes	1990	444	Prentice	7	1.5%
Structural Analysis	Hibbeler	1997	716	Prentice	12	1.7%
Structural Analysis	Hibbeler	1999	566	Prentice	8	1.4%
Structural Modeling and Analysis	Dym	1997	248	Cambridge	3	1.2%
Structural Analysis	Ghali, Neville	1997	743	E & FN Spon	5	0.7%
Matrix Methods of Structural Analysis	Kanchi	1993	521	Wiley	0	0
Structural Analysis	Laursen	1988	408	McGraw-Hill	107	2.5%
Structural Analysis: A Classical and Matrix Approach	McCormac, Nelson	1997	573	Addison-Wesley	10	1.7%
Introduction to Structural Mechanics and Analysis	Dadeppo	1999	423	Prentice	0	0
Computer Assisted Structural Analysis and Modeling	Hoit	1995	405	Prentice	0	0
BasicStructural Analysis	Gerstle	1974	498	Prentice	10	2%

Table 1.1: Summary of the Structural Analysis Books, (Godoy, 2007)

Thandavamoothy (2011) includes historic development in the form of arches and their applications. It illustrates the application of elastic theory towards analysis of modern arches using multiple examples.

Timoshenko (1953) gives a brief account of the history of theory of elasticity and theory of structure. Further, it describes influential work of some of mathematicians and physicist in detail.

Ruddock (2000) includes information on historic masonry bridges, viaducts and aqueducts and it provides critical analysis of their failure. It also describes the studies conducted to preserve historic masonry structures.

West (1989) integrates the classical and modern methods of structural analysis. It illustrates the applications of these methods through examples.

Kinney (1957) presents methods of analysis for statically indeterminate arches. It illustrates their applications through various examples.

1.3 Thesis Organization

The thesis comprises analysis of circular arches and it is arranged in four chapters.

Chapter 2 includes study of historic arches, development of the elastic theory and its influence on the modern arches. The historic arch section describes the primitive stages of circular arch before 600 B.C.E, the significant development in the form and application occurred during the Roman and Greek civilizations and the various forms that stem from the circular arch during medieval period. The elastic theory section documents the relevant work of mathematicians and physicists occurred between 16th and 18th century. The modern arch section discusses the most common types of arch used in modern structures.

Chapter 3 focuses on analysis of most commonly used types of the circular arch – Three-hinged, Two-hinged and Hingeless and summarizes their structural behavior. A section is dedicated for each type of the arch in which, analytical equations are developed and validated. The equations are further used to plot the internal stresses and deflection in the arch and to discuss its behaviors under different loading conditions. The conclusion section discusses the similarities and differences between the behaviors of the above–mentioned types of the circular arch under symmetric and asymmetric loading conditions.

Chapter 4 includes application of the analytical equations towards comparison of internal stresses in a circular and a parabolic arch and provides a preliminary design for the compared circular arch rib. For this purpose parabolic arch of the Hoover Dam Bridge is used. In the comparison sections, internal stresses in the parabolic arch are determined using the Sap 2000 program and they are compared with the internal stresses in the circular arch found using the analytical equations. In the preliminary design section, internal stresses in the compared circular arch are used to develop and optimized its rib design.

Chapter 5 includes comparison of structural behavior of the above-mentioned types of circular arch under similar loading conditions. Additionally it includes a study of rise-to span ratio and its effect on the internal stress of each type of the arch. A brief description of future work that can be done to further develop this thesis is also provided in this chapter.

Chapter 2

Evolution of Arch

2.1 Introduction

Through out the history of architecture, arches have been used as a main structural component. With their unique compressive mechanism of resisting load, arches can be categorized as special class of structural systems. They are capable of spanning long distances while supporting significant weight, which makes them highly efficient and visually powerful structural systems. Unlike modern concrete or steel arches in which the members are continuous and monolithic, historically arches were built with masonry and were commonly used to span small distance. As stone is quite durable material under compression, many impressive examples of early masonry arches exist to this day (Thandavamoothy, 2011, pg1017-1019).

This chapter focuses on the development of an arch form, all the way from the prehistoric period to the modern period. It discusses the development in the theory of analysis of an arch and its influence on the modern arch design.

2.2 Historic Arch

2.2.1 Before 600 B.C.E

2.2.1.1 Trabeated style Architraves

The arch in its most primitive form was first used by Mesopotamian, Persian and Egyptian civilizations. Ancient builders accomplished the challenge of creating the doors and passageways by the trabeated style architraves, commonly known in today's date as a lintel. It is a horizontal structural element that carries the weight of the overlying elements by transferring it to the abutments or piers. With this configuration, the longest available beam restricted the opening size. Even though the stone architraves were simple in nature, they were considered progression of the ancient wooden framework that was subject to decay with time. From a static point of view this system involves all structural configurations that transfer weight in a vertical direction. Vertical elements like pilasters, columns and abutments are subjected to compressive stresses, while horizontal one like lintels or beams are subjected to both compressive and tensile stresses. (Acocella, 2006, pg24).

2.2.1.2 False /Corbelled Arch

In terms of execution, the Architrave structures with considerable depth that can span large openings were extremely laborious technical solution. New structural configuration was adopted due to lack of readily available large stone elements, which initiated future developments towards a more rational use of rigid material that is not resistant to tensile stress. The earlier examples are consisted of two stone slabs, laid diagonally against each other, which would transfer the applied load to the masonry abutments through diagonal thrust. In this configuration, the diagonal thrust tend to widen the structure itself in the absence of adequate abutments. This structural solution is commonly referred as a false arch. More sophisticated version of the false arch was a corbelled arch shown in Figure 2.1(a). Corbelled arch consisted of a series of cantilevers that were superimposed upon and projecting a little beyond the cantilever below. This created two slanting sets of stone steps that met at the top to form the apex of a triangle. In this configuration the load was transferred vertically by compressions to the piers below without any outward thrust, enabling the omission of buttresses on either sides. Corbel arches required significantly thickened walls and abutments to counteract the effects of gravity (Thandavamoothy, 2011, pg1017-1019). The corbelled arch was used extensively in ancient Egypt as an architectural unit. Earliest application of the Corbel vault chambers and tunnels are seen in the Egyptian pyramids. Also the ruins of ancient Greek structures show use of corbel vault and arches for entrance gate structures and bridges. One

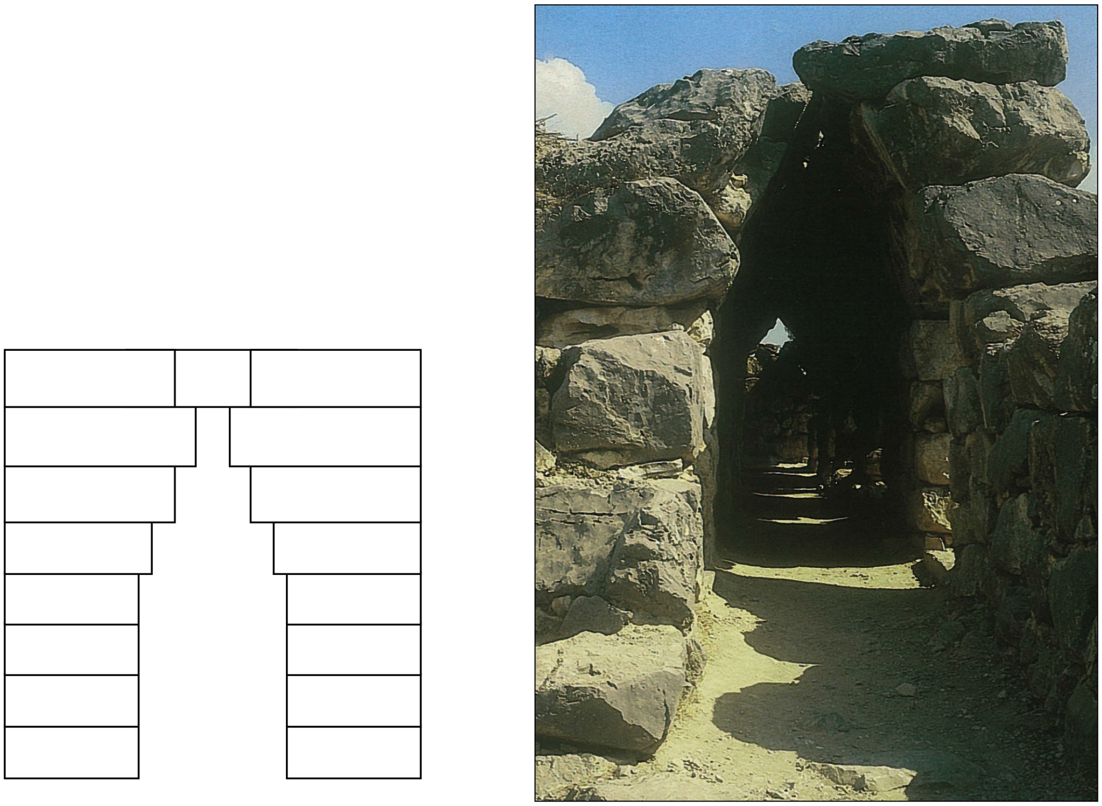

(a) Typical Corbelled Arch (b) Mycenaean Fortress of Tiryns

Figure 2.1: Corbelled Arch - False Arch

example of it is Mycenaean Fortress of Tiryns shown in Figure 2.1(b). In order to determining safe dimensions of members the ancient builders valued the information regarding the strength of structural materials. The Egyptians had some empirical rules, with help of which they erected great monuments, temples, pyramids, and obelisks, some of which still exist. Mesopotamian civilization gave great importance to the corbelled arch and vault in numerous buildings demonstrating a deeper understanding of their technical potential. The corbeled arch adopted in ancient time was in some respect a transitional stage between the architrave structures and the more sophisticated arcuated system commonly called as true arch (Acocella, 2006, pg30).

2.2.2 Greek and Romans

There was long absence of any technical development of the arch, until the last five centuries of B.C.E, where initiative towards the technical analysis and symbolic and spatial application of the arch was observed. The Greeks developed statics and theories on equilibrium, which led towards the progress in mechanics of materials. Archimedes derived the conditions of equilibrium of a lever and outlined methods of determining centers of gravity of bodies.

In Greek civilization, the loads applied on the arch structures were no longer distributed in a vertical direction but they were obliquely directed outwards. As a consequence the arch structure required adjoining piers, which can absorb the transferred thrust. Hence there was a tendency to build safe and heavy structures, which resisted outward thrust.


(a) Falerii Novi Arch

(b) Falerii Novi Arch Abutment

Figure 2.2: Arcuated Arch - True Arch

Falerii Novis arcuated system shown in Figure 2.2(a) marked the beginning of greatly developed Roman arch system. The third and fourth centuries B.C.E paved the way for various forms of arches. From the second century B.C.E significant application of arches was made in city gates. The arch used in Roman architecture reflected understanding of stones inelastic characteristic, which resulted in greater compressive strength and enabled larger spans using small masonry unit. This played a fundamental role in wide spread application of the arcuated system in the Roman spatial architecture (Acocella, 2006, pg36).

2.2.2.1 True /Arcuated Arch

The arcuated arch also known as true arch, can be defined as a structure, which depends in considerable degree on the development of horizontal outward thrust at the abutments in order to support applied vertical loads. Figure 2.3 show geometry of a true arch. The individual pieces are in the shape of truncated wedges and they are arranged on a curved line so as to retain their position by mutual pressure. The individual stones or bricks, which form the curve of an arch, are called voussoirs. The lowest voussoirs are called springers and the central voussoir is called the keystone. The under or concave side of the voussoir is called intrados and the upper or convex side, the extrados of the arch. The end supports to which the load is transferred by the arch are called piers or abutments. The span of an arch is, the distance between the apposite springs. The rise of an arch is the height of the highest point of its intrados above the line connecting the springer. The highest point of the extrados is called crown of the arch (Thandavamoothy, 2011, pg1018). A true arch transfers the weight outward and then downward into the ground, rather than bearing it solely upon itself. Engineers in Roman civilization were able to construct vaults that served as tunnels by building a series of back-to-back true arches. In addition to forming passageways, the arch was a strong and efficient way of supporting a superstructure. The horizontal reaction component was the main difference between a true arch and a corbelled arch.

The Romans developed ability to build bridges to provide for their rapidly growing armies. They developed the semicircular true masonry arch and used it extensively in both bridges and aqueducts. The Roman builders were guided only by empirical rules, as there was no theory developed for determining the safe dimensions of arches. The skills of the Roman builders were so

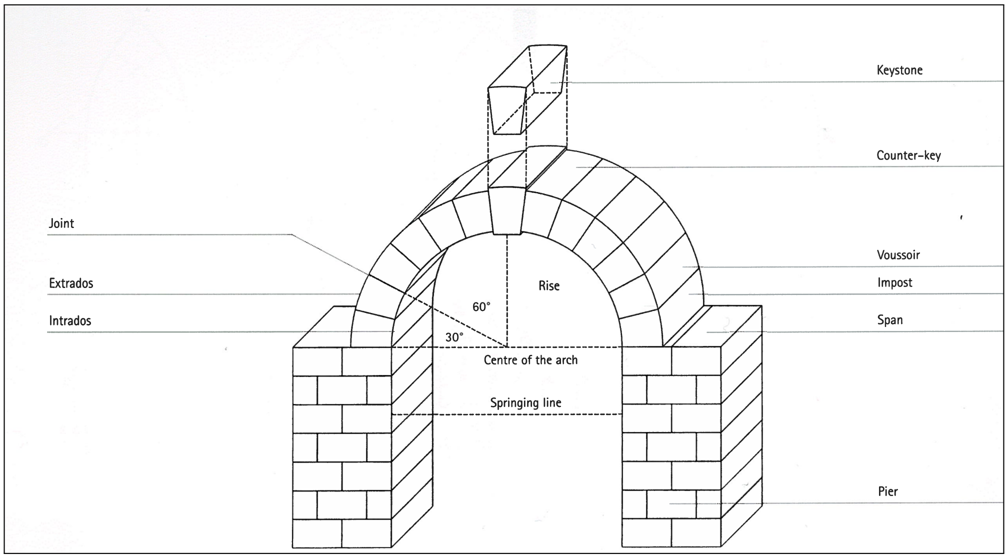

Figure 2.3: Geometry of True Arch

developed that some of their structures remain intact to this day and reflect the proportions and the methods of construction that they used. An important aspect the Romans paid attention to was the choice of materials. The Romans invented concrete for greater economy of material as well as for convenient constructability. Their masonry bridges rested mostly on semi-circular arches or on segmental circular arches (Thandavamoothy, 2011, pg1020).

2.2.2.2 Compositional Arrangement of Roman Arches

Though the concept of arch was already existent, Roman architect were responsible for its enormous development. They experimented with the archs application beyond singular use, which enhanced compositional potential on a more significant scale. They transformed the single arch into sequential arrangements of increasing dimension that resulted in the monumental string of arches for the aqueducts. In this configuration, arches effectively exploit the static principle of equilibrium of adjoining arches positioned to provide mutual support. This distribution of thrust caused excessive stress on element that open and close the sequence and, as a consequence, it was structurally the most elaborate part of the construction. In order to widen the span between the supporting piers of bridges, Roman engineers pushed the construction limits of the arch with a radial configuration of stones. This challenge was met by the constructing a series of daring arched structures with gradually increasing spans, particularly those at the bottom playing the crucial role of supporting buttresses while resisting the water pressure (Acocella, 2006).

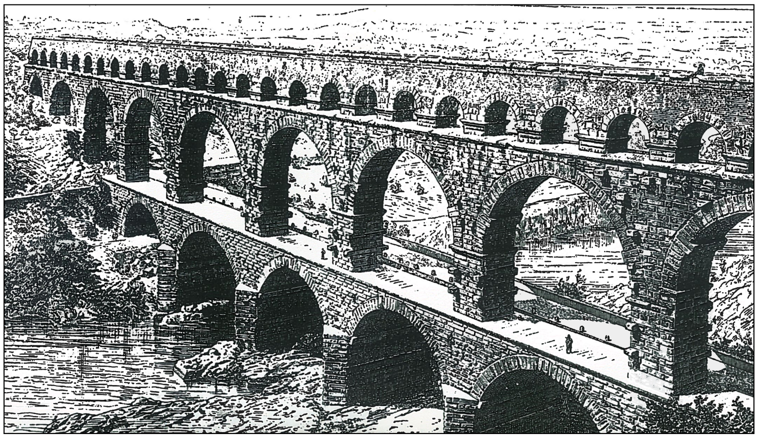

Figure 2.4: Roman Aqueduct - Pont du Gard

Some of the Aqueducts constructed by Romans are considered an unequalled infrastructural work in terms of their architectural equilibrium and the technical skill. One such example is the Pont du Gard shown Figure 2.4, where the structural section of the bridge gets slimmer as it rises and it features two enormous superimposed orders of circular arches, on top of which is a more close-knit series of smaller arches supporting the actual conduit of the aqueduct. Roman structures reflected innovative building methods, cement-based technique, and fresh compositional design based on multiple arches. With the ever-growing demand of the bridge construction, the circular arch was a deliberate choice over the drop arch, which cause greater outwards thrust and impose problem in the presence of considerable span (Acocella, 2006).

The construction of curved masonry walls is combination with the curvilinear arches and vaults widened the ranges of experiments carried out into Roman building types. Some of the Examples are found in traditional Roman theaters and amphitheaters. Innovation consisted of curving masonry walls and arches and laying two or three orders of arches on top of one another

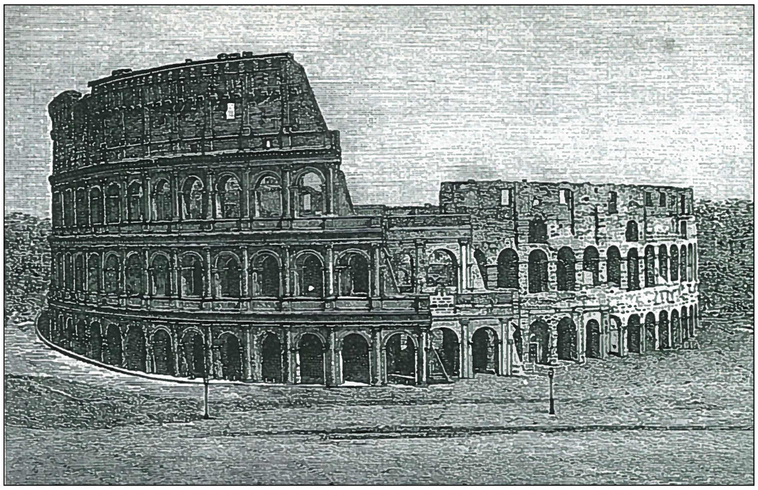

Figure 2.5: Roman Amphitheater - Colosseum

absorbing the thrust of the internal vaults and terrace of the theater. It almost took two centuries to classify the typology of the Roman amphitheater and achieve unique models such as the Colosseum shown in Figure 2.5. This horseshoe-shaped auditorium is supported by a sequence of radial-vaulted structures capable of incorporating flights of steps for the incoming and outgoing flow of spectators. The mass of the building is perforated on three levels by a sequence of rhythmic arches with toothed voussoirs and uniformly divided arched lintels (Acocella, 2006).

2.2.3 Medieval Period

2.2.3.1 Pointed Gothic Arch

The Roman semicircular arch was followed by the pointed Gothic arch, which was originally derived from the Islamic pointed arch. Its centerline more closely followed the compressive force and hence has a stronger geometrical form. The Gothic high-rise arch and the buttresses required to absorb its thrust shown in Figure 2.6 are of one of the important achievements in historic architectural design. High-rise of the arch reduced the thrust and lightened flying buttresses. A Gothic cathedral can be compared with a framed building in which the curved frame elements develop almost exclusively compressive stresses. The Gothic cathedrals spanned up to one hundred feet and covered hundreds of square yards by making use of the pointed arch (Salvadori and Heller, 1986).

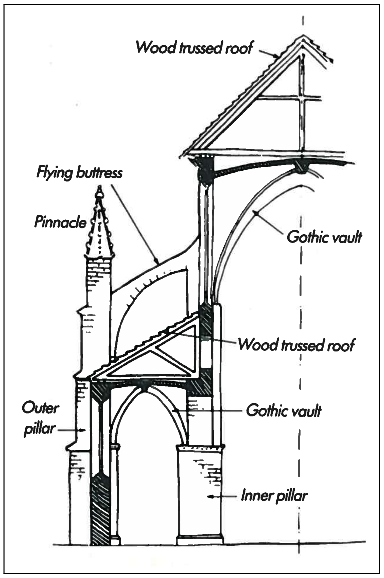

Figure 2.6: Pointed Gothic Arch

2.2.3.2 Arabic Arch

The horseshoe arch or Arabic arch shown in Figure 2.7 is based on the semicircular arch, but its lower ends are extended further round the circle until they start to converge. It was used in the Spanish Visigoth architecture, Islamic architecture, and Mudejar architecture. It was used mainly for aesthetic purpose rather that the strength (Thandavamoothy, 2011, pg1024).

The use of a semicircular arch was continued for centuries and was represented as a typical feature of Byzantine architecture of the eastern Roman Empire and of the later Romanesque architecture of Western Europe. The round arch was the principal element in a long sequence of curvilinear structures and its geometrical form influenced the subsequent developments. The modifications including reductions, transpositions and small variations made in the round arch characterized several historical eras.

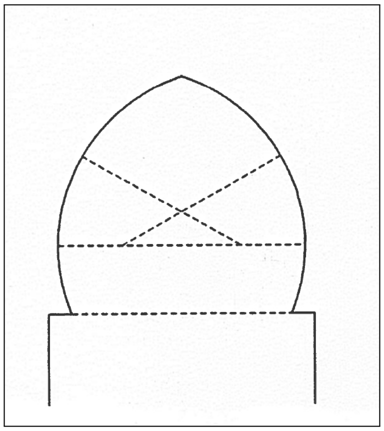

Figure 2.7: Arabic Arch

2.2.4 Geometric Forms of An Arch

With the introduction of efficient construction materials and advancement in construction techniques, arches were used in numerous geometrical forms. Such as: 1) Rounded or Semicircular, 2) Stilted; 3) Segmental; 4) Horseshoe;5) Pointed; 6) Three centered or Elliptical; 7) Four- Centered or Tudor; 8) Ogee; 9) Foiled Cusped; 10) Shoulder; and 11) Flat.

Broadly the arches are categorized in four classes based on the way they are formed. The first class of arches is struck from single center, where the center is located in middle of the diameter. In the case where the center is at a point above the diameter, it is called a stilted arch. When the arch is formed of curve that is less than a semicircle it is called segmented arch. If the curve is greater than a semicircular and has a center above the springing line it is called horseshoe arch as shown Figure 2.8(a). The second class of the arches is struck from two centers as shown in Figure 2.8(b). There are three main types under this category. The first is equilateral where the two centers coincide with the ends of the diameter. The second, more acutely pointed is lancet and its centers are on the line of diameter but outside it. The third is the obtuse or drop arch in which the centers are still on the line of the diameter, but outside the arch.

The third class consists of arches formed with three centers and these arches are elliptical in shape. The fourth class consists of arches formed from four centers. One of the most prominent

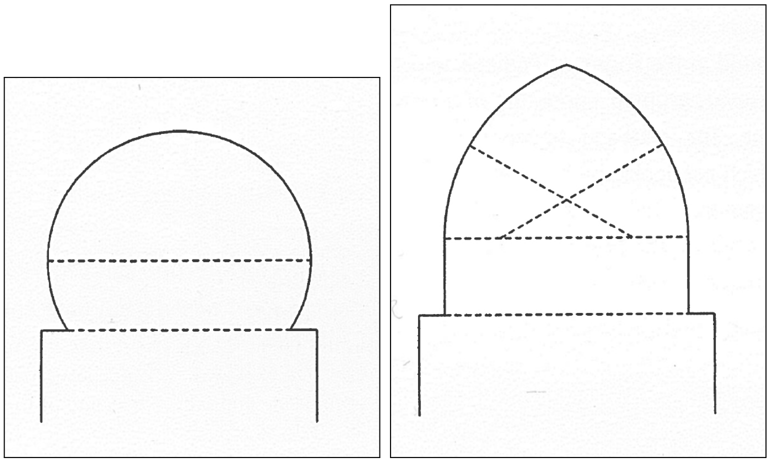

(a) Horseshoe Arch (b) Pointed Arch

types under this class is the Tudor arch. It is a low and wide arch of elliptical shape. In the Gothic period pointed arch was transformed and blunted into the flattened Tudor arch. Another variety of arch is based on the three or four center arch is the Ogee arch as shown inf Figure 2.8(c). In this one or two of the centers are below but other two are above the arch creating a concave upper arc flowing into a convex and convex lower arc. Similarly the Foiled arch shown in Figure 2.8(d) have three or more lobes or leaves and are created from the combination of above-mentioned four classes of arches (Thandavamoothy, 2011, pg1024).

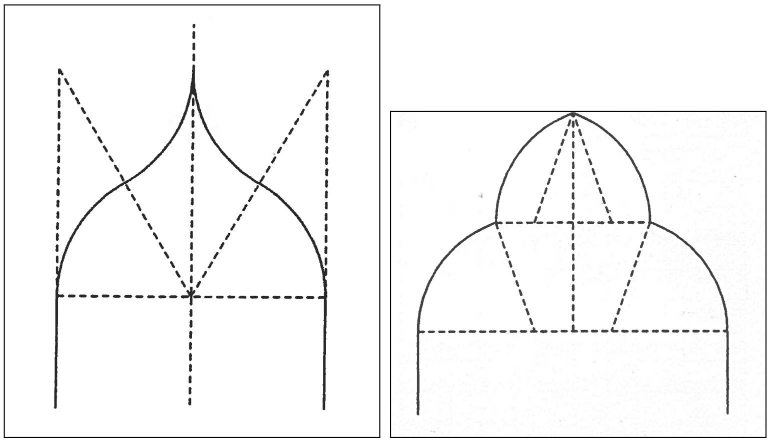

(c) Orgee Arch (d) Folied Cusped Arch

Keeping in consideration the original compressive mechanism of the arch, geometrical variations were made, which broaden the family of curvilinear forms. It led to the development of the pointed arch in the medieval times, the elliptical and mixed arches in the Renaissance and Baroque eras, and to the parabolic arch between the late nineteenth and early twentieth century(Acocella, 2006).

2.3 Elastic Arch Theory

2.3.1 Developments (1400 -1900)

Most of the knowledge that the Greeks and Romans accumulated in the way of structural engineering was lost during the Middle Ages with decline of civilization throughout Europe. Beginning in the fourteenth century in Italy, the Renaissance was a period of general revival where roads and bridges were needed and the builders had to learn again how to construct arches. Like the arches of the Romans, these were built by rule of thumb. The renewal of interest in field of art and science led to development of architecture and engineering (Kinney, 1957, pg537).

2.3.1.1 Strength of Materials and Structural Behavior

Some of the early attempts to apply statics in finding the forces acting in structural members and also the first experiments for determining the strength of structural materials were seen in the work of Leonardo Da Vinci. He stated the law of the lever that introduced the concept of the moment of a force. He also correctly presented the idea of the thrust produced by an arch. In one of his manuscripts, he indicated a vertical load Q applied on two slanting members shown in Figure 2.8. With the help of the dotted-line parallelogram, he derived the forces needed at the supports a and b to achieve an equilibrium (McCurdy, 1939). His work was followed by Galileos attempt to analyze the cantilever beam in 1638. Although these were important advances in understanding the structural behaviors, the engineers of the fifteenth and sixteenth centuries, like the Roman era continued to fix the dimensions of arches by relying only on experience and judgment (Timoshenko, 1953, pg6).

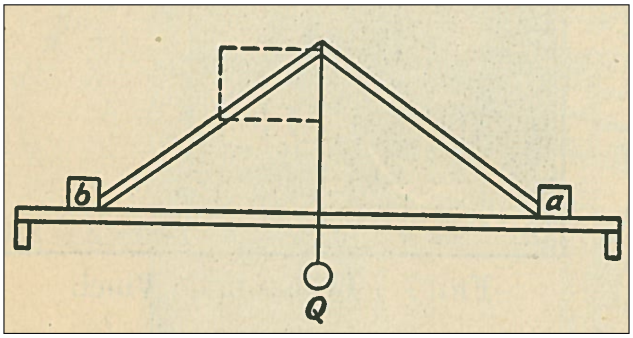

Figure 2.8: Application of Statics

2.3.1.2 Hooke's experimental approach to the arch (1675)

As hangs a flexible cable, so, inverted stand the touching piece of an arch - Robert Hooke (1675).

Robert Hooke stated the idea that an arch was simply the inverted shape of a loaded chain hanging across a span. He stated, based on his experiment that the line of the chain represented the line of thrust. It connects the points of greatest stress in each block across the span of an arch. As shown in Figure 2.9 Hooke used two different types of models consisting of flexible cable and rods joined together with pins to show the funicular behavior of an arch . A cable can take different shapes to support the same load. In each case, the tension in the cable is different and if the cable is displaced, it will swing back to its initial position. He also used jointed rods to form a shape similar to that of a cable supporting different weight and then inverted it to represent an arch. He indicated that many lines of thrust will fit in an arch with deep voussoirs making it over-stable and hence it will take large forces to displace it. Once the forces are removed, the arch will snap back into position. An arch with much thinner ring allows only one line of thrust to fit within the arch (Bertrand, 1869).

In 1678 Hooke published a paper containing the results of his experiments with elastic bodies. This is the first published paper that discussed the elastic properties of materials and the relation between the magnitude of forces and the deformations (Timoshenko, 1953).

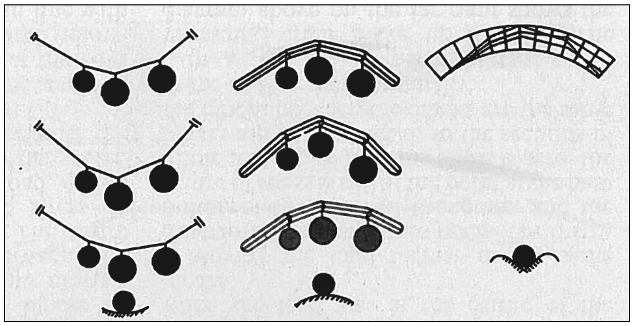

Figure 2.9: Experimental Approach - Line of thrust in an arch

2.3.1.3 Philippe de la Hire's application of statics to the solution of arch problem (1695)

The first application of statics to the solution of arch problem was seen in Lahires work. He indicated use of the funicular polygon in the analysis of arch as shown in Figure 2.10 (de la Hire, 1679). He considered a semicircular arch consisted of wedge shaped units with perfectly smooth surface of contact transmitting only normal pressure. The shape ABCDE represents the funicular polygon of the arch. He then geometrically found the required weights P1, P2 and P3 to ensure the stability by projecting the radii boarding the wedges on to a horizontal tangent MN. He stated that magnitude of P1, P2,P3 , are in the same ratio as MK,KL and LN respectively and lengths of radii between the wedges of the arch represent the pressure acting between them. With this assumption the radius CE parallel to MN indicates very large thrust and hence he concluded that stability of

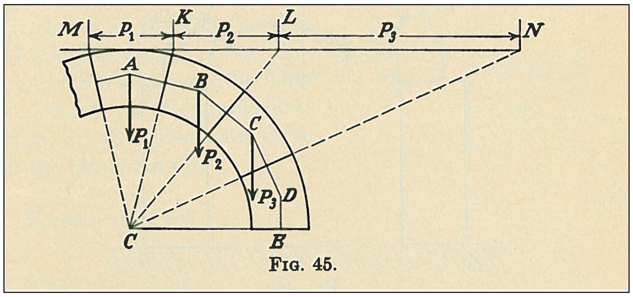

Figure 2.10: Analysis of an arch using funicular polygon

semicircular arch couldnt exist under the assumption of perfectly smooth wedge surfaces. In actual arch the cement will contribute to the stability by preventing the wedges from sliding. He later

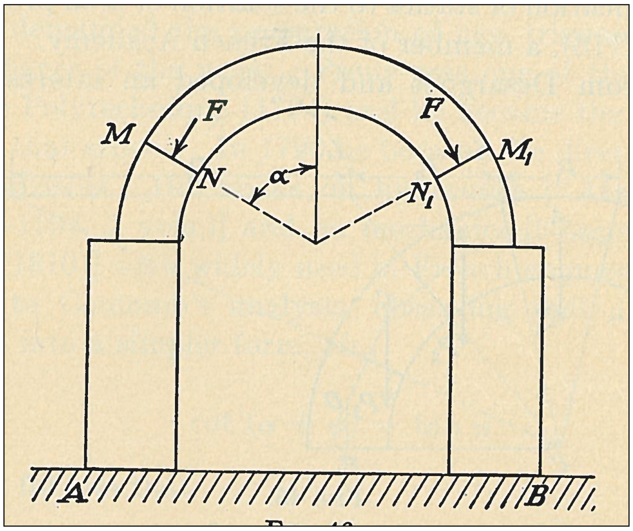

Figure 2.11: Analysis of Pillar supporting a semicircular arch

applied his theory to determine the adequate dimension of pillar supporting the semicircular arch shown in Figure 2.11. He assumed that the fractures would occur in most critical location (MN and M1N1) and calculated the required weight of the pillar to counteract the Force F at the fractures while perverting the rotation of pillars at point A and B. Lahires method was used later in the preparation of a table for use in calculations of the thickness of arches (Timoshenko, 1953, pg63).

2.3.1.4 Charles-Augustin de Coulomb Theory of arch failure (1773)

Coulomb made further progress in the theory of arches. In his memoir of 1773, Coulomb stated that for arch stability both relative sliding as well as relative rotation of the wedges must be checked (Coulomb, 1773). His experiments with models showed that typical failures of arches occur at the locations indicated in the figure 2.12. He studied one-half of a symmetrically loaded arch denoted by ABCD in Figure 2.13. By taking in consideration the horizontal thrust H acting at the cross section AB and the weight Q of the segment ABmn, he derived the normal and tangential forces acting on the plane mn.

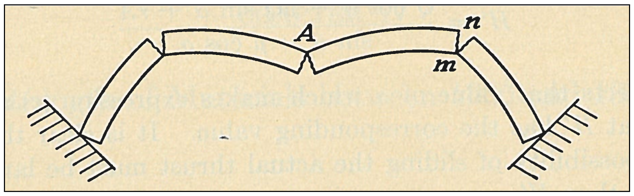

Figure 2.12: Typical failure of arches

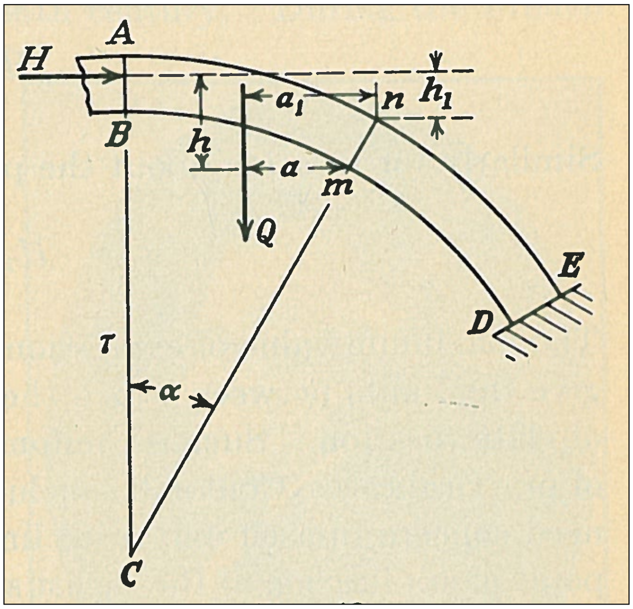

Figure 2.13: Typical failure of arches

$$\begin{aligned} \text{Normal component} \quad & H\cos\alpha + Q\sin\alpha \\ \text{Tangential Component} \quad & Q\cos\alpha - H\sin\alpha \end{aligned} \tag{2.1}$$

Within all ranges of α , he derived the smallest and the largest values of H required to prevent the portion ABmn of the arch from sliding down along the plane mn. They are give by the equations,

$$\begin{aligned} H &= \frac{Q\cos\alpha - \mu Q\sin\alpha - \tau A}{\sin\alpha + \mu cos\alpha} \\ H\prime &= \frac{Q\cos\alpha + \mu Q\sin\alpha + \tau A}{\sin\alpha - \mu cos\alpha} \end{aligned} \tag{2.2}$$

Where μ is the coefficient of friction and τ the total resistance of the arch to shearing along the plane mn. It is clear that to eliminate any possibility of sliding the actual thrust must be larger than H and smaller than $H\prime$. Considering the possible rotation about the point m the limiting value H1 of the thrust is derived.

$$H_1 = \frac{Q_a}{h} \tag{2.3}$$

Similarly for rotation about the point n

$$H_1\prime = \frac{Q_a 1}{h_1} \tag{2.4}$$

Coulomb does not give definite rules for designing arches but only determines limits for the thrust, which is necessary for stability. For this reason his work was not appreciated by the engineers of his time but arch builders used his ideas extensively in the nineteenth century, when graphical methods were developed for calculating the limiting values of thrust (Timoshenko, 1953, pg66).

2.3.1.5 The theories of arch bridges during 1800-1833

During the period 1800-1833, designers of arches followed Coulombs theory and assumed that arch fails when it breaks into four pieces as shown Figure 2.12. With this assumption, it was challenging to find the location of the cross section of fracture BC shown in Figure 2.14. The theory supposes that the resultant R of the horizontal thrust H and the weight of ABCD portion of the arch passes through B and the fracture location BC is located when H is maximum. The problem of finding the location of this cross section of fracture was usually solved by a trial-and error method (Coulomb, 1773). To simplify the work, tables were prepared giving the weight and the position of the center of gravity of the portion BCAD of the arch for any location of BC in certain types of arches (Timoshenko, 1953, pg84).

2.3.1.6 Claude-Louis Navier's application theory of bending curved member towards arches (1826)

Navier made an important contribution to the theory of bending of curved bars, which he later used towards parabolic and circular arches. He took the formula already developed by Euler based on the assumption that, when an initially curved bar is bent, the bending moment is proportional to the change in curvature and applied it to investigate the bending of a curved bar shown in Figure

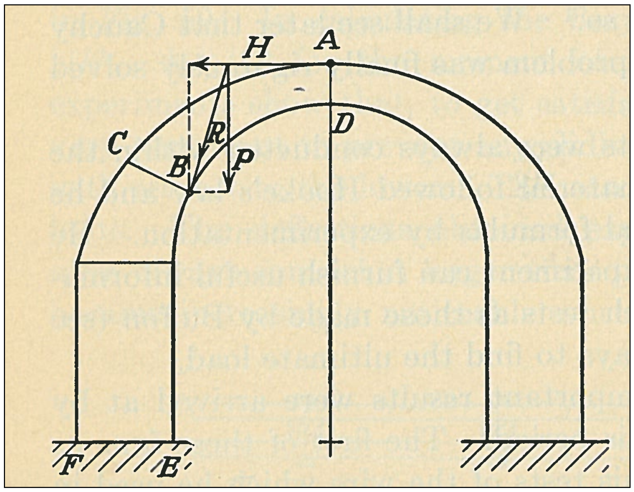

Figure 2.14: Location of fractures in arch bridges

2.15 (Navier, 1826).

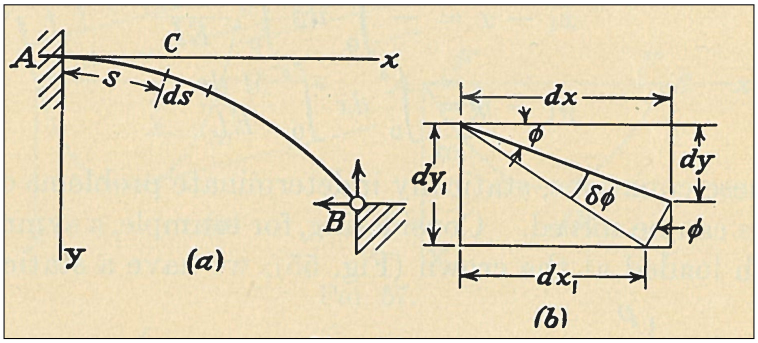

Figure 2.15: Analysis of bending curved bar

$$EI\left(\frac{1}{\rho} - \frac{1}{\rho_0}\right) = M \tag{2.5}$$

Taking an element ds at a point C, he concluded using the above equation that the angle between the two adjacent cross sections changes, due to bending, by $\frac{Mds}{EI}$. The cross section C rotates during bending , through the angle

$$\delta\phi = \int_0^s \frac{Mds}{EI} \tag{2.6}$$

Due to this rotation, the initial projections dx and dy of the element ds will be changed to dx_1 and dy_1. Integrating these formulas, he obtains the components of the displacement of any point

C during bending in the following form:

$$x_1 - x = -\int_0^s dy \int_0^s \frac{Mds}{EI} \tag{2.7}$$

$$y_1 - y = \int_0^s dx \int_0^s \frac{Mds}{EI} \tag{2.8}$$

These equations can be used to determine the thrust H in a symmetrical two - hinged arch loaded at the crown, from the condition that the horizontal displacement at hinge B vanishes as shown in Figure 2.16.Using this equation, he calculated the thrust in parabolic and circular arch (Timoshenko, 1953, pg78).

$$\int_0^s dy \int_0^s \frac{Mds}{EI} = 0 \tag{2.9}$$

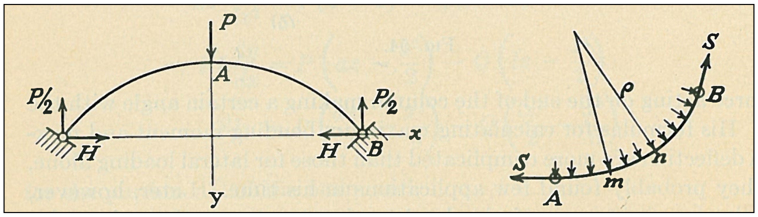

Figure 2.16: Two-Hinged Arch

2.3.1.7 Bresse's application theory of bending curved member towards arches (1865)

Similar to Naviers work, Bresse developed the theory of the deflection of for a curved bar and in it he included the effects of both axial and flexural strains and demonstrated the application of his theory in the design of arches (Bresse, 1859). The axial tensile force and the bending moment at any cross-section of the bar in Figure 2.17 are N and M respectively. The horizontal displacement of a point due to stretching of the element mn will be equal to $\frac{Ndx}{AE}$. Summation of the displacements Resulting from the deformations of all the elements of the bar, were used to find the total horizontal

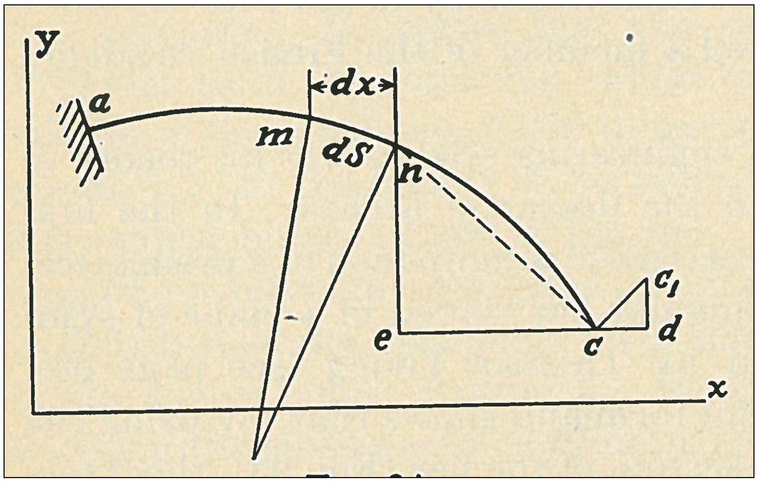

Figure 2.17: Analysis of bending curved bar

displacement u of the point c.

$$u = \int_a^c \frac{Ndx}{AE} + \int_a^c \frac{Mds}{EI}(y - y_c) \tag{2.10}$$

similarly to obtain the displacement v

$$v = \int_a^c \frac{Ndy}{AE} + \int_a^c \frac{Mds}{EI}(x - x_c) \tag{2.11}$$

and for angle of rotation α

$$\alpha = \int_a^c \frac{Mds}{EI} \tag{2.12}$$

Breese used these equation towards finding thrust H in two hinge arch shown in Figure 2.18 by using the condition that the horizontal distance at point C must be zero.

$$N = N_1 - H\frac{dx}{ds} \tag{2.13}$$

$$M = M_1 - H_y \tag{2.14}$$

To find Thrust H

$$H = \frac{\int_a^c \frac{N_1 dx}{AE} + \int_a^c \frac{M_1 y}{EI} ds}{\int_a^c \frac{dx^2}{AEds} + \int_a^c \frac{y^2 ds}{EI} ds} \tag{2.15}$$

Breese applied his theoretical considerations to specific problems of symmetrical circular two-hinged arches of constant cross section. He gave numerical tables for such arches of various proportions,

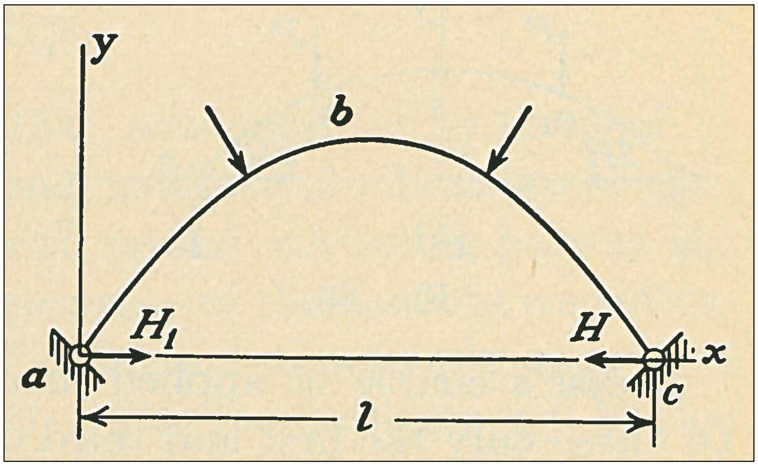

Figure 2.18: Two-Hinged Arch

by the use of which the thrust may readily be obtained for a single load, for a load uniformly distributed along the axis of the arch or along the horizontal Projection of this axis. All these carefully prepared tables are still of some practical value (Timoshenko, 1953, pg148).

The development of theory of analysis of statically indeterminate structures by James Maxwell and Alberto Castigliano closely relates to the above discussed two- hinged arch analysis by Navier and Bresse. James Maxwell based his theory on internal strain energy and external applied load, where as Alberto Castigliano used theorem the of least work.

2.3.1.8 Winkler's analysis of arches based on least work and strain energy method (1868)

Winkler studied Two-hinged and Hingelss arches hinges in great detail. He applied the notions of influence lines to arches. Using the principle of least work, he investigated the positions of pressure lines in arches and formulated the related principle. It states that from all the funicular curves which can be constructed for the acting loads, the true pressure line is that which deviates as little as possible from the center line of the arch (Winkler, 1880). Per Winklers principle, if the funicular curve constructed for the acting loads is taken as the center line of an arch, the pressure line coincides with the center line causing no bending. Winkler ignored the bending caused due to axial compression in the strain energy expression for the arch, which is usually considered small. It has become the usual practice to take the funicular curve constructed for the dead loads for the centerline of an arch (Timoshenko, 1953, pg155).

2.3.1.9 Christian Otto Mohr's graphical methods of arch analysis and Elastic center (1870)

Mohr made two important contributions to the elastic theory of arches. The first was the idea of computing the influence line for the horizontal reaction component of a two- hinged arch as equivalent to the bending moment diagram for a conjugate beam loaded with the y/EI diagram for arch.The term y is the vertical distance from the plane of the hinge to the arch axis at any section. Mohr obtained this moment diagram by graphical methods. His second contribution was an extension of the concept of the elastic center (neutral point) to include articulated arches (Kinney, 1957, pg538).

Throughout the nineteenth century, method of computing the thrust line of an arch was develoved by many practicing engineers. Most of them realized that it was sufficient to find any line of thrust, which would support the required loads. As the result of work by Winkler and Mohr, supplemented by carefully controlled tests conducted by the society of Austrian Engineers and Architects, the elastic theory was finally accepted for the analysis of arches (Ruddock, 2000, pg7).

2.4 Modern Arches

The period of 1800-1900 century is considered to be a golden age of structural engineering as during this period most of the present day theories of mechanics of material and structural analysis were developed. These developments were accompanied by the advancement in construction techniques and building material. As steel and reinforced concrete exhibited elastic properties much better than those of wood and stone, their arrival declining the popularity of masonry arches towards early 20th century. New theories were applied to enable more daring steel and concrete arch forms. New advancement in structural forms included the perfection of long-span arch bridges of various configuration (West, 1989, pg9).

2.4.1 Geometry of Modern Arches

Two forms that are most commonly used in the modern arches are the parabolic and circular arches. The Semicircular arches have been used and evolved right from the period of Roman civilization. On the other hand the parabolic arches have comparatively lesser presence throughout the history. One of the landmark examples of parabolic arch developed based on elastic theory of analysis is the Gateway Arch, St. Louis shown in Figure 2.19(b). While the theory of elasticity is the most commonly used method of analysis in modern arches, some of the parabolic arch application in late 19th and early 20th century were derived from experimental approach.

Antonio Gaudis parabolic or Catenary masonry arches show originality and independence, particularly with their integration in the process of architectural design. He resolved the equilibrium problem of the arch by comparing it with the behavior of hanging cable. The challenge was to find the shape of a cable that supports a load proportional to the vertical distance between its directrix and a horizontal extrados. To use a symmetric catenary to support an asymmetric load, it needed transformation for which Gaudi used iterative graphic method. He first hung a cable and measure the vertical distances of various point across the cable under it own weight. To this cable he added the corresponding weight of the floor, which caused change in shape of the cable. Vertical distances were measured again and accordingly the self-weight was modified. The cable under these loads adopted a shape that was very close to the exact mathematical shape. Application of this method can be seen in the design of diaphragm arches in the Mila house in Barcelona shown in Figure 2.19(a) (Huerta, 2006).

2.4.2 Types of Modern Arches

From 19th century on wards the theory of elasticity was commonly used for the analysis of arches and on the basis of requirements and limitations, certain types of arches were put in to

(a) Parabolic diaphragm arches, Mila House, Barcelona

(b) Gateway Arch, St. Louis

design application. Based on the material of construction, arches are classified as steel, concrete, timber, brick or stone. In the standpoint of support conditions and structural behavior they are classified as follows,

(1) Three-Hinged - Hinges at the crown and abutment

(2) Two-Hinged – Hinges at the abutments only

(3) Hingeless – No hinges at all

2.4.2.1 Three-Hinged Arch

The support reaction and stresses in the Three-hinged arch can be statically derived and hence application of the elastic theory is not required for the analysis. The Salginatobel Bridge in Schiers, Switzerland by Rober Malliart shown in Figure 2.19 is a three- hinged arch hollow box reinforced concrete bridge. It is a statically determinant and therefore analysis of the bending moments was simpler. A Three-hinged arch was an appropriate design solution due to its ability to move and adjust to the slight movements of the adjoining mountain which minimized the stresses developed due to the movement or temperature changes(West, 1989, pg10).

Figure 2.19: The Salginatobel Bridge, Schiers, Switzerland

2.4.2.2 Two-Hinged Arch and Hinge Less Arch

These two classes of arches belongs to the classes of structures whose stresses cannot be computed by the ordinary method of statics alone as the equilibrium between the exterior forces and interior stresses in the arch is dependent in part on its change of form. The rainbow Arch at Niagara Falls Spanning 950 feet is a hinge less arch. For the purpose of preliminary study of the Rainbow arch a two hinge arch design was considered and it was found that the deflection of the rib increased the stress at the critical location by about four times as compared to the hinge less arch which was actually erected. Thus the greater stiffness of the hinge less arch is a distinct advantage in long span arches (Kinney, 1957, pg540).

2.4.2.3 Other classification of modern arch

According to the shape and structural arrangement of the arch rib, several types of arches are available. A solid arch also known, as closed arch is a type of arch, where the space between the loaded area and the rib is filled as shown in Figure 2.20(a). These arches are either Hinge less or Two-hinged. Solid rib reinforced concrete arches are mostly hinge less and are used for long spans, where as solid rib steel arches are usually two-hinged when used for shorter spans (500-600 feet) and are hinge less when used for longer spans. The horizontal thrust developed in an arch under the applied load is an essential design component, which calls for excellent foundation or abutments for the arch. When the site conditions do not permit for the required abutments, horizontal thrust is resisted by providing a tie between the supports. This type of arch is called as tied arch shown in Figure 2.20(b).

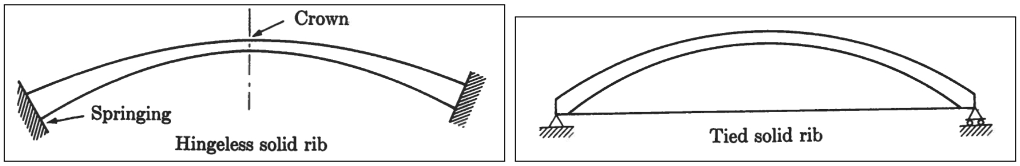

(a) Hingeless Solid Rib Arch

(b) Tied Solid Rib Arch

Figure 2.20: Modern Arches

The spandrel braced arch shown in Figure 2.21(a) also called, as open arch is a type of arch where the space between the loaded area and the rib is not filled. It is essentially a deck truss with horizontal thrust developed at the two ends. A two- hinged braced rib arch shown in Figure 2.21(b) is a type of spandrelbraced arch where the deck is hung form the arch. This type or arch is used in the places where there are no limitations associated with the space under the deck.

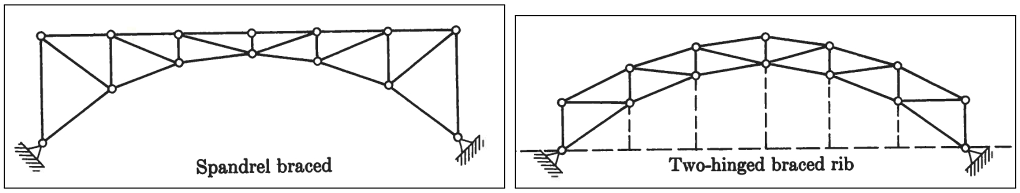

(a) Spandrel Braced Arch

(b) Two Hinged Braced Rib Arch

Figure 2.21: Modern Arches

2.5 Conclusion

The rational behind the structural behavior of an arch was not completely understood by the ancient builders and they used the intuitive understanding to develop the empirical rules to erected great monuments. Structural engineering existed as an art down through the ancient and medieval period. During this period circular arches were primarily used to span moderated distances. Some of the important developments in the application of an arch form were seen the

Roman and Gothic periods. The Romans explored compositional potential of a circular arch by using it in a sequential arrangement and there by effectively used the static principal of equilibrium of the adjoining arches. The Greek on other hand transformed the circular arch into a pointed arch and used flying buttresses to resist the outward thrust.

Renewal of interest in the filed of science and its application towards understanding the behavior of structures was seen from 14th century onward. From 14th century to 19th century many mathematicians and physicist developed theories based on their understanding of elastic properties of the materials. Even though the elastic theory of analysis progressed during this period, the practicing structural engineers continued relying on their experience and judgment to design arch structures. By 18th century the elastic theory of analysis was fully accepted and was used towards analysis of the arches.

The development in the theory of analysis was paralleled by the advancement in building material and construction techniques. Arrival of steel and reinforced concrete had revolutionary impact on application of arch structures. In contemporary world arches have gained a special importance and are primarily used in ambitious projects like long span bridges.

Chapter 3

Analysis of Elastic Arches

3.1 Introduction

In the previous chapter development of the elastic theory has been discussed briefly. Some of the influential work that has direct application in the analysis of arches includes, computing influence line and elastic center by Otto Mohr, principle of least work and strain energy method by E. Winkler, virtual work method by John Bernoulli and method of least work by Alberto Castigliano.

This chapter particularly focuses on application of statics, principal of least work and virtual work method towards developing analytical equations for symmetric Three-hinged, Two-hinged and Hingeless circular arches under different loading conditions. The analytical equations are made generic by the introduction of certain trigonometric variables that define geometry of each type of the arch. The equations are validated using examples discussed in existing literature. Additional, a structural analysis program, Sap 2000 is used to develop models for the three types of arches mentioned above and their analysis is compared with the solutions obtained using the analytical equations. The solutions of the analytical equations are further used to discuss the structural behavior of each type of arch.

3.1.1 Structure and Geometry of an Arch

The application of the elastic theory for the analysis of an arch is based on the assumption that it is a constrained curved beam and its ends are connected with rigid support. These connections may be made to allow an angular movement at the point of connection, as in the case of Two -hinged arches or the connection may be made rigid as in the case of Hingeless arch. These two forms of arches fall in a type of statically indeterminate curved beams whose stresses cannot be computed by the ordinary method of statics alone. The equilibrium between the exterior forces and the interior stresses in these arches is dependent in part on its change of form. Therefore, computation of the interior stresses requires the static equilibrium of the forces, the static equilibrium of the material, and the form of the arch. The static indeterminateness is terminated when a third hinge is introduced, usually at the crown of the arch. This transforms the arch into two curved beams, each freely supported at two points.

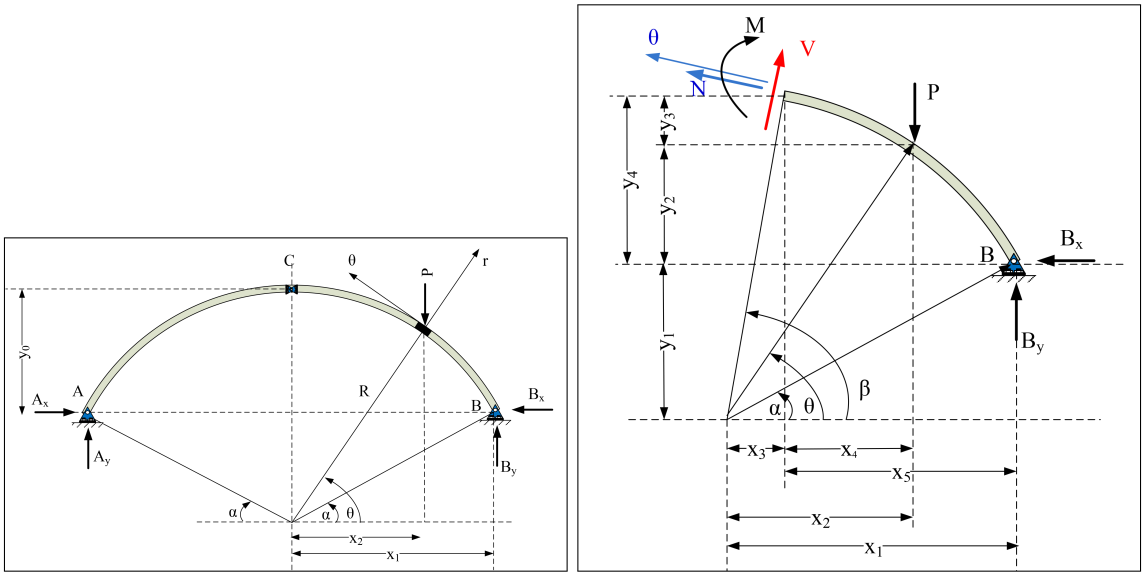

(a) Reactions

(b) Internal Forces

Figure 3.1: Geometry of circular arch

Trignometric Variables

$\mathrm{x1}=\boldsymbol{R}\ \mathrm{Cos}[\boldsymbol{\alpha}];\ \mathrm{x2}=\boldsymbol{R}\ \mathrm{Cos}[\boldsymbol{\theta}\ ];\ \mathrm{x3}=\ \boldsymbol{R}\ \mathrm{Cos}[\boldsymbol{\beta}];\ \mathrm{x4}=\mathrm{x2}-\mathrm{x3};\ \mathrm{x5}=\mathrm{x1}-\mathrm{x3};$

$\mathrm{y0}=\boldsymbol{R}(\mathbf{1}-\mathrm{Sin}[\boldsymbol{\alpha}]);\ \mathrm{y1}=\boldsymbol{R}\ \mathrm{Sin}[\boldsymbol{\alpha}];\ \mathrm{y2}=\boldsymbol{R}\ (\mathrm{Sin}[\boldsymbol{\theta}\ ]-\mathrm{Sin}[\boldsymbol{\alpha}]);\ \mathrm{y3}=\boldsymbol{R}\ \mathrm{Sin}[\boldsymbol{\beta}]-\mathrm{y1}-\mathrm{y2};\ \mathrm{y4}=\boldsymbol{R}\ \mathrm{Sin}[\boldsymbol{\beta}]-\mathrm{y1};$

A Three-hinged arch in Figure 3.1 represents the trigonometric variables defining the geometry of a symmetric circular arch that are used in deriving the analytical equations. Similar variables are used for a Two-hinged and a Hingeless arch. The shape ACB represents an arch, where A and B are the abutments and point C is crown of the arch. Distance y0 represents rise of the arch where as distance x1 represents half of the arch span. Letter α indicates an angle made by a line connecting center of the circle and the abutment with the horizontal, consequently when α is zero it is a semicircular arch. All the dimensions and angles are measured for the abutment B. Letter θ indicates an angle at which a load P is applied on the arch rib. Forces Ax and Bx are the horizontal reactions and forces Ay and By are the vertical reactions at the abutments. Shear force (V), axial force (N) and Moment (M) are the internal forces at any angle β across the arch span. Figure 3.1(b) indicates the sign convention used for the internal forces, where positive sign is assumed for clock wise Moment, outward Shear force and tensile Axial force. Overall the nomenclature used in defining the geometry of the arch, includes upper case letters to indicate all forces and lower case letters to indicate all dimensions.

3.2 Three-Hinged Circular Arch

A symmetrical Three-hinged circular arch has overall four reactions - two at each support. The primary difference between a Three- hinged arch and a Two-hinged or Hingless arch is the discontinuity of the arch rib due to the hinge at the crown, which converts a Three-hinged arch into two independently supported curved components. In each of the independent component, there are two equal and apposite reactions. Thus with two unknown reactions and three equations of equilibrium for each component, a symmetrical Three-hinged circular arch is a statically determinate structure.

3.2.1 Analysis Procedure

For the purpose of analysis, three loading conditions are considered; a point load , self-weight of the arch and applied uniformly distributed load across the arch. The self- weight and the uniformly distributed load are symmetric about the center of the arch where as a point load, when applied anywhere but at the crown is asymmetric about the center of the arch. Hence to illustrate the analysis, same figures are used for the self-weight and the uniformly distributed loading conditions where as different set of figures is used for the point load condition. The analysis for all three loading conditions is performed in three steps using Mathematica, where reactions at the support are computed in the first step, internal forces across arch are computed in the second step and using the equations for internal forces from the second step, the deflection in the arch is computed in third step. The Mathematica files for all steps are included in relevant sections and for simplification only final equations for reactions and internal forces are expanded. The analytical equations for support reactions and internal forces are in terms of the trigonometric variables defined above. For computing deflection, a specific design of a symmetric circular arch is considered (Kinney, 1957, pg 547-558). This reduced the complexity of the deflection equation as well as the time to process Mathematica files.

3.2.2 Point Load

In this case the elementary applied force is given by

$$dp = P \tag{3.1}$$

3.2.2.1 Reactions

Considering Figure 3.2, the horizontal and vertical reactions at the supports are determined. When a point load is applied anywhere but at the crown of an arch it creates an asymmetric loading condition about the center of the arch. As the expression for the vertical reaction By is dependent on the location of the point load P with respect to the crown C, two different set of equations are developed, one for the condition $\theta < \frac{\Pi}{2}$ and other for the condition $\theta \geq \frac{\Pi}{2}$.

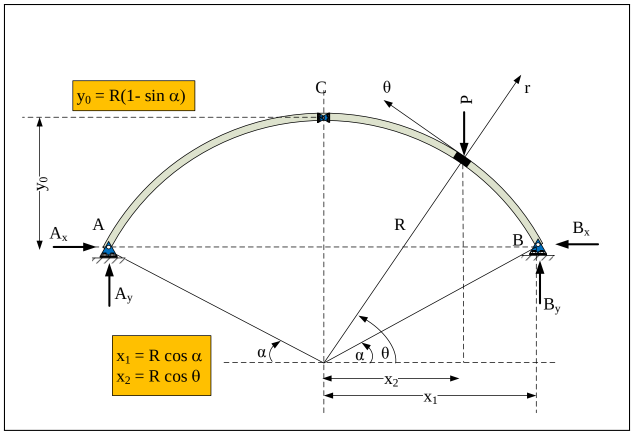

Figure 3.2: Three-hinged circular arch under point load

Following is the output from Mathematica illustrating the derivation for computing support reaction.

Reactions

Define the load

```
P=P;
```

Determine vertical reaction at B by taking moment with respect to A (CCW +ve)

```
SigMA=BY2x1 − P(x1 + x2);
```

```
Sol1=Solve[SigMA==0,BY]; BY=BY/.Sol1[[1]]
```

$\frac{1}{2}P(\mathrm{Cos}[\alpha] + \mathrm{Cos}[\theta])\mathrm{Sec}[\alpha]$

Determine vertical reaction at A by taking summation of forces in the y direction

```
Sol2=Solve[BY − P + AY==0,AY]; AY=AY/.Sol2[[1]]
```

$\frac{1}{2}(P - P\mathrm{Cos}[\theta]\mathrm{Sec}[\alpha])$

$\theta < \frac{\pi}{2}$

Determine horizontal reaction at B by taking moment with respect to C (CCW +ve)

```
SigMC= − BXy0 + BYx1 − Px2;
```

```
Sol3=Solve[SigMC==0,BX]; BX=BX/.Sol3[[1]]
```

$$\frac{-P\text{Cos}[\alpha]+P\text{Cos}[\theta]}{2(-1+\text{Sin}[\alpha])}$$

```
AX=BX;
```

Check statics by taking moment about O CCW +ve

```
MO=FullSimplify[−AXy1 − AYx1 − Px2 + BXy1 + BYx1]
```

```
0
```

```
Clear[AX]; Clear[BX];
```

$\theta > \frac{\pi}{2}$

Determine horizontal reaction at B by taking moment with respect to C (CCW +ve)

```
SigMC= − BXy0 + BYx1;
```

```
Sol3=Solve[SigMC==0,BX]; BX=BX/.Sol3[[1]]
```

$$-\frac{P(\text{Cos}[\alpha]+\text{Cos}[\theta])}{2(-1+\text{Sin}[\alpha])}$$

```
AX=BX;
```

Check statics by taking moment about O CCW +ve

```
MO=FullSimplify[−AXy1 − AYx1 − Px2 + BXy1 + BYx1]
```

```
0
```

3.2.2.2 Internal Forces

While the location of a point load anywhere but at the crown of an arch, creates an asymmetric loading condition, it also causes discontinuity in the internal forces. This discontinuity in the internal forces in shown in Figure 3.3. Hence the expression for the internal forces at any angle β across the arch span is dependent on its relation with respect to the angle θ at which the point load is applied. By taking in consideration following conditions, different sets of equations are developed for the internal forces.

$$\theta < \frac{\Pi}{2} \longrightarrow \beta < \theta, \beta \geq \theta, \;\; \theta \geq \frac{\Pi}{2} \longrightarrow \beta < \theta, \beta \geq \theta \tag{3.2}$$

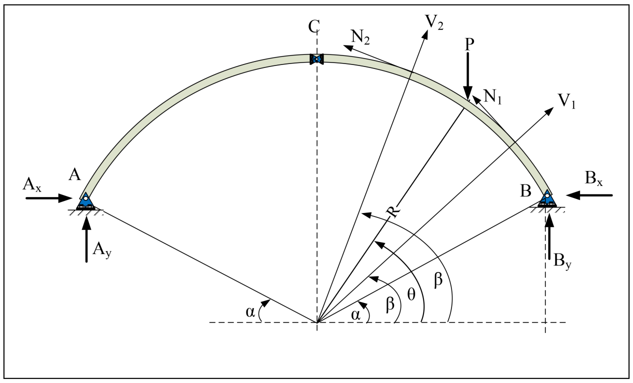

Figure 3.3: Relation of β with respect to θ

The free body diagram in Figure 3.4 is used to determine the internal forces - axial, shear and moment at any angle β across the arch span.

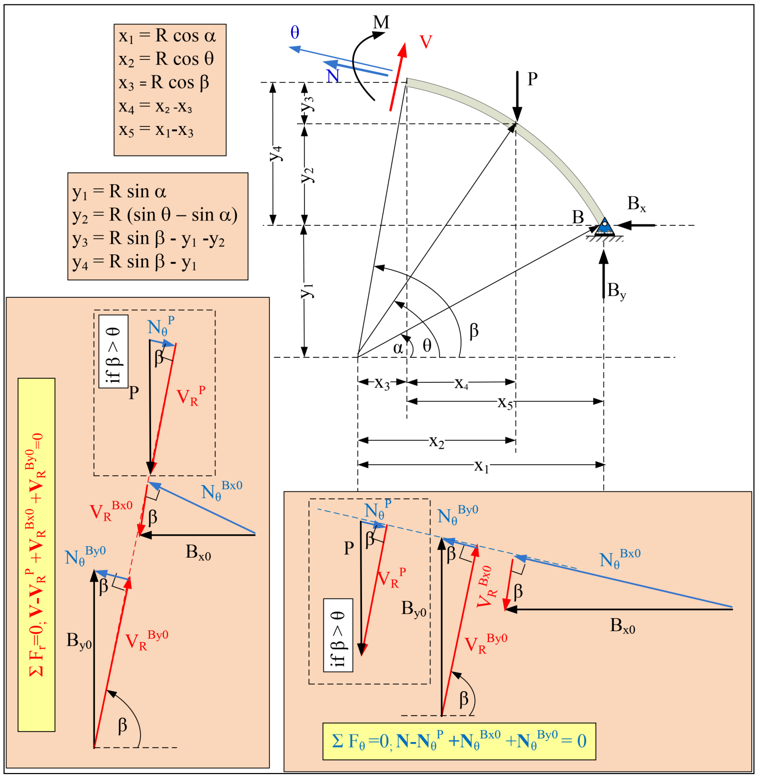

Figure 3.4: FBD of three-hinged, circular arch under point load

Following is the output from Mathematica illustrating the derivation for internal forces -

axial, shear and moment at any angle β across the arch span.

Internal Forces

$\theta < \frac{\pi}{2}$ & $\beta < \theta$

Summation of forces in the radial direction; Shear (+ve outward)

```
SigFV1= − BXCos[β] + BYSin[β] + V1;
```

```
Sol4=FullSimplify[Solve[SigFV1==0,V1]]; V1[β_]=V1/.Sol4[[1]]
```

$$-\frac{P(\mathrm{Cos}[\alpha]\mathrm{Cos}[\beta]-\mathrm{Cos}[\beta]\mathrm{Cos}[\theta]+\mathrm{Sin}[\beta](-1+\mathrm{Sin}[\alpha]+\mathrm{Cos}[\theta](-\mathrm{Sec}[\alpha]+\mathrm{Tan}[\alpha])))}{2(-1+\mathrm{Sin}[\alpha])}$$

Summation of forces in the tangential direction; Normal force (+ve Tension)

```
SigFN1=BXSin[β] + BYCos[β] + N1;
```

```
Sol5=FullSimplify[Solve[SigFN1==0,N1]]; N1[β_]=N1/.Sol5[[1]]
```

$$\frac{P((\mathrm{Cos}[\alpha]-\mathrm{Cos}[\theta])\mathrm{Sin}[\beta]+\mathrm{Cos}[\beta](1-\mathrm{Sin}[\alpha]+\mathrm{Cos}[\theta](\mathrm{Sec}[\alpha]-\mathrm{Tan}[\alpha])))}{2(-1+\mathrm{Sin}[\alpha])}$$

Summation of moments; Internal moment (CW +ve)

```
SigM1=BXy4 − BYx5 + M1;
```

```
Sol6=Solve[SigM1==0,M1]; M1[β_]=M1/.Sol6[[1]]
```

$$\frac{1}{2(-1+\mathrm{Sin}[\alpha])}(-PR\mathrm{Cos}[\alpha]+PR\mathrm{Cos}[\beta]-PR\mathrm{Cos}[\theta]+PR\mathrm{Cos}[\beta]\mathrm{Cos}[\theta]\mathrm{Sec}[\alpha]-PR\mathrm{Cos}[\beta]\mathrm{Sin}[\alpha]+2PR\mathrm{Cos}[\theta]\mathrm{Sin}[\alpha]+PR\mathrm{Cos}[\alpha]\mathrm{Sin}[\beta]-PR\mathrm{Cos}[\theta]\mathrm{Sin}[\beta]-PR\mathrm{Cos}[\beta]\mathrm{Cos}[\theta]\mathrm{Tan}[\alpha])$$

$\theta < \frac{\pi}{2}$ & $\beta > \theta$

Summation of Forces in the radial direction; Shear (+ve outward)

```
SigFV2= − BXCos[β] + BYSin[β] − PSin[β] + V2;
```

```
Sol7=FullSimplify[Solve[SigFV2==0,V2]]; V2[β_]=V2/.Sol7[[1]]
```

$$\frac{P(-\mathrm{Cos}[\alpha]\mathrm{Cos}[\beta]+\mathrm{Cos}[\beta]\mathrm{Cos}[\theta]+\mathrm{Sin}[\beta](-1+\mathrm{Sin}[\alpha]+\mathrm{Cos}[\theta](\mathrm{Sec}[\alpha]-\mathrm{Tan}[\alpha])))}{2(-1+\mathrm{Sin}[\alpha])}$$

Summation of forces in the tangential direction; Normal force (+ve Tension)

```
SigFN2=BXSin[β] + BYCos[β] − PCos[β] + N2;
```

```
Sol8=FullSimplify[Solve[SigFN2==0,N2]]; N2[β_]=N2/.Sol8[[1]]
```

$$\frac{P((\mathrm{Cos}[\alpha]-\mathrm{Cos}[\theta])\mathrm{Sin}[\beta]+\mathrm{Cos}[\beta](-1+\mathrm{Sin}[\alpha]+\mathrm{Cos}[\theta](\mathrm{Sec}[\alpha]-\mathrm{Tan}[\alpha])))}{2(-1+\mathrm{Sin}[\alpha])}$$

Summation of moments; Internal moment (CW +ve)

```
SigM2=BXy4 − BYx5 + Px4 + M2;
```

```
Sol9=Solve[SigM2==0,M2]; M2[β_]=M2/.Sol9[[1]]
```

$$\frac{1}{2(-1+\text{Sin}[\alpha])}(-PR\text{Cos}[\alpha]-PR\text{Cos}[\beta]+PR\text{Cos}[\theta]+PR\text{Cos}[\beta]\text{Cos}[\theta]\text{Sec}[\alpha]+PR\text{Cos}[\beta]\text{Sin}[\alpha]+PR\text{Cos}[\alpha]\text{Sin}[\beta]-PR\text{Cos}[\theta]\text{Sin}[\beta]-PR\text{Cos}[\beta]\text{Cos}[\theta]\text{Tan}[\alpha])$$

Internal Forces

$\theta > \frac{\pi}{2}$ & $\beta < \theta$

Summation of forces in the radial direction; Shear (+ve outward)

```
SigFV1= − BXCos[β] + BYSin[β] + V1;
```

```
Sol4=FullSimplify[Solve[SigFV1==0,V1]]; V1[β_]=V1/.Sol4[[1]]
```

$$-\frac{P(\text{Cos}[\alpha]\text{Cos}[\beta]+\text{Cos}[\beta]\text{Cos}[\theta]+\text{Sin}[\beta](-1+\text{Sin}[\alpha]+\text{Cos}[\theta](-\text{Sec}[\alpha]+\text{Tan}[\alpha])))}{2(-1+\text{Sin}[\alpha])}$$

Summation of forces in the tangential direction; Normal force (+ve Tension)

```
SigFN1=BXSin[β] + BYCos[β] + N1;
```

```
Sol5=FullSimplify[Solve[SigFN1==0,N1]]; N1[β_]=N1/.Sol5[[1]]
```

$$\frac{P((\text{Cos}[\alpha]+\text{Cos}[\theta])\text{Sin}[\beta]+\text{Cos}[\beta](1-\text{Sin}[\alpha]+\text{Cos}[\theta](\text{Sec}[\alpha]-\text{Tan}[\alpha])))}{2(-1+\text{Sin}[\alpha])}$$

Summation of moments; Internal moment (CW +ve)

```
SigM1=BXy4 − BYx5 + M1;
```

```
Sol6=Solve[SigM1==0,M1]; M1[β_]=M1/.Sol6[[1]]
```

$$\frac{1}{2(-1+\text{Sin}[\alpha])}(-PR\text{Cos}[\alpha]+PR\text{Cos}[\beta]-PR\text{Cos}[\theta]+PR\text{Cos}[\beta]\text{Cos}[\theta]\text{Sec}[\alpha]-PR\text{Cos}[\beta]\text{Sin}[\alpha]+PR\text{Cos}[\alpha]\text{Sin}[\beta]+PR\text{Cos}[\theta]\text{Sin}[\beta]-PR\text{Cos}[\beta]\text{Cos}[\theta]\text{Tan}[\alpha])$$

$\theta > \frac{\pi}{2}$ & $\beta > \theta$

Summation of Forces in the radial direction; Shear (+ve outward)

```
SigFV2= − BXCos[β] + BYSin[β] − PSin[β] + V2;
```

```
Sol7=FullSimplify[Solve[SigFV2==0,V2]]; V2[β_]=V2/.Sol7[[1]]
```

$$-\frac{P(\text{Cos}[\alpha]\text{Cos}[\beta]+\text{Cos}[\beta]\text{Cos}[\theta]-\text{Sin}[\beta](-1+\text{Sin}[\alpha]+\text{Cos}[\theta](\text{Sec}[\alpha]-\text{Tan}[\alpha])))}{2(-1+\text{Sin}[\alpha])}$$

Summation of forces in the tangential direction; Normal force (+ve Tension)

```
SigFN2=BXSin[β] + BYCos[β] − PCos[β] + N2;
```

```
Sol8=FullSimplify[Solve[SigFN2==0,N2]]; N2[β_]=N2/.Sol8[[1]]
```

$$\frac{P((\text{Cos}[\alpha]+\text{Cos}[\theta])\text{Sin}[\beta]+\text{Cos}[\beta](-1+\text{Sin}[\alpha]+\text{Cos}[\theta](\text{Sec}[\alpha]-\text{Tan}[\alpha])))}{2(-1+\text{Sin}[\alpha])}$$

Summation of moments; Internal moment (CW +ve)

```
SigM2=BXy4 − BYx5 + Px4 + M2;
```

```
Sol9=Solve[SigM2==0,M2]; M2[β_]=M2/.Sol9[[1]]
```

$$\frac{1}{2(-1+\mathrm{Sin}[\alpha])}(-PR\mathrm{Cos}[\alpha]-PR\mathrm{Cos}[\beta]+PR\mathrm{Cos}[\theta]+PR\mathrm{Cos}[\beta]\mathrm{Cos}[\theta]\mathrm{Sec}[\alpha]+PR\mathrm{Cos}[\beta]\mathrm{Sin}[\alpha]-2PR\mathrm{Cos}[\theta]\mathrm{Sin}[\alpha]+ PR\mathrm{Cos}[\alpha]\mathrm{Sin}[\beta]+PR\mathrm{Cos}[\theta]\mathrm{Sin}[\beta]-PR\mathrm{Cos}[\beta]\mathrm{Cos}[\theta]\mathrm{Tan}[\alpha])$$

3.2.2.3 Deflection

Some unseen challenges occurred in the application of the Three-hinged arch's analytical equations towards computing the deflection which provided complex solution. Therefore it needs further investigation in future work.

3.2.2.4 Summary Of Results

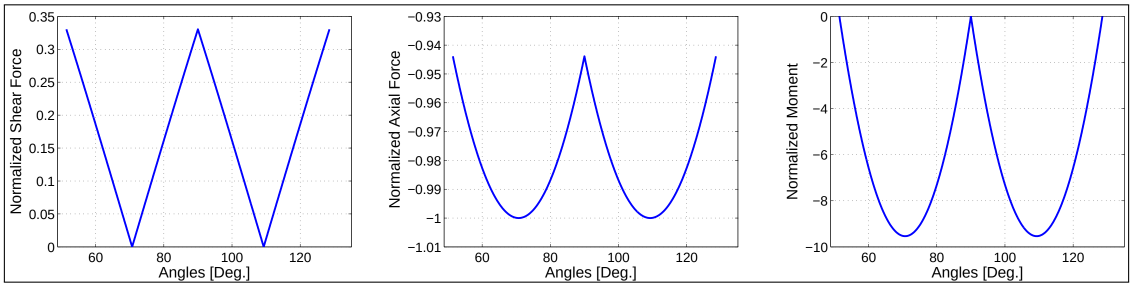

Figure 3.5: Plots of internal forces for Three-hinged circular arch under point load

Figure 3.5 show plots for a Three-hinged arch example discussed in the above section. A point load is applied at the crown of the arch. The internal axial force and shear force are normalized with respect to the resultant of vertical reaction and thrust at the abutments. The internal moment is normalized with respect to the product of internal axial force and the rise. As indicated by the plot, all internal forces are symmetric about the crown of the arch and the Three-hinged arch behaves like two independent curved components. The axial compressive force is highest at the mid point of each component and it decreases toward the hinged supports with the difference of about 5% between the high and low axial forces. The internal moment is zero at the hinges and it is highest at the mid point of each component. The shear force on other hand is comparatively lower than the internal axial force and moment and it is zero at the locations of maximum internal moment.

3.2.3 Self Weight

In this case the elementary applied force is given by

$$dP = wds = wRd\theta \tag{3.3}$$

3.2.3.1 Reactions

Considering Figure 3.6, the horizontal and vertical reactions at the supports are determined.

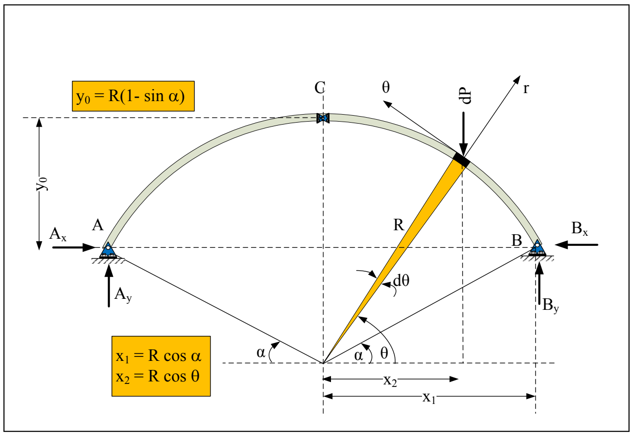

Figure 3.6: Three-hinged circular arch under self weight

Following is the output from Mathematica illustrating the derivation for computing support reaction.

Reactions

Define the load (omitting the $d\theta$)

```
dP′=wR;
```

Determine vertical reaction by taking summation of forces in the y direction

$\text{BY}=\int_{\alpha}^{\pi/2}\text{dP}'\boldsymbol{d\theta}$

$$Rw\left(\frac{\pi}{2}-\alpha\right)$$

Determine horizontal reaction at B by taking moment with respect to C (CCW +ve)

$\text{SigMC}=-\text{BXy0}+\text{BYx1}-\int_{\alpha}^{\pi/2}\text{x2dP}'\boldsymbol{d\theta};$

$\text{Sol1}=\text{Solve}[\text{SigMC}==\mathbf{0},\text{BX}];\ \text{BX}=\text{BX}/.\text{Sol1}[[\mathbf{1}]]$

$$-\frac{R(-2w+\pi w\text{Cos}[\alpha]-2w\alpha\text{Cos}[\alpha]+2w\text{Sin}[\alpha])}{2(-1+\text{Sin}[\alpha])}$$

$\text{CX}=\text{BX};$

Check statics by taking moment about O (CCW +ve)

$\text{MO}=\text{FullSimplify}\left[\text{BXy1}+\text{BYx1}-\text{CX}(\text{y1}+\text{y0})-\int_{\alpha}^{\pi/2}\text{x2dP}'\boldsymbol{d\theta}\right]$

$$0$$

3.2.3.2 Internal Forces

The free body diagram in Figure 3.7 is used to determine the internal forces - axial, shear and moment at any angle β across the arch span.

Following is the output from Mathematica illustrating the derivation for internal forces - axial, shear and moment.

Internal Forces

Summation of forces in the Radial direction ; Shear (+ve outward)

$\text{SigFV}=-\text{BXCos}[\boldsymbol{\beta}]+\text{BYSin}[\boldsymbol{\beta}]-\int_{\alpha}^{\beta}\text{dP}'\text{Sin}[\boldsymbol{\beta}]\boldsymbol{d\theta}+\boldsymbol{V};$

$\text{Sol2}=\text{FullSimplify}[\text{Solve}[\text{SigFV}==\mathbf{0},\boldsymbol{V}]];\ \boldsymbol{V}[\boldsymbol{\beta}\_]=\boldsymbol{V}/.\text{Sol2}[[\mathbf{1}]]$

$$-\frac{Rw(\text{Cos}[\beta](-2+(\pi-2\alpha)\text{Cos}[\alpha]+2\text{Sin}[\alpha])+(\pi-2\beta)(-1+\text{Sin}[\alpha])\text{Sin}[\beta])}{2(-1+\text{Sin}[\alpha])}$$

Summation of forces in the tangential direction; Normal force +(ve Tension)

$\text{SigFN}=\text{BXSin}[\boldsymbol{\beta}]+\text{BYCos}[\boldsymbol{\beta}]-\int_{\alpha}^{\beta}\text{dP}'\text{Cos}[\boldsymbol{\beta}]\boldsymbol{d\theta}+\boldsymbol{N};$

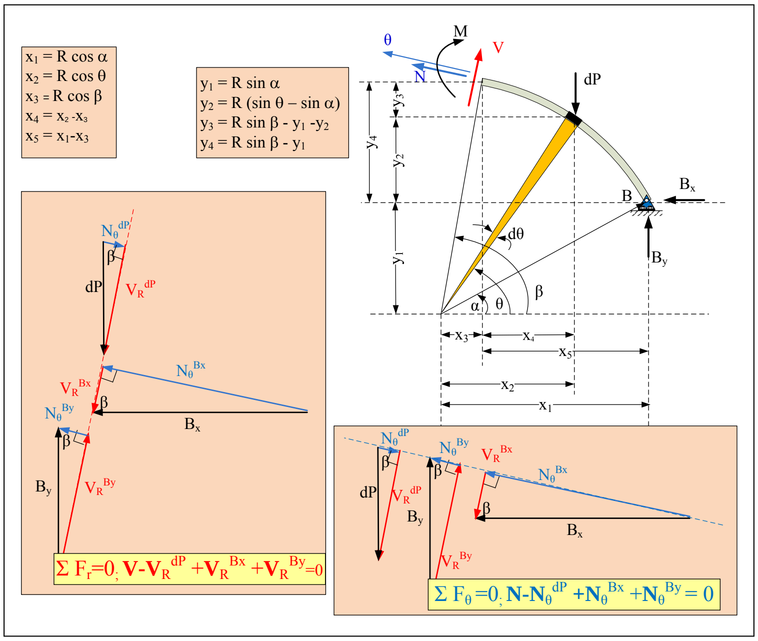

Figure 3.7: FBD of Three-hinged circular arch under self weight

```
Sol3=FullSimplify[Solve[SigFN==0,N]]; NN[β_]=N/.Sol3[[1]]
```

$$\frac{1}{2}Rw\left(-(\pi-2\beta)\mathrm{Cos}[\beta]+\frac{(-2+(\pi-2\alpha)\mathrm{Cos}[\alpha]+2\mathrm{Sin}[\alpha])\mathrm{Sin}[\beta]}{-1+\mathrm{Sin}[\alpha]}\right)$$

Summation of moments; Internal moment (CW +ve)

$$\text{SigM=BXy4} - \text{BYx5} + \int_{\alpha}^{\beta}\text{dP}'\text{x4}\,d\theta + M;$$

```
Sol4=FullSimplify[Solve[SigM==0,M]]; M[β_]=M/.Sol4[[1]]
```

$$\frac{R^2w(-(\pi-2\beta)\mathrm{Cos}[\beta](-1+\mathrm{Sin}[\alpha])+(\pi-2\alpha)\mathrm{Cos}[\alpha](-1+\mathrm{Sin}[\beta]))}{2(-1+\mathrm{Sin}[\alpha])}$$

3.2.3.3 Deflection

The analytical equations developed above are used to compute deflection in a symmetric circular arch (Kinney, 1957, pg 547-558).Following are the numerical values used for the trigonometric variable,

Arch Rib Width (b) = 2 ft, Arch Rib Depth(d) = 3 ft, Area(a) = 6 ft^2, Moment of Inertia (i) =

4.5 ft^4, Modulus of Elasticity(e) = 3645 Ksi, α= 0.8975 rad., Radius(R) = 160.35 ft., Span = 200 ft, Rise = 35 ft, W=2.275 kip/ft

Following equation of virtual work is used to compute defection in the considered arch example.

$$\delta P.\,\Delta = \left[\int_{\alpha}^{\theta} \frac{M\ \delta\mathrm{M1}}{e\ i}\ Rd\beta + \int_{\theta}^{\frac{\pi}{2}} \frac{M\ \delta\mathrm{M2}}{e\ i}\ Rd\beta + \int_{\frac{\pi}{2}}^{\theta} \frac{M\ \delta\mathrm{M3}}{e\ i}\ Rd\beta + \int_{\theta}^{(\pi-\alpha)} \frac{M\ \delta\mathrm{M4}}{e\ i}\ Rd\beta\right] \tag{3.4}$$

Where

δP	External Virtual unit load applied in the direction of Δ
Δ	External displacement caused by the real applied load
M	Internal moment in the beam caused by real load
$\delta\mathrm{M1}(\beta < \theta)$,	
$\delta\mathrm{M2}(\beta \geq \theta)$	Internal moment caused due to external virtual unit load when $\theta < \frac{\pi}{2}$
$\delta\mathrm{M3}(\beta < \theta)$,	
$\delta\mathrm{M4}(\beta \geq \theta)$	Internal moment caused due to external virtual unit load when $\theta \geq \frac{\pi}{2}$

3.2.3.4 Summary of Results

YOU CAN NOT HAVE A SUBSUBSECTION WITHOUT TEXT

Figure 3.8 show plots for the Three-hinged arch example under self-weight discussed in the above section.The internal axial force and shear force are normalized with respect to the resultant of vertical reaction and thrust at the abutments. The axial compressive force is highest at the abutments and it decreases toward the crown to about 81% of the maximum value. The shear force on other hand is comparatively low and it varies between about 4% and 1%, respectively from the abutment to the crown. The internal moment is normalized with respect to the product of internal axial force and the rise. The internal moment is zero at the location of the hinges and it is highest between the hinges. With no inflection point in the moment diagram between the hinges, it can be said that a Three-hinged arch under self-weight behaves like two independently supported curved

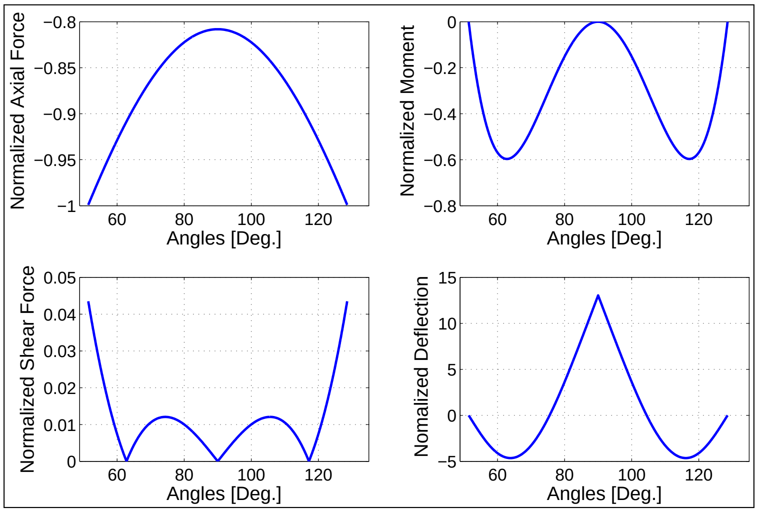

Figure 3.8: Plots for Three-hinged circular arch under self-weight

components. Deflection in a Three-hinged arch is highest at the crown and it reduces to about 40% of the maximum at $\frac{1}{6}$ of the span from the abutments. As the supports are immovable, the downward deflection caused in individual curved components pushes the crown upward.

3.2.4 Uniformly Distributed Load

In this case the elementary applied force is given by

$$dp = wdx = wRSin\theta \tag{3.5}$$

3.2.4.1 Reactions

Considering Figure 3.6, the horizontal and vertical reactions at the supports are determined. Following is the output from Mathematica illustrating the derivation for computing support reaction.

Reactions

Define the load (omitting the $d\theta$)

$$\mathrm{dP'}=\boldsymbol{wR}\mathrm{Sin}[\boldsymbol{\theta}];$$

Determine vertical reaction by taking summation of forces in the y direction

$$\mathrm{BY}=\int_{\boldsymbol{\alpha}}^{\boldsymbol{\pi/2}}\mathrm{dP'}\boldsymbol{d\theta}$$

$$Rw\mathrm{Cos}[\alpha]$$

Determine horizontal reaction at B by taking moment with respect to C (CCW +ve)

$$\mathrm{SigMC}=-\mathrm{BXy0}+\mathrm{BYx1}-\int_{\boldsymbol{\alpha}}^{\boldsymbol{\pi/2}}\mathrm{x2dP'}\boldsymbol{d\theta};$$

$$\mathrm{Sol1=Solve[SigMC==\mathbf{0},BX]; BX=BX/.Sol1[[\mathbf{1}]]}$$

$$-\frac{Rw\mathrm{Cos}[\alpha]^2}{2(-1+\mathrm{Sin}[\alpha])}$$

$$\mathrm{CX=BX;}$$

Check statics by taking moment about O (CCW +ve)

$$\mathrm{MO=FullSimplify}\left[\mathrm{BXy1}+\mathrm{BYx1}-\mathrm{CX(y1+y0)}-\int_{\boldsymbol{\alpha}}^{\boldsymbol{\pi/2}}\mathrm{x2dP'}\boldsymbol{d\theta}\right]$$

$$0$$

3.2.4.2 Internal Forces

The free body diagram in Figure 3.7 is used to determine the internal forces - axial, shear and moment at any angle β across the arch span. Following is the output from Mathematica, illustrating the derivation for internal forces - axial, shear and moment at any angle β across the arch span.

Internal Forces

Summation of forces in the Radial direction ; Shear (+ve outward)

$$\mathrm{SigFV}=-\mathrm{BXCos}[\boldsymbol{\beta}]+\mathrm{BYSin}[\boldsymbol{\beta}]-\int_{\boldsymbol{\alpha}}^{\boldsymbol{\beta}}\mathrm{dP'Sin}[\boldsymbol{\beta}]\boldsymbol{d\theta}+\boldsymbol{V};$$

$$\mathrm{Sol2=FullSimplify[Solve[SigFV==\mathbf{0},\boldsymbol{V}]];}\ \boldsymbol{V}[\boldsymbol{\beta\_}]=\boldsymbol{V}/.\mathrm{Sol2[[\mathbf{1}]]}$$

$$\frac{1}{2}Rw\mathrm{Cos}[\beta](1+\mathrm{Sin}[\alpha]-2\mathrm{Sin}[\beta])$$

Summation of forces in the tangential direction; Normal force +(ve Tension)

$$\text{SigFN=BXSin}[\boldsymbol{\beta}] + \text{BYCos}[\boldsymbol{\beta}] - \int_{\boldsymbol{\alpha}}^{\boldsymbol{\beta}} \text{dP}'\text{Cos}[\boldsymbol{\beta}]\boldsymbol{d\theta} + \boldsymbol{N};$$

$$\text{Sol3=FullSimplify[Solve[SigFN==}\mathbf{0},\boldsymbol{N}]];\ \text{NN}[\boldsymbol{\beta}\_]=\boldsymbol{N}/.\text{Sol3}[[\mathbf{1}]]$$

$$\frac{1}{2}Rw\left(-2\text{Cos}[\beta]^2 + \frac{\text{Cos}[\alpha]^2\text{Sin}[\beta]}{-1+\text{Sin}[\alpha]}\right)$$

Summation of moments; Internal moment (CW +ve)

$$\text{SigM=BXy4} - \text{BYx5} + \int_{\boldsymbol{\alpha}}^{\boldsymbol{\beta}} \text{dP}'\text{x4}\boldsymbol{d\theta} + \boldsymbol{M};$$

$$\text{Sol4=FullSimplify[Solve[SigM==}\mathbf{0},\boldsymbol{M}]];\ \boldsymbol{M}[\boldsymbol{\beta}\_]=\boldsymbol{M}/.\text{Sol4}[[\mathbf{1}]]$$

$$\frac{1}{2}R^2w(-1+\text{Sin}[\beta])(-\text{Sin}[\alpha]+\text{Sin}[\beta])$$

3.2.4.3 Deflection

The process to compute the deflection in Three-hinged circular arch under uniformly distributed load as well as the the numerical values used for the trigonometric variable are similar to that under Self-weight discussed in Section 3.2.3.3 and therefore it is not shown here.

3.2.4.4 Summary of Results

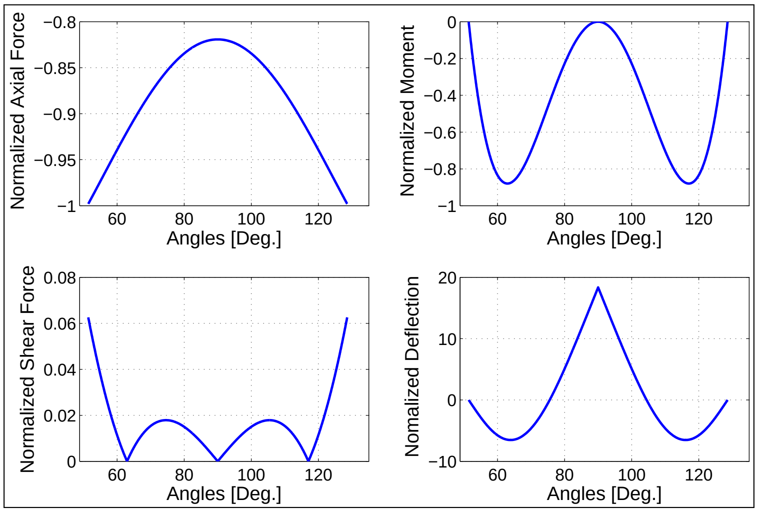

Figure 3.9: Plots for Three-hinged circular arch under uniformly distribute load

Figure 3.9 show plots for the Three-hinged arch under uniformly distributed load discussed in above section. The internal axial force and shear force are normalized with respect to the resultant of vertical reaction and thrust at the abutments. The axial compressive force is highest at the abutments and it decreases toward the crown to about 82.5% of the maximum value. The shear force on other hand is comparatively low and it varies between about 6% and 2%, respectively from the abutment to the crown. The internal moment is normalized with respect to the product of internal axial force and the rise. The internal moment is zero at the location of the hinges and it is highest between the hinges. Deflection in a Three-hinged arch is highest at the crown and it reduces to about 33 % of the maximum at $\frac{1}{6}$ of the span from the abutments. As the supports are immovable, the downward deflection caused in individual curved components pushes the crown upward.

3.2.5 Three-Hinged Circular Arch: Validation

The analytical equations developed above for the Three-hinged circular arch under point load, self-weight and uniformly distributed load are validated in two steps. Firstly, the self weight and uniformly distributed load applied across the arch span are divided in series of 20 point loads. The graphs of internal forces are plotted using the analytical equations for self weight and uniformly distributed load together with their respective point loads. These graphs are superimposed to check the validity of the analytical solutions. As the self-weight or the uniformly distributed load are equivalent to their respective series of point loads their plots closely match with each other.

Figure 3.10 and Figure 3.11 illustrates the above discussed process used for validating the analytical equations. Secondly, a Sap 2000 model is developed for the Three-hinged circular arch under self-weight case. The moment, shear force and axial force diagrams of its analysis are compared with the graphs plotted using the analytical equation.

The numerical values on the moment diagram in Figure 3.12, axial force diagram in Figure

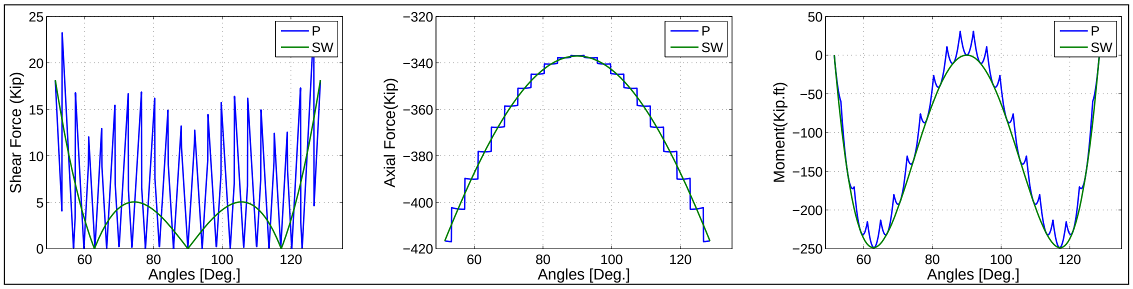

Figure 3.10: Three-hinged circular arch under self-weight vs. series of point load

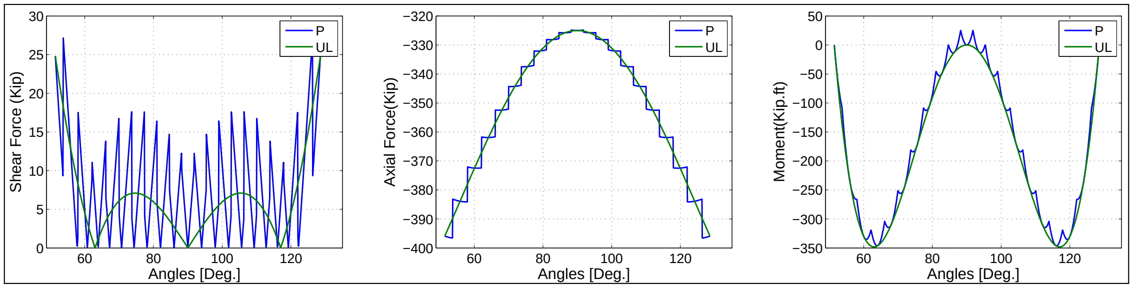

Figure 3.11: Three-hinged circular arch under uniformly distribute load vs.series of point load

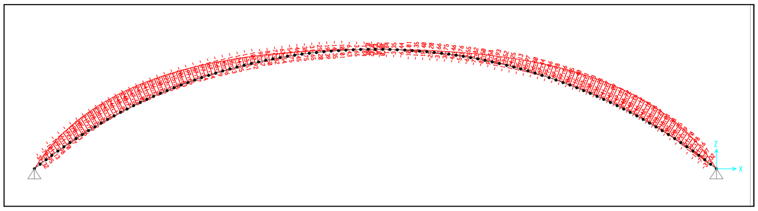

Figure 3.12: SAP 2000 - Moment diagram of Three-hinged circular arch under self-weight

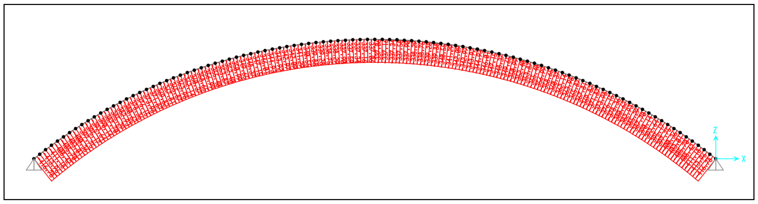

Figure 3.13: SAP 2000 - Axial force diagram of Three-hinged circular arch under self-weight

3.13 and shear force diagram in Figure 3.14 matches with their respective values on the graphs in

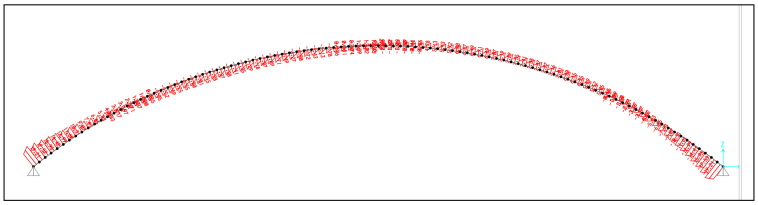

Figure 3.14: SAP 2000 - Shear force diagram of Three-hinged circular arch under self-weight

Figure 3.10.

3.2.6 Conclusion

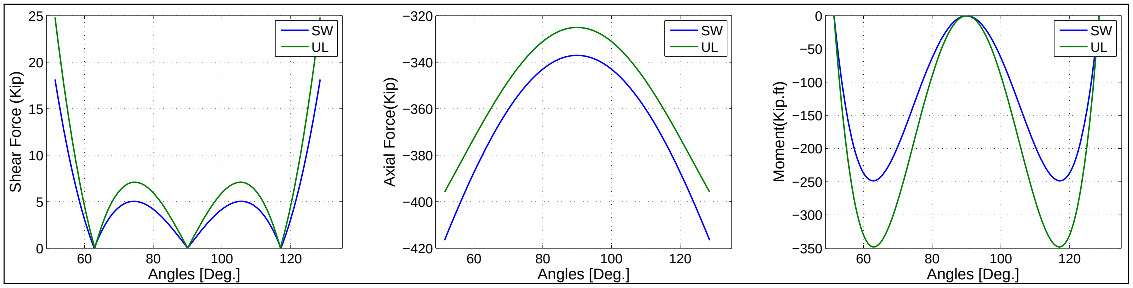

Figure 3.15: Three-hinged circular arch under self-weight vs. UDL

This section discusses the structural behavior of a Three-hinged arch under point load, Self-weight and Uniformly distributed load in terms of internal forces and deflection. Figure 3.15 compares the self- Weight loading condition with the uniformly distributed loading condition under an equal load w=2.275 kip/ft. Compared to the self-weight, a uniformly distributed load causes more internal shear force and moment, and it causes less internal compressive axial force. Figure 3.16 show plots of an asymmetric loading condition.For this purpose, a unit load is applied at the crown and at the quarter of the span. Under this condition, the maximum moment due to the point load applied at the quarter of the span is about 1.5 times more than that applied at the crown. The maximum axial force due to the point load applied at the quarter of the span is closer to that applied at the crown.

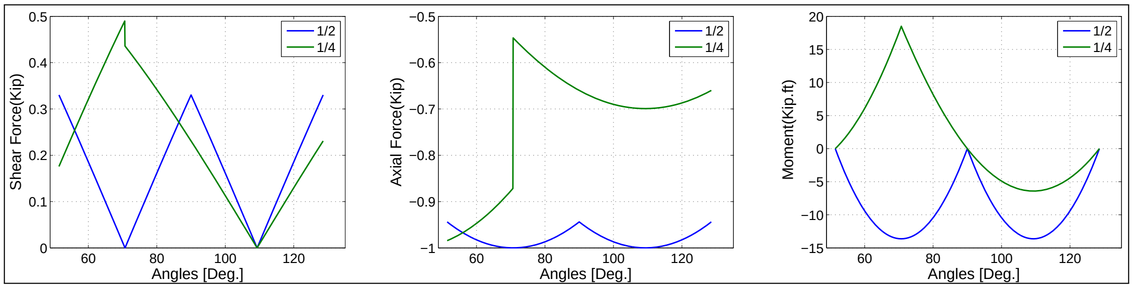

Figure 3.16: Three-hinged circular arch under point load at 1/2 and 1/4 span

3.3 Two - Hinged Circular Arch

A symmetrical Two-hinged circular arch has total four reactions - two at each support. Since the arch rib of a Two hinged arch is continuous between the supports and the point of the supports are immovable, applied load not only produce vertical but also horizontal reactions, commonly know as a thrust. With only three equation of equilibrium to solve the four unknown reactive forces, a Two- hinged arch is statically indeterminate to first degree.

3.3.1 Analysis Procedure

To begin with, a redundant reaction of the statically indeterminate Two-hinged arch, henceforth called as an original structure is removed, converting it into a statically determinate arch, henceforth called as a primary structure. Using the ordinary method of statics, the support reaction and internal forces in the primary structure due to the applied load are computed. Later, assuming that no external force exists on the primary structure, a unit virtual force is applied at the location of the removed redundant force and the internal forces caused from the unit load are computed. Compatibility equation for the deformation of an arch under applied load is considered to compute the redundant reaction in the original statically indeterminate Two-hinged arch. Once all the support reactions are found, the internal forces in the arch are computed using ordinary method of statics. Further, these internal forces are used to compute the deflection in the arch under the applied load. The analysis process described here is performed in seven steps using Mathematica.The Mathematica files for all steps are included in relevant sections and for simplification only final equations for reactions and internal forces are expanded.

For the purpose of analysis, three loading conditions are considered; a point load , self-weight of the arch and applied uniformly distributed load across the arch. The self- weight and the uniformly distributed load are symmetric about the center of the arch where as a point load, when applied anywhere but at the crown is asymmetric about the center of the arch. Hence to illustrate the analysis, same figures are used for the self-weight and the uniformly distributed loading conditions where as different set of figures is used for the point load condition.The analytical equations for support reactions and internal forces are in terms of the trigonometric variables defined above. For computing deflection, a specific design of a symmetric circular arch is considered (Kinney, 1957, pg 547-558). This reduced the complexity of the deflection equation as well as the time to process Mathematica files.

3.3.2 Point Load

In this case the elementary applied force is given by

$$dp = P \tag{3.6}$$

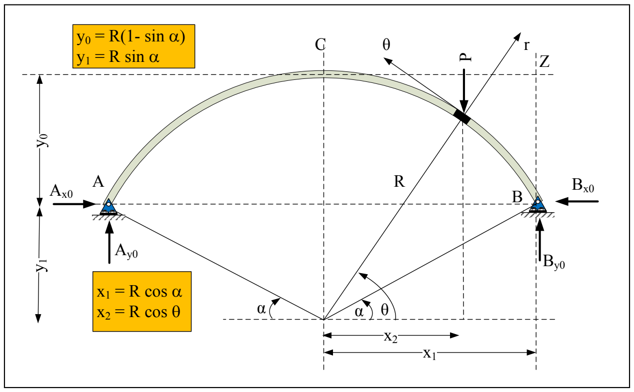

Figure 3.17: Two-Hinged circular arch under point load

3.3.2.1 Primary Structure: Reactions and Internal Forces

The redundant force Bxo at the abutment B in the original Two-hinged arch shown in Figure 3.17 is removed converting it into a primary structure. The location of a point load anywhere on the arch causes discontinuity in the internal forces. This discontinuity in the internal forces in shown in Figure 3.3.Hence the expression for the internal forces at any angle β across the arch span is dependent on its relation with respect to the angle θ at which the point load is applied. By taking in consideration following conditions, different sets of equations are developed for the internal forces.

$$\beta < \theta,\ \beta \geq \theta \tag{3.7}$$

The free body diagram in Figure 3.18, is used to determine the horizontal, vertical reactions at the supports as well as the internal forces - axial, shear and moment at any angle β across the arch span. Following is the output from Mathematica, illustrating the derivation for computing support reaction.

Primary Structure: Reactions

Define the load

```
P=P;
```

Determine vertical reaction at B by taking moment with respect to A (CCW +ve)

```
SigMA=BY2x1 − P(x1 + x2);
```

```
Sol1=Solve[SigMA==0,BY]; BY=BY/.Sol1[[1]]
```

$\frac{1}{2}P(\mathrm{Cos}[\alpha] + \mathrm{Cos}[\theta])\mathrm{Sec}[\alpha]$

Determine vertical reaction at A by taking summation of forces in the y direction

```
Sol2=Solve[BY − P + AY==0,AY]; AY=AY/.Sol2[[1]]
```

$\frac{1}{2}(P - P\mathrm{Cos}[\theta]\mathrm{Sec}[\alpha])$

Determine horizontal reaction at A by taking moment with respect to Z (CCW +ve)

```
BX=0;
```

```
SigMZ=AXy0 − AY2x1 + P(x1 − x2) − BXy0;
```

```
Sol3=Solve[SigMZ==0,AX]; AX=AX/.Sol3[[1]];
```

Check statics by taking moment about O CCW +ve

```
MO=FullSimplify[BXy1 + BYx1 − AXy1 − AYx1 − x2P]
```

```
0
```

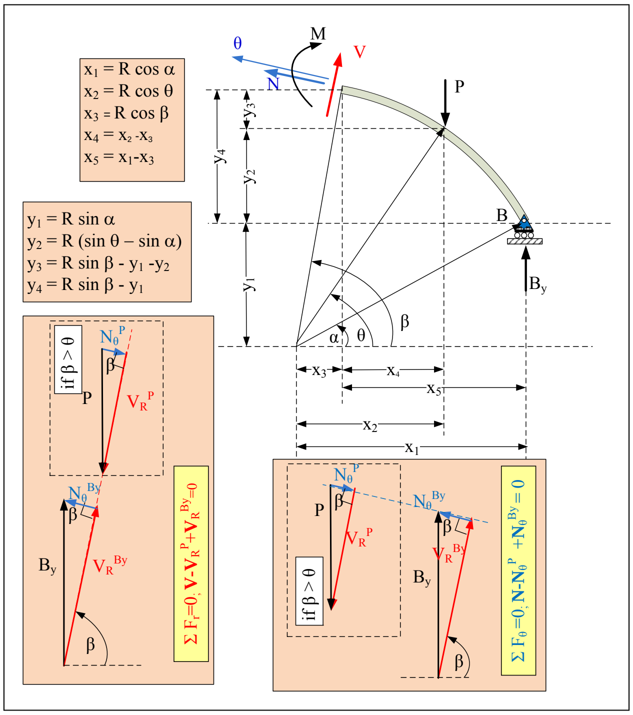

Figure 3.18: Two-Hinged circular arch after removing redundant thrust at abutment' B'

Following is the output from Mathematica illustrating the derivation for internal forces - axial, shear and moment at any angle β across the arch span.

Primary Structure: Internal Forces

For $\beta < \theta$

Summation of forces in the radial direction; Shear (+ve outward)

```
SigFV1=BYSin[β] + V1;
```

```
Sol4=FullSimplify[Solve[SigFV1==0,V1]]; V1[β_]=V1/.Sol4[[1]]
```

$$-\frac{1}{2}P(\text{Cos}[\alpha]+\text{Cos}[\theta])\text{Sec}[\alpha]\text{Sin}[\beta]$$

Summation of forces in the tangential direction; Normal force (+ve Tension)

```
SigFN1=BYCos[β] + NN1;
```

```
Sol5=FullSimplify[Solve[SigFN1==0,NN1]]; NN1[β_]=NN1/.Sol5[[1]]
```

$$-\frac{1}{2}P\mathrm{Cos}[\beta](\mathrm{Cos}[\alpha]+\mathrm{Cos}[\theta])\mathrm{Sec}[\alpha]$$

Summation of moments; Internal moment (CW +ve)

```
SigM1= − BYx5 + M1;
```

```
Sol6=Solve[SigM1==0,M1]; M1[β_]=M1/.Sol6[[1]]
```

$$\frac{1}{2}P(R\mathrm{Cos}[\alpha]-R\mathrm{Cos}[\beta])(\mathrm{Cos}[\alpha]+\mathrm{Cos}[\theta])\mathrm{Sec}[\alpha]$$

For $\beta > \theta$

Summation of Forces in the radial direction; Shear (+ve outward)

```
SigFV2=BYSin[β] − PSin[β] + V2;
```

```
Sol7=FullSimplify[Solve[SigFV2==0,V2]]; V2[β_]=V2/.Sol7[[1]]
```

$$-\frac{1}{2}P(-1+\mathrm{Cos}[\theta]\mathrm{Sec}[\alpha])\mathrm{Sin}[\beta]$$

Summation of forces in the tangential direction; Normal force (+ve Tension)

```
SigFN2=BYCos[β] − PCos[β] + NN2;
```

```
Sol8=FullSimplify[Solve[SigFN2==0,NN2]]; NN2[β_]=NN2/.Sol8[[1]]
```

$$-\frac{1}{2}P\mathrm{Cos}[\beta](-1+\mathrm{Cos}[\theta]\mathrm{Sec}[\alpha])$$

Summation of moments; Internal moment (CW +ve)

```
SigM2= − BYx5 + Px4 + M2;
```

```
Sol9=Solve[SigM2==0,M2]; M2[β_]=M2/.Sol9[[1]]
```

$$\frac{1}{2}(PR\mathrm{Cos}[\alpha]+PR\mathrm{Cos}[\beta]-PR\mathrm{Cos}[\theta]-PR\mathrm{Cos}[\beta]\mathrm{Cos}[\theta]\mathrm{Sec}[\alpha])$$

3.3.2.2 Primary Structure: Virtual Unit Force

A unit virtual force is applied at the location Bxo in the direction of displacement of abutment B under real load. The free body diagram in Figure 3.19, is used to determine the internal forces at any angle β across the arch span caused due to the virtual unit load . Following is the output from Mathematica illustrating the derivation for computing internal forces caused due to virtual force.

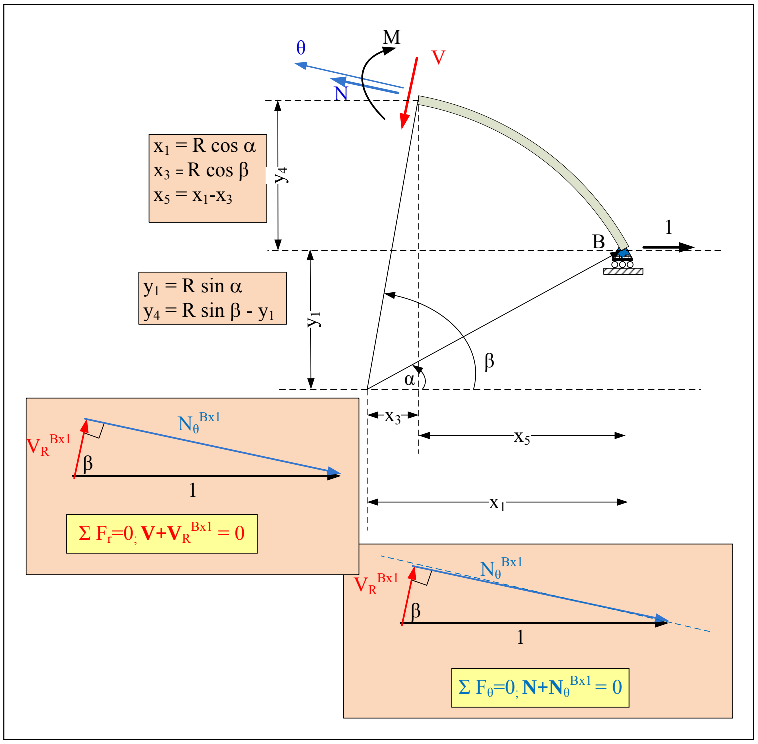

Figure 3.19: Two-Hinged circular arch with applied virtual force

Primary Structure: Virtual Force

Apply virtual horizontal force at B

```
BX1=1;
```

Summation of forces in the radial direction; Shear (+ve outward)

```
SigFδV=FullSimplify[BX1Cos[β] − δV];
```

```
Sol10=Solve[SigFδV==0,δV]; δV[β_]=δV/.Sol10[[1]]
```

```
Cos[β]
```

Summation of forces in the tangential direction; Normal force (+ve Tension)

```
SigFδN=FullSimplify[−BX1Sin[β] + δN];
```

```
Sol11=Solve[SigFδN==0,δN]; δN[β_]=δN/.Sol11[[1]]
```

```
Sin[β]
```

Summation of moments; Internal moment (CW +ve)

```
SigδM=FullSimplify[−BX1y4 + δM];
```

```
Sol12=Solve[SigδM==0,δM]; δM[β_]=δM/.Sol12[[1]]
```

```
-RSin[α] + RSin[β]
```

3.3.2.3 Original Structure: Redundant Force

Following Compatibility equation for the deformation of an arch under applied load together with the virtual work method are used to determine the redundant force Bxo at the abutment B. For this process both flexural and axial components of the compatibility equation as well as the discontinuity in the internal forces are considered.

$$1.\ \Delta_B = \left[\int_\alpha^\theta \frac{M1\ \delta\text{M}1}{e\ i}\,d\beta + \int_\theta^{(\pi-\alpha)} \frac{M2\ \delta\text{M}2}{e\ i}\,d\beta + \int_\alpha^\theta \frac{N1\ \delta\text{N}1}{a\ e}\,d\beta\ + \int_\alpha^{(\pi-\alpha)} \frac{N2\ \delta\text{N}2}{a\ e}\,d\beta\right] \tag{3.8}$$

Where

$M1(\beta < \theta),\ M2(\beta \geq \theta)$	Internal moment in the beam caused by real load
$\delta\text{M}1(\beta < \theta)$,$\delta\text{M}2(\beta \geq \theta)$	Internal moment caused due to external virtual unit load
$N1(\beta < \theta)$,$N2(\beta \geq \theta)$	Internal axial force in the beam caused by real load
$\delta N1(\beta < \theta),\ \delta N2(\beta \geq \theta)$	Internal axial force caused due to external virtual unit load

Following is the output from Mathematica illustrating the derivation for computing the redundant force.

Original Structure: Redundant Force

Deformation due to real load (Flexural + Axial)

Displacement at B

$$\text{DeltaBX1F=FullSimplify}\left[\int_{\alpha}^{\theta} \frac{\text{M1}[\beta]\delta\text{M}[\beta]}{ei} d\beta + \int_{\theta}^{\pi-\alpha} \frac{\text{M2}[\beta]\delta\text{M}[\beta]}{ei} d\beta\right];$$

$$\text{DeltaBX1A=FullSimplify}\left[\int_{\alpha}^{\theta} \frac{\text{NN1}[\beta]\delta\text{N}[\beta]}{ae} d\beta + \int_{\theta}^{\pi-\alpha} \frac{\text{NN2}[\beta]\delta\text{N}[\beta]}{ae} d\beta\right];$$

```
DeltaBX1=DeltaBX1F + DeltaBX1A;
```

Deformation due to virtual load (Flexural + Axial)

$\text{F11F=FullSimplify}\left[\int_{\alpha}^{\pi-\alpha}\frac{\delta\text{M}[\beta]\delta\text{M}[\beta]}{ei}d\beta\right];$

$\text{F11A=FullSimplify}\left[\int_{\alpha}^{\pi-\alpha}\frac{\delta\text{N}[\beta]\delta\text{N}[\beta]}{ae}d\beta\right];$

F11=F11F + F11A;

Redundant force in original structure

Solve[{BXOF11==DeltaBX1},{BXO}];

FullSimplify[BXO]

$$\frac{P\left(-\left(i-3aR^2\right)\text{Cos}[2\alpha]+\left(i-aR^2\right)\text{Cos}[2\theta]+aR^2(-2+2\text{Sin}[\alpha](-(\pi-2\alpha)\text{Cos}[\alpha]+(\pi-2\theta)\text{Cos}[\theta]+2\text{Sin}[\theta]))\right)}{2(\pi-2\alpha)\left(i+2aR^2-aR^2\text{Cos}[2\alpha]\right)+2\left(i-3aR^2\right)\text{Sin}[2\alpha]}$$

3.3.2.4 Original Structure: Reactions and Internal Forces

After the redundant force in the original structure Bxo is computed, remaining support reaction and the internal forces in the original structure are determined using the free body diagram in Figure 3.20. Following is the output from Mathematica illustrating the derivation for computing the support reactions

Original Structure: Reactions

Determine Vertical reaction at B by taking moment with respect to A (CCW +ve)

SigMAO=BYO**2**x1 − ***P***(x1 + x2);

Sol13=Solve[SigMAO==**0**,BYO]; BYO=BYO/.Sol13[[**1**]]

$\frac{1}{2}P(\text{Cos}[\alpha]+\text{Cos}[\theta])\text{Sec}[\alpha]$

Determine vertical reaction at A by taking summation of forces in the y direction

Sol14=Solve[BYO − ***P*** + AYO==**0**,AYO]; AYO=AYO/.Sol14[[**1**]]

$\frac{1}{2}(P-P\text{Cos}[\theta]\text{Sec}[\alpha])$

Determine horizontal reaction at A by taking summation of forces in the x direction

AXO=BXO;

Check statics by taking summation of moments with respect to O CCW +ve

Clear[MO];

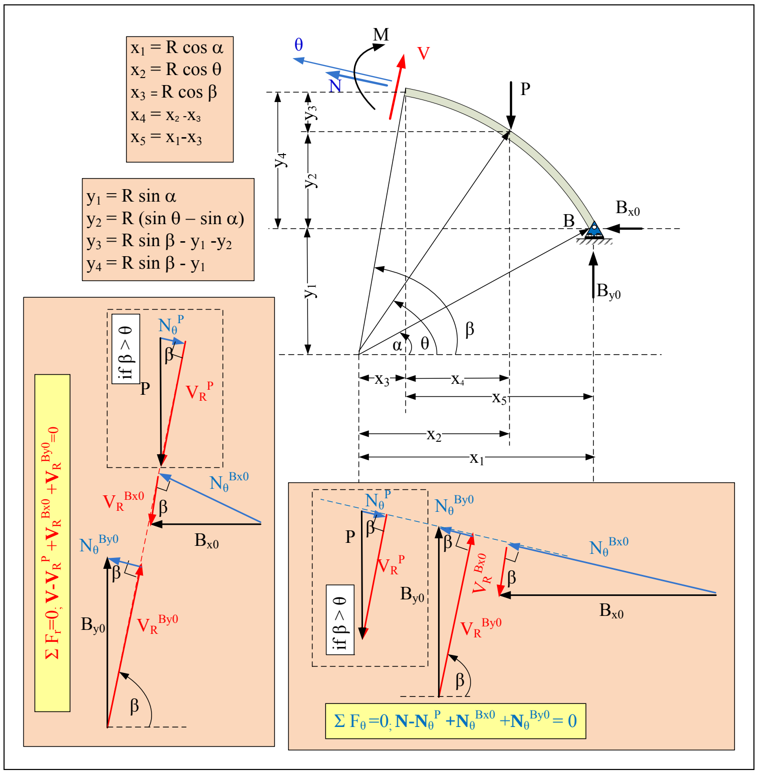

Figure 3.20: FBD of the original Two-hinged circular arch under point load

```
MO=FullSimplify[BYOx1 + BXOy1 − AYOx1 − AXOy1 − Px2]
```

```
0
```

Following is the output from Mathematica illustrating the derivation for computing the internal forces.

Original Structure: Internal Forces

For $\beta < \theta$

Summation of forces in the Radial direction ; Shear (+ve outward)

```
SigFVO1= − BXOCos[β] + BYOSin[β] + VO1;
```

```
Sol15=Solve[SigFVO1==0,VO1]; VO1[β_]:=VO1/.Sol15[[1]];
```

```
FullSimplify[VO1[β]]
```

$$\begin{aligned}&\frac{1}{2}P\left(-(\text{Cos}[\alpha]+\text{Cos}[\theta])\text{Sec}[\alpha]\text{Sin}[\beta]\right.\\&+\left(\text{Cos}[\beta]\left(-\left(i-3aR^2\right)\text{Cos}[2\alpha]+\left(i-aR^2\right)\text{Cos}[2\theta]+aR^2(-2+2\text{Sin}[\alpha](-(\pi-2\alpha)\text{Cos}[\alpha]+(\pi-2\theta)\text{Cos}[\theta]+\right.\right.\\&\left.\left.\left.2\text{Sin}[\theta]))\right)\right)/\left((\pi-2\alpha)\left(i+2aR^2-aR^2\text{Cos}[2\alpha]\right)+\left(i-3aR^2\right)\text{Sin}[2\alpha]\right)\right)\end{aligned}$$

Summation of forces in the tangential direction; Normal force (+ve Tension)

```
SigFNO1=BXOSin[β] + BYOCos[β] + NO1;
```

```
Sol16=Solve[SigFNO1==0,NO1]; NO1[β_]:=NO1/.Sol16[[1]];
```

```
FullSimplify[NO1[β]]
```

$$\begin{aligned}&\frac{1}{2}P\left(-\text{Cos}[\beta](\text{Cos}[\alpha]+\text{Cos}[\theta])\text{Sec}[\alpha]\right.\\&+\left(\text{Sin}[\beta]\left(\left(i-3aR^2\right)\text{Cos}[2\alpha]+\left(-i+aR^2\right)\text{Cos}[2\theta]+aR^2(2+(\pi-2\alpha)\text{Sin}[2\alpha]-2\text{Sin}[\alpha]((\pi-2\theta)\text{Cos}[\theta]+\right.\right.\\&\left.\left.\left.2\text{Sin}[\theta]))\right)\right)/\left((\pi-2\alpha)\left(i+2aR^2-aR^2\text{Cos}[2\alpha]\right)+\left(i-3aR^2\right)\text{Sin}[2\alpha]\right)\right)\end{aligned}$$

Summation of moments; Internal moment (CW +ve)

```
SigMO1=BXOy4 − BYOx5 + MO1;
```

```
sol17=Solve[SigMO1==0,MO1]; MO1[β_]:=MO1/.sol17[[1]];
```

```
FullSimplify[MO1[β]]
```

$$\begin{aligned}&\frac{1}{2}P\left(R(\text{Cos}[\alpha]-\text{Cos}[\beta])(\text{Cos}[\alpha]+\text{Cos}[\theta])\text{Sec}[\alpha]\right.\\&-\left(R(\text{Sin}[\alpha]-\text{Sin}[\beta])\left(\left(i-3aR^2\right)\text{Cos}[2\alpha]+\left(-i+aR^2\right)\text{Cos}[2\theta]+aR^2(2+(\pi-2\alpha)\text{Sin}[2\alpha]-2\text{Sin}[\alpha]((\pi-2\theta)\text{Cos}[\theta]+\right.\right.\\&\left.\left.\left.2\text{Sin}[\theta]))\right)\right)/\left((\pi-2\alpha)\left(i+2aR^2-aR^2\text{Cos}[2\alpha]\right)+\left(i-3aR^2\right)\text{Sin}[2\alpha]\right)\right)\end{aligned}$$

For $\beta > \theta$

Summation of forces in the Radial direction ; Shear (+ve outward)

```
SigFVO2= − BXOCos[β] + BYOSin[β] − PSin[β] + VO2;
```

```
Sol18=Solve[SigFVO2==0,VO2]; VO2[β_]:=VO2/.Sol18[[1]];
```

```
FullSimplify[VO2[β]]
```

$$\begin{aligned}&\frac{1}{2}P\left(2\text{Sin}[\beta]-(\text{Cos}[\alpha]+\text{Cos}[\theta])\text{Sec}[\alpha]\text{Sin}[\beta]\right.\\&+\left(\text{Cos}[\beta]\left(-\left(i-3aR^2\right)\text{Cos}[2\alpha]+\left(i-aR^2\right)\text{Cos}[2\theta]+aR^2(-2+2\text{Sin}[\alpha](-(\pi-2\alpha)\text{Cos}[\alpha]+(\pi-2\theta)\text{Cos}[\theta]+\right.\right.\\&\left.\left.\left.2\text{Sin}[\theta]))\right)\right)/\left((\pi-2\alpha)\left(i+2aR^2-aR^2\text{Cos}[2\alpha]\right)+\left(i-3aR^2\right)\text{Sin}[2\alpha]\right)\right)\end{aligned}$$

Summation of forces in the tangential direction; Normal force (+ve Tension)

```
SigFNO2=BXOSin[β] + BYOCos[β] − PCos[β] + NO2;
```

```
Sol19=Solve[SigFNO2==0,NO2]; NO2[β_]:=NO2/.Sol19[[1]];
```

```
FullSimplify[NO2[β]]
```

$$\frac{1}{2}P\left(2\mathrm{Cos}[\beta]-\mathrm{Cos}[\beta](\mathrm{Cos}[\alpha]+\mathrm{Cos}[\theta])\mathrm{Sec}[\alpha]+\left(\mathrm{Sin}[\beta]\left(\left(i-3aR^2\right)\mathrm{Cos}[2\alpha]+\left(-i+aR^2\right)\mathrm{Cos}[2\theta]+aR^2(2+(\pi-2\alpha)\mathrm{Sin}[2\alpha]-2\mathrm{Sin}[\alpha]((\pi-2\theta)\mathrm{Cos}[\theta]+2\mathrm{Sin}[\theta]))\right)\right)/\left((\pi-2\alpha)\left(i+2aR^2-aR^2\mathrm{Cos}[2\alpha]\right)+\left(i-3aR^2\right)\mathrm{Sin}[2\alpha]\right)\right)$$

Summation of moments; Internal moment (CW +ve)

```
SigMO2=BXOy4 − BYOx5 + Px4 + MO2;
```

```
sol20=Solve[SigMO2==0,MO2]; MO2[β_]:=MO2/.sol20[[1]];
```

```
FullSimplify[MO2[β]]
```

$$\frac{1}{2}PR\left(2(\mathrm{Cos}[\beta]-\mathrm{Cos}[\theta])+(\mathrm{Cos}[\alpha]-\mathrm{Cos}[\beta])(\mathrm{Cos}[\alpha]+\mathrm{Cos}[\theta])\mathrm{Sec}[\alpha]+\left((\mathrm{Sin}[\alpha]-\mathrm{Sin}[\beta])\left(-\left(i-3aR^2\right)\mathrm{Cos}[2\alpha]+\left(i-aR^2\right)\mathrm{Cos}[2\theta]+aR^2(-2+2\mathrm{Sin}[\alpha](-(\pi-2\alpha)\mathrm{Cos}[\alpha]+(\pi-2\theta)\mathrm{Cos}[\theta]+2\mathrm{Sin}[\theta]))\right)\right)/\left((\pi-2\alpha)\left(i+2aR^2-aR^2\mathrm{Cos}[2\alpha]\right)+\left(i-3aR^2\right)\mathrm{Sin}[2\alpha]\right)\right)$$

3.3.2.5 Deflection

Figure 3.21 and the analytical equations developed above are used to compute deflection in the symmetric Two-hinged circular arch example discussed in Section 3.2.2.2 (Kinney, 1957, pg 547-558). Following equation of virtual work is used to compute deflection.

$$\delta P.\,\Delta=\left[\int_{\alpha}^{\theta}\frac{M1\ \delta\mathrm{M1}}{e\ i}\,Rd\beta+\int_{\theta}^{(\pi-\alpha)}\frac{M2\ \delta\mathrm{M2}}{e\ i}\,Rd\beta\right] \tag{3.9}$$

Where

δP	External Virtual unit load applied in the direction of Δ
Δ	External displacement caused by the real applied load
$M1(\beta<\theta),\ M2(\beta\geq\theta)$	Internal moment in the beam caused by real point load
$\delta M1(\beta<\theta),\ \delta M2(\beta\geq\theta)$	Internal moment caused due to external virtual unit load

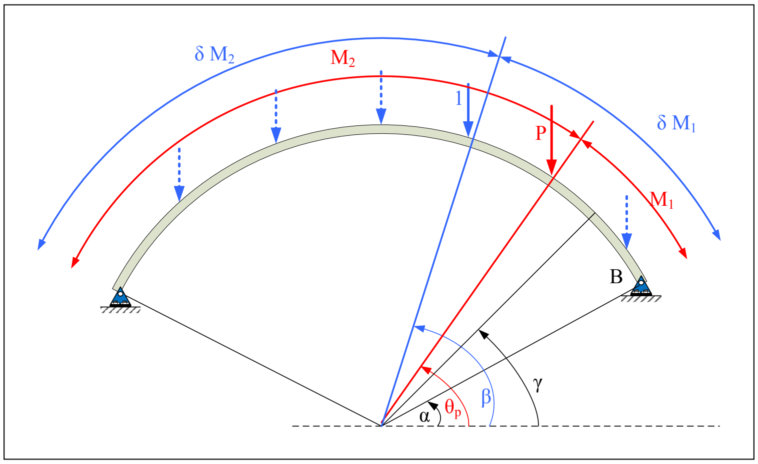

Figure 3.21: FBD to compute deflection in Two-hinged circular arch

3.3.2.6 Summary Of Results

Figure 3.22 show plots for a Two-hinged arch example discussed above. A point load is applied at the crown of the arch. The internal axial force and shear force are normalized with respect to the resultant of vertical reaction and thrust at the abutments. The internal moment is normalized with respect to the product of internal axial force and the rise. As indicated by the plot, all internal forces are symmetric about the crown of the arch. The axial compressive force is highest at about $\frac{1}{6}$ of the span from both abutments and it decrease to about 91% of the maximum value at the crown. The internal moment is zero at the hinges and it is highest at the crown. The shear force on other hand is comparatively lower than the internal axial force and moment. The deflection is zero at the hinges and it maximum at about $\frac{1}{6}$ of the span from both abutments.

3.3.3 Self weight

In this case the elementary applied force is given by

$$dP = wds = wRd\theta \tag{3.10}$$

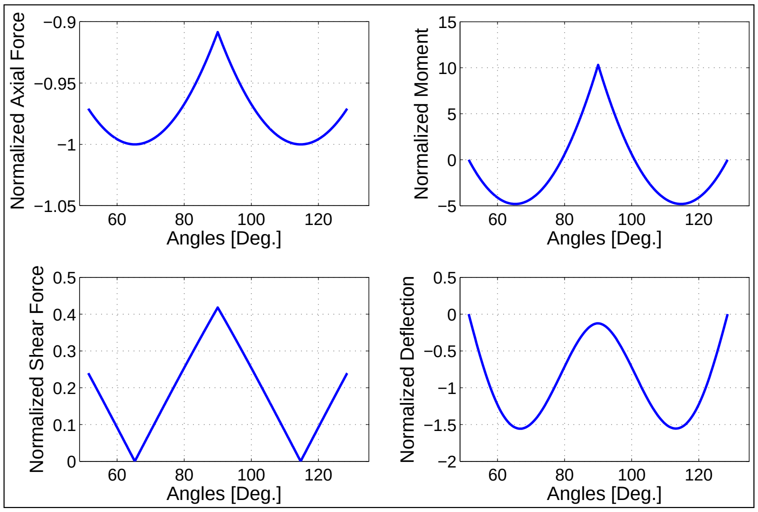

Figure 3.22: Plots for Two-hinged circular arch under point load

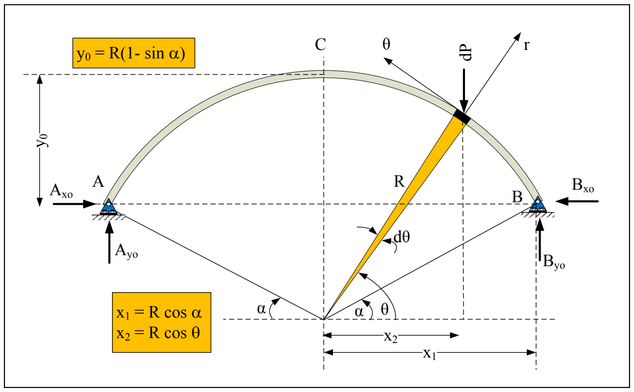

Figure 3.23: Two-Hinged circular arch under self weight

3.3.3.1 Primary Structure: Reactions and Internal Forces

The redundant force Bxo at the abutment B in the original Two-hinged arch shown in Figure 3.23 is removed converting it into a primary structure. The free body diagram in Figure 3.24, is used to determine the horizontal, vertical reactions at the supports as well as the internal forces - axial, shear and moment at any angle β across the arch span. Following is the output from Mathematica illustrating the derivation for computing support reaction.

Primary Strucure: Reactions

Define the load (omitting the $d\theta$)

$$\text{dP}'\boldsymbol{=}\boldsymbol{wR};$$

Determine reaction at B by taking moment with respect to A (CCW +ve)

$$\text{SigMA}=\text{BY}\mathbf{2}\text{x1}-\int_{\boldsymbol{\alpha}}^{\boldsymbol{\pi-\alpha}}(\text{x1}+\text{x2})\text{dP}'\boldsymbol{d\theta};$$

$$\text{Sol1}=\text{Solve}[\text{SigMA}==\mathbf{0},\text{BY}];\ \text{BY}=\text{BY}/.\text{Sol1}[[\mathbf{1}]]$$

$$\frac{1}{2}Rw(\pi-2\alpha)$$

Determine vertical reaction at A by taking summation of forces in the y direction

$$\text{Sol2}=\text{Solve}\left[\text{BY}-\int_{\boldsymbol{\alpha}}^{\boldsymbol{\pi-\alpha}}\text{dP}'\boldsymbol{d\theta}+\text{AY}==\mathbf{0},\text{AY}\right];\ \text{AY}=\text{AY}/.\text{Sol2}[[\mathbf{1}]]$$

$$\frac{1}{2}Rw(\pi-2\alpha)$$

Determine horizontal reaction at A by taking moment with respect to Z (CCW +ve)

$$\text{BX}=\mathbf{0};$$

$$\text{SigMZ}=\text{AXy0}-\text{AY}\mathbf{2}\text{x1}+\int_{\boldsymbol{\alpha}}^{\boldsymbol{\pi-\alpha}}\text{dP}'(\text{x1}-\text{x2})\boldsymbol{d\theta}-\text{BXy0};$$

$$\text{Sol3}=\text{Solve}[\text{SigMZ}==\mathbf{0},\text{AX}];\ \text{AX}=\text{AX}/.\text{Sol3}[[\mathbf{1}]];$$

Check statics by taking moment about O CCW +ve

$$\text{MO}=\text{FullSimplify}\left[\text{BXy1}+\text{BYx1}-\text{AXy1}-\text{AYx1}-\int_{\boldsymbol{\alpha}}^{\boldsymbol{\pi-\alpha}}\text{x2dP}'\boldsymbol{d\theta}\right]$$

$$0$$

Following is the output from Mathematica illustrating the derivation for internal forces - axial, shear and moment at any angle β across the arch span.

Primary Structure: Internal Forces

Summation of forces in the radial direction; Shear (+ve outward)

$$\text{SigFV}=\text{BYSin}[\boldsymbol{\beta}]-\int_{\boldsymbol{\alpha}}^{\boldsymbol{\beta}}\text{dP}'\text{Sin}[\boldsymbol{\beta}]\boldsymbol{d\theta}+\boldsymbol{V};$$

$$\text{Sol4}=\text{FullSimplify}[\text{Solve}[\text{SigFV}==\mathbf{0},\boldsymbol{V}]];\ \boldsymbol{V}[\boldsymbol{\beta\_}]=\boldsymbol{V}/.\text{Sol4}[[\mathbf{1}]]$$

$$-\frac{1}{2}Rw(\pi-2\beta)\text{Sin}[\beta]$$

Summation of forces in the tangential direction; Normal force (+ve Tension)

$$\text{SigFN}=\text{BYCos}[\boldsymbol{\beta}]-\int_{\boldsymbol{\alpha}}^{\boldsymbol{\beta}}\text{dP}'\text{Cos}[\boldsymbol{\beta}]\boldsymbol{d\theta}+\boldsymbol{N};$$

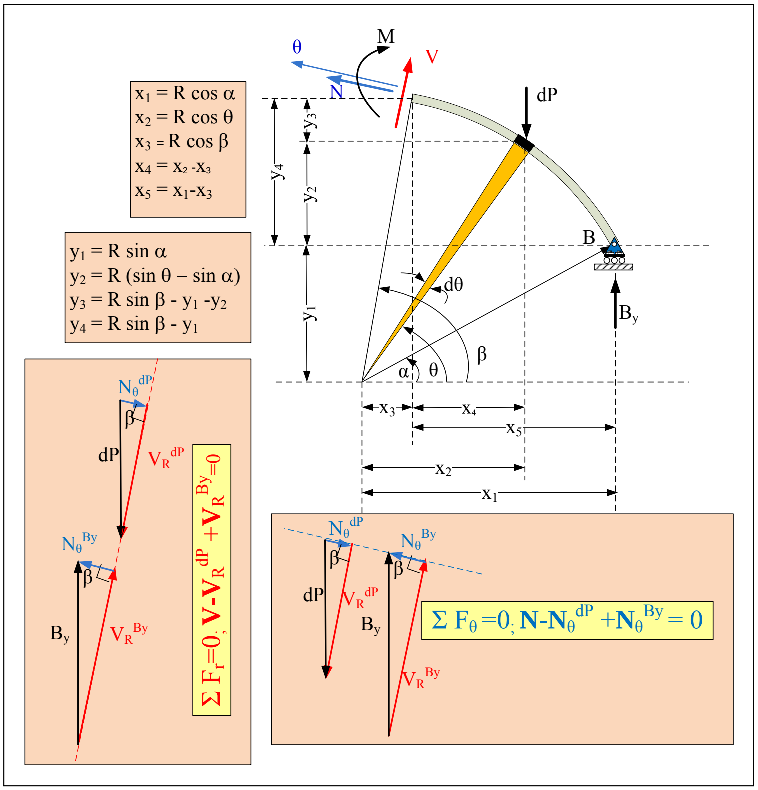

Figure 3.24: FBD of Two-Hinged circular arch after removing redundant thrust at abutment' B'

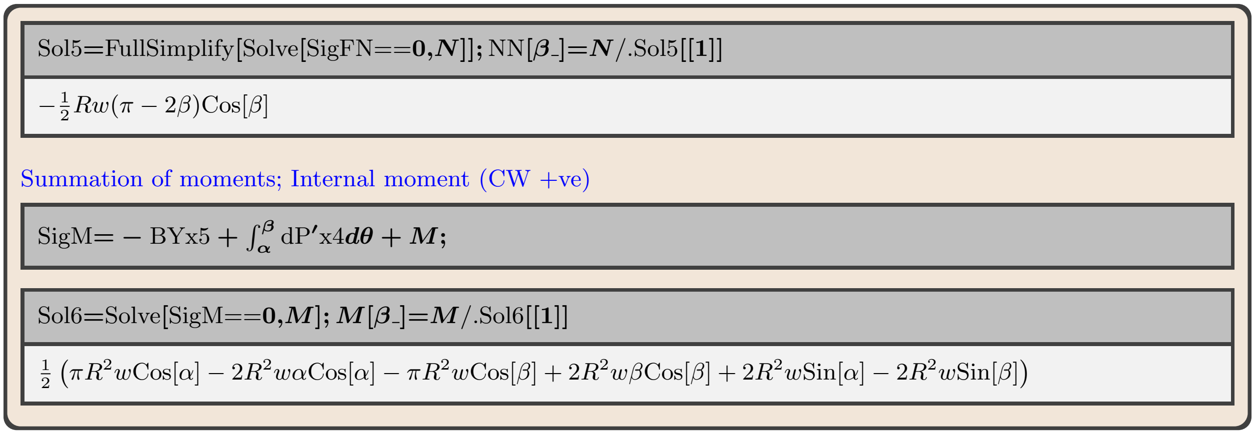

```
Sol5=FullSimplify[Solve[SigFN==0,N]]; NN[β_]=N/.Sol5[[1]]
```

$$-\frac{1}{2}Rw(\pi-2\beta)\mathrm{Cos}[\beta]$$

Summation of moments; Internal moment (CW +ve)

$$\mathrm{SigM}=-\mathrm{BYx5}+\int_{\alpha}^{\beta}\mathrm{dP}'\mathrm{x4}\,d\theta+M;$$

```
Sol6=Solve[SigM==0,M]; M[β_]=M/.Sol6[[1]]
```

$$\frac{1}{2}\left(\pi R^2w\mathrm{Cos}[\alpha]-2R^2w\alpha\mathrm{Cos}[\alpha]-\pi R^2w\mathrm{Cos}[\beta]+2R^2w\beta\mathrm{Cos}[\beta]+2R^2w\mathrm{Sin}[\alpha]-2R^2w\mathrm{Sin}[\beta]\right)$$

3.3.3.2 Primary Structure: Virtual Unit Force

Figure 3.19 and a similar process used for Two-hinged circular arch under point load is followed to determine the internal forces at any angle β across the arch span caused due to virtual unit load . Following is the output from Mathematica, illustrating the derivation for computing internal forces caused due to virtual forces.

Primary Structure: Virtual Force

Apply virtual horizontal force at B

```
BX1=1;
```

Summation of forces in the radial direction; Shear (+ve outward)

```
SigFδV=FullSimplify[BX1Cos[β] − δV];
```

```
Sol10=Solve[SigFδV==0,δV]; δV[β_]=δV/.Sol10[[1]]
```

```
Cos[β]
```

Summation of forces in the tangential direction; Normal force (+ve Tension)

```
SigFδN=FullSimplify[−BX1Sin[β] + δN];
```

```
Sol11=Solve[SigFδN==0,δN]; δN[β_]=δN/.Sol11[[1]]
```

```
Sin[β]
```

Summation of moments; Internal moment (CW +ve)

```
SigδM=FullSimplify[−BX1y4 + δM];
```

```
Sol12=Solve[SigδM==0,δM]; δM[β_]=δM/.Sol12[[1]]
```

```
−RSin[α] + RSin[β]
```

3.3.3.3 Original Structure: Redundant Force

Using the following Compatibility equation for the deformation of an arch under applied load together with the virtual work method is used to determine the redundant force Bxo at the abutment B. For this process both flexural and axial components of the compatibility equation are considered.

$$1.\ \Delta_B = \left[\int_{\alpha}^{(\pi-\alpha)} \frac{M\ \delta\mathrm{M}}{e\ i}\,d\beta + \int_{\alpha}^{(\pi-\alpha)} \frac{N\ \delta\mathrm{N}}{a\ e}\,d\beta\right] \tag{3.11}$$

Where

M Internal moment in the beam caused by real load

δM Internal moment caused due to external virtual unit load

N Internal axial force in the beam caused by real load

δN Internal axial force caused due to external virtual unit load

Following is the output from Mathematica illustrating the derivation for computing the redundant force.

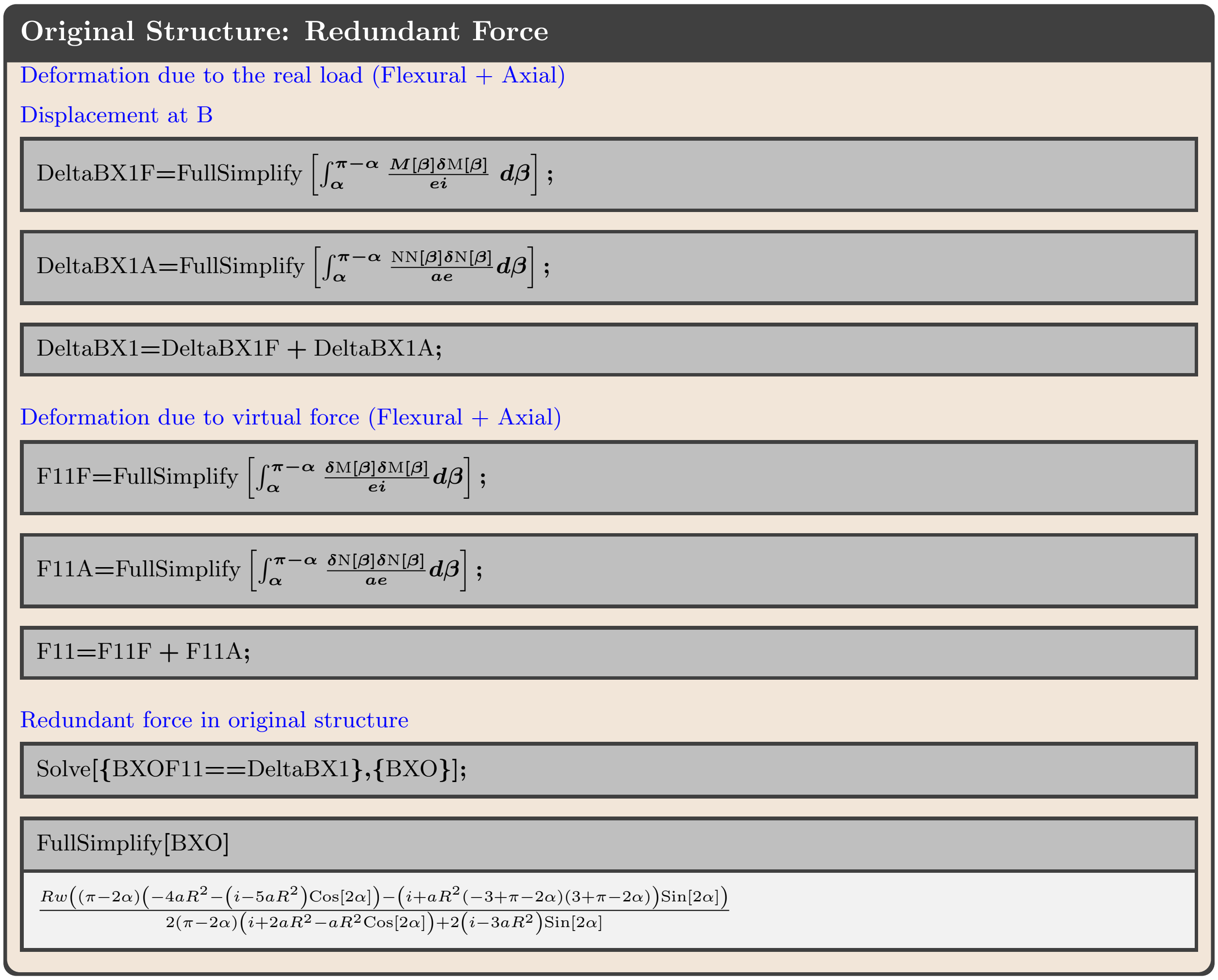

Original Structure: Redundant Force

Deformation due to the real load (Flexural + Axial)

Displacement at B

DeltaBX1F=FullSimplify $\left[\int_{\alpha}^{\pi-\alpha} \frac{M[\beta]\delta\text{M}[\beta]}{ei}\, d\beta\right]$;

DeltaBX1A=FullSimplify $\left[\int_{\alpha}^{\pi-\alpha} \frac{\text{NN}[\beta]\delta\text{N}[\beta]}{ae} d\beta\right]$;

DeltaBX1=DeltaBX1F + DeltaBX1A;

Deformation due to virtual force (Flexural + Axial)

F11F=FullSimplify $\left[\int_{\alpha}^{\pi-\alpha} \frac{\delta\text{M}[\beta]\delta\text{M}[\beta]}{ei} d\beta\right]$;

F11A=FullSimplify $\left[\int_{\alpha}^{\pi-\alpha} \frac{\delta\text{N}[\beta]\delta\text{N}[\beta]}{ae} d\beta\right]$;

F11=F11F + F11A;

Redundant force in original structure

Solve[{BXOF11==DeltaBX1},{BXO}];

FullSimplify[BXO]

$$\frac{Rw\left((\pi-2\alpha)\left(-4aR^2-\left(i-5aR^2\right)\text{Cos}[2\alpha]\right)-\left(i+aR^2(-3+\pi-2\alpha)(3+\pi-2\alpha)\right)\text{Sin}[2\alpha]\right)}{2(\pi-2\alpha)\left(i+2aR^2-aR^2\text{Cos}[2\alpha]\right)+2\left(i-3aR^2\right)\text{Sin}[2\alpha]}$$

3.3.3.4 Original Structure: Reactions and Internal Forces

After the redundant force in the original structure Bxo is computed, remaining support reaction and the internal forces in the original structure are determined using the free body diagram in Figure 3.25. Following is the output from Mathematica illustrating the derivation for computing the support reactions.

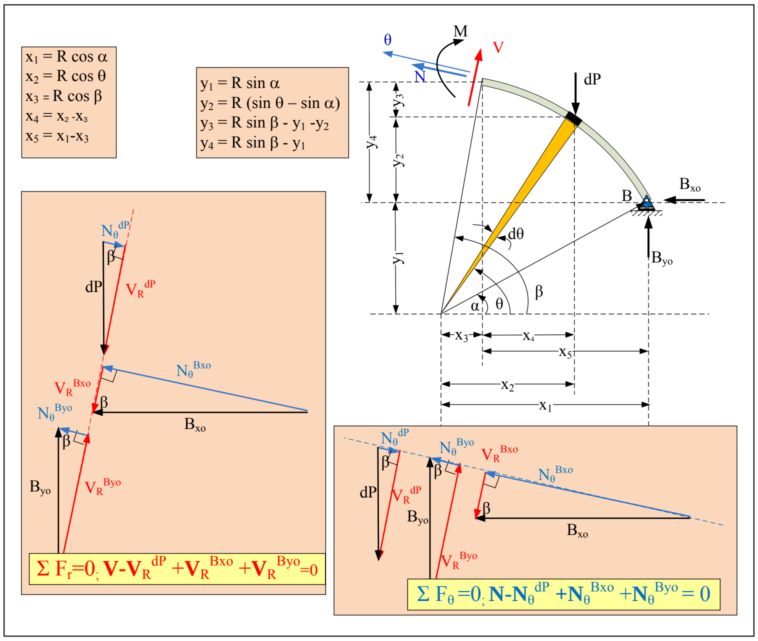

Figure 3.25: FBD of the original Two-hinged circular arch under self-weight

Original Structure: Reactions

Determine vertical reaction at B by taking moment with respect to A (CCW +ve)

SigMAO=BYO**2**x1 $-\int_{\alpha}^{\pi-\alpha}$(x1 + x2)dP′$\boldsymbol{d\theta}$**;**

Sol10=Solve[SigMAO==**0**,BYO]**;** BYO=BYO/.Sol10[[**1**]]

$\frac{1}{2}Rw(\pi-2\alpha)$

Determine vertical reaction at A by taking summation of forces in the y direction

Sol11=Solve $\left[\text{BYO} - \int_{\alpha}^{\pi-\alpha} \text{dP}'\boldsymbol{d\theta} + \text{AYO}==\mathbf{0},\text{AYO}\right]$ **;** AYO=AYO/.Sol11[[**1**]]

$\frac{1}{2}Rw(\pi-2\alpha)$

Determine horizontal reaction at A by taking summation of forces in the x direction

AXO=BXO**;**

Check statics by taking summation of moments with respect to O CCW +ve

Clear[MO]**;**

MO=FullSimplify $\left[\text{BYOx1} + \text{BXOy1} - \text{AYOx1} - \text{AXOy1} - \int_{\alpha}^{\pi-\alpha} \text{dP}'\text{x2}\boldsymbol{d\theta}\right]$

0

Following is the output from Mathematica, illustrating the derivation for computing the internal forces.

Original Structure: Internal Forces

Summation of forces in the Radial direction ; Shear (+ve outward)

$$\text{SigFVO} = -\text{BXOCos}[\boldsymbol{\beta}] + \text{BYOSin}[\boldsymbol{\beta}] - \int_{\boldsymbol{\alpha}}^{\boldsymbol{\beta}} \text{dP}'\text{Sin}[\boldsymbol{\beta}]\,\boldsymbol{d\theta} + \text{VO};$$

$$\text{Sol12=Solve[SigFVO==}\mathbf{0}\text{,VO]; VO}[\boldsymbol{\beta}\_]\text{:=VO/.Sol12[[}\mathbf{1}\text{]];}$$

$$\text{FullSimplify[VO}[\boldsymbol{\beta}]]$$

$$\begin{aligned}&-\Big(Rw\left(\text{Cos}[\beta]\left(4aR^2(\pi-2\alpha)+\left(i-5aR^2\right)(\pi-2\alpha)\text{Cos}[2\alpha]+\left(i+aR^2(-3+\pi-2\alpha)(3+\pi-2\alpha)\right)\text{Sin}[2\alpha]\right)\right.\\&\quad\left.+(\pi-2\beta)\left((\pi-2\alpha)\left(i+2aR^2-aR^2\text{Cos}[2\alpha]\right)+\left(i-3aR^2\right)\text{Sin}[2\alpha]\right)\text{Sin}[\beta]\right)\Big)/\\&\quad\left(2\left((\pi-2\alpha)\left(i+2aR^2-aR^2\text{Cos}[2\alpha]\right)+\left(i-3aR^2\right)\text{Sin}[2\alpha]\right)\right)\end{aligned}$$

Summation of forces in the tangential direction; Normal force +(ve Tension)

$$\text{SigFNO=BXOSin}[\boldsymbol{\beta}] + \text{BYOCos}[\boldsymbol{\beta}] - \int_{\boldsymbol{\alpha}}^{\boldsymbol{\beta}} \text{dP}'\text{Cos}[\boldsymbol{\beta}]\,\boldsymbol{d\theta} + \text{NO};$$

$$\text{Sol13=Solve[SigFNO==}\mathbf{0}\text{,NO]; NNO}[\boldsymbol{\beta}\_]\text{:=NO/.Sol13[[}\mathbf{1}\text{]];}$$

$$\text{FullSimplify[NNO}[\boldsymbol{\beta}]]$$

$$\begin{aligned}&\Big(Rw\left((\pi-2\beta)\text{Cos}[\beta]\left(-(\pi-2\alpha)\left(i+2aR^2-aR^2\text{Cos}[2\alpha]\right)-\left(i-3aR^2\right)\text{Sin}[2\alpha]\right)\right.\\&\quad\left.+\left(4aR^2(\pi-2\alpha)+\left(i-5aR^2\right)(\pi-2\alpha)\text{Cos}[2\alpha]+\left(i+aR^2(-3+\pi-2\alpha)(3+\pi-2\alpha)\right)\text{Sin}[2\alpha]\right)\text{Sin}[\beta]\right)\Big)/\\&\quad\left(2\left((\pi-2\alpha)\left(i+2aR^2-aR^2\text{Cos}[2\alpha]\right)+\left(i-3aR^2\right)\text{Sin}[2\alpha]\right)\right)\end{aligned}$$

Summation of moments; Internal moment (CW +ve)

$$\text{Clear[MO];}$$

$$\text{SigMO=BXOy4} - \text{BYOx5} + \int_{\boldsymbol{\alpha}}^{\boldsymbol{\beta}} \text{dP}'\text{x4}\,\boldsymbol{d\theta} + \text{MO};$$

$$\text{sol14=Solve[SigMO==}\mathbf{0}\text{,MO]; MO}[\boldsymbol{\beta}\_]\text{:=MO/.sol14[[}\mathbf{1}\text{]];}$$

$$\text{FullSimplify[MO}[\boldsymbol{\beta}]]$$

$$\begin{aligned}&\frac{1}{2}R^2w\Big((\pi-2\alpha)(\text{Cos}[\alpha]-\text{Cos}[\beta])\\&-\left(\left(4aR^2(\pi-2\alpha)+\left(i-5aR^2\right)(\pi-2\alpha)\text{Cos}[2\alpha]+\left(i+aR^2(-3+\pi-2\alpha)(3+\pi-2\alpha)\right)\text{Sin}[2\alpha]\right)(\text{Sin}[\alpha]-\text{Sin}[\beta])\right)/\\&\left((\pi-2\alpha)\left(i+2aR^2-aR^2\text{Cos}[2\alpha]\right)+\left(i-3aR^2\right)\text{Sin}[2\alpha]\right)-2((\alpha-\beta)\text{Cos}[\beta]-\text{Sin}[\alpha]+\text{Sin}[\beta])\Big)\end{aligned}$$

3.3.3.5 Deflection

The analytical equations developed above are used to compute deflection in the symmetric circular arch example discussed in Section 3.2.3.3 (Kinney, 1957, pg 547-558).Following equation of virtual work is used to compute deflection.

$$\delta P.\,\Delta = \left[\int_{\alpha}^{\theta} \frac{M\ \delta\mathrm{M1}}{e\ i}\ Rd\beta + \int_{\theta}^{(\pi-\alpha)} \frac{M\ \delta\mathrm{M2}}{e\ i}\ Rd\beta\right] \tag{3.12}$$

Where

δP	External Virtual unit load applied in the direction of Δ
Δ	External displacement caused by the real applied load
M	Internal moment in the beam caused by real load
$\delta M1(\beta < \theta),\ \delta M2(\beta \geq \theta)$	Internal moment caused due to external virtual unit load

3.3.3.6 Summary Of Results

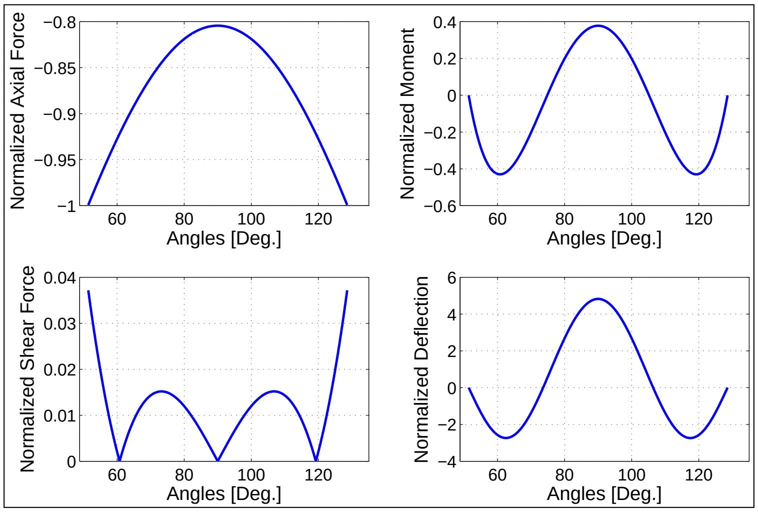

Figure 3.26: Plots for Two-hinged circular arch under self-weight

Figure 3.26 show plots for the Two-hinged arch under self-weight discussed in section above. The internal axial force and shear force are normalized with respect to the resultant of vertical reaction and thrust at the abutments. The axial compressive force is highest at the abutments and it decreases toward the crown to about 80.5% of the maximum value. The shear force on other hand is comparatively low and it varies between about 3.75% and 1.5%, respectively from the abutment to the crown. The internal moment is normalized with respect to the product of internal axial force and the rise. The internal moment is zero at the location of the hinges and it is highest at about $\frac{1}{6}$ of span from the abutments. There are two inflection points in the moment diagram and they correspond with the zero deflection points in the arch. The Deflection is highest at the crown and the graph of deflection follows similar profile as that of the moment diagram. Maximum positive and negative deflection corresponds with the point of maximum positive and negative moment in the arch respectively.

3.3.4 Uniformly Distributed Load

In this case the elementary applied force is given by

$$dp = wdx = wRSin\theta \tag{3.13}$$

The redundant force Bxo at the abutment B in the original Two-hinged arch shown in Figure 3.23 is removed converting it into a primary structure. First three steps including support reaction and internal forces caused due to the real load and internal forces caused due to the virtual load are similar to that for the Two-hinged circular arch under self-weight. For simplicity only the steps involving computation of the redundant force, support reactions and the internal forces in the original structure are shown here.

3.3.4.1 Original Structure: Redundant Force

The process used for the Two-hinged arch under self weight repeated here.The Compatibility equation for the deformation of an arch under applied load together with the virtual work method are used to determine the redundant force Bxo at the abutment B. For this process both flexural and axial components of the compatibility equation are considered.Following is the output from

Mathematica illustrating the derivation for computing the redundant force.

Original Structure: Redundant Force

Deformation due to the real load (Flexural + Axial)

Displacement at B

DeltaBX1F=FullSimplify $\left[\int_{\alpha}^{\pi-\alpha} \frac{M[\beta]\delta\mathrm{M}[\beta]}{ei}\, d\beta\right]$;

DeltaBX1A=FullSimplify $\left[\int_{\alpha}^{\pi-\alpha} \frac{\mathrm{NN}[\beta]\delta\mathrm{N}[\beta]}{ae} d\beta\right]$;

DeltaBX1=DeltaBX1F + DeltaBX1A;

Deformation due to virtual force (Flexural + Axial)

F11F=FullSimplify $\left[\int_{\alpha}^{\pi-\alpha} \frac{\delta\mathrm{M}[\beta]\delta\mathrm{M}[\beta]}{ei} d\beta\right]$;

F11A=FullSimplify $\left[\int_{\alpha}^{\pi-\alpha} \frac{\delta\mathrm{N}[\beta]\delta\mathrm{N}[\beta]}{ae} d\beta\right]$;

F11=F11F + F11A;

Redundant force in original structure

Solve[{BXOF11==DeltaBX1},{BXO}];

FullSimplify[BXO]

$$\frac{w\left(9aR^3\mathrm{Cos}[\alpha]-16iR\mathrm{Cos}[\alpha]^3+aR^3(7\mathrm{Cos}[3\alpha]+3(\pi-2\alpha)(\mathrm{Sin}[\alpha]-\mathrm{Sin}[3\alpha]))\right)}{12\left((\pi-2\alpha)\left(i+2aR^2-aR^2\mathrm{Cos}[2\alpha]\right)+\left(i-3aR^2\right)\mathrm{Sin}[2\alpha]\right)}$$

3.3.4.2 Original Structure: Reactions and Internal Forces

After the redundant force in the original structure Bxo is computed, remaining support reaction and the internal forces in the original structure are determined using the free body diagram in Figure 3.25. Following is the output from Mathematica illustrating the derivation for computing the support reactions.

Original Structure: Reactions

Determine vertical reaction at B by taking moment with respect to A (CCW +ve)

SigMAO=BYO**2**x1 − $\int_{\alpha}^{\pi-\alpha}$(x1 + x2)dP′$d\theta$;

Sol10=Solve[SigMAO==**0**,BYO]**;** BYO=BYO/.Sol10[[**1**]]

$Rw\mathrm{Cos}[\alpha]$

Determine vertical reaction at A by taking summation of forces in the y direction

$\mathrm{Sol11{=}Solve}\left[\mathrm{BYO} - \int_{\boldsymbol{\alpha}}^{\boldsymbol{\pi-\alpha}} \mathrm{dP}'\boldsymbol{d\theta} + \mathrm{AYO{=}{=}}\mathbf{0}\mathrm{,AYO}\right]\mathbf{;}\ \mathrm{AYO{=}AYO/.Sol11}[[\mathbf{1}]]$

$Rw\mathrm{Cos}[\alpha]$

Determine horizontal reaction at A by taking summation of forces in the x direction

AXO=BXO**;**

Check statics by taking summation of moments with respect to O CCW +ve

Clear[MO]**;**

$\mathrm{MO{=}FullSimplify}\left[\mathrm{BYOx1} + \mathrm{BXOy1} - \mathrm{AYOx1} - \mathrm{AXOy1} - \int_{\boldsymbol{\alpha}}^{\boldsymbol{\pi-\alpha}} \mathrm{dP}'\mathrm{x2}\boldsymbol{d\theta}\right]$

0

Following is the output from Mathematica illustrating the derivation for computing the internal forces.

Original Structure: Internal Forces

Summation of forces in the Radial direction ; Shear (+ve outward)

$\mathrm{SigFVO{=}} - \mathrm{BXOCos}[\boldsymbol{\beta}] + \mathrm{BYOSin}[\boldsymbol{\beta}] - \int_{\boldsymbol{\alpha}}^{\boldsymbol{\beta}} \mathrm{dP}'\mathrm{Sin}[\boldsymbol{\beta}]\boldsymbol{d\theta} + \mathrm{VO};$

Sol12=Solve[SigFVO==**0**,VO]**;** VO[***β***_]:=VO/.Sol12[[**1**]]**;**

FullSimplify[VO[***β***]]

$$\begin{aligned}&\left(Rw\left(3\left(-4i+3aR^2\right)\mathrm{Cos}[\alpha]\mathrm{Cos}[\beta]+\left(-4i+7aR^2\right)\mathrm{Cos}[3\alpha]\mathrm{Cos}[\beta]+3aR^2(\pi-2\alpha)\mathrm{Cos}[\beta](\mathrm{Sin}[\alpha]-\mathrm{Sin}[3\alpha])\right.\right.\\&\quad\left.\left.-\,6\left((\pi-2\alpha)\left(i+2aR^2-aR^2\mathrm{Cos}[2\alpha]\right)+\left(i-3aR^2\right)\mathrm{Sin}[2\alpha]\right)\mathrm{Sin}[2\beta]\right)\right)/\\&\quad\left(12\left((\pi-2\alpha)\left(i+2aR^2-aR^2\mathrm{Cos}[2\alpha]\right)+\left(i-3aR^2\right)\mathrm{Sin}[2\alpha]\right)\right)\end{aligned}$$

Summation of forces in the tangential direction; Normal force +(ve Tension)

$\mathrm{SigFNO{=}BXOSin}[\boldsymbol{\beta}] + \mathrm{BYOCos}[\boldsymbol{\beta}] - \int_{\boldsymbol{\alpha}}^{\boldsymbol{\beta}} \mathrm{dP}'\mathrm{Cos}[\boldsymbol{\beta}]\boldsymbol{d\theta} + \mathrm{NO};$

Sol13=Solve[SigFNO==**0**,NO]**;** NNO[***β***_]:=NO/.Sol13[[**1**]]**;**

FullSimplify[NNO[$\boldsymbol{\beta}$]]

$$\left(Rw\left(12\text{Cos}[\beta]^2\left(-(\pi-2\alpha)\left(i+2aR^2-aR^2\text{Cos}[2\alpha]\right)-\left(i-3aR^2\right)\text{Sin}[2\alpha]\right)\right.\right.$$
$$\left.\left.+\left(3\left(4i-3aR^2\right)\text{Cos}[\alpha]+\left(4i-7aR^2\right)\text{Cos}[3\alpha]+3aR^2(\pi-2\alpha)(-\text{Sin}[\alpha]+\text{Sin}[3\alpha])\right)\text{Sin}[\beta]\right)\right)/$$
$$\left(12\left((\pi-2\alpha)\left(i+2aR^2-aR^2\text{Cos}[2\alpha]\right)+\left(i-3aR^2\right)\text{Sin}[2\alpha]\right)\right)$$

Summation of moments; Internal moment (CW +ve)

Clear[MO];

SigMO=BXOy4 − BYOx5 + $\int_{\alpha}^{\beta}$ dP′x4$\boldsymbol{d\theta}$ + MO;

sol14=Solve[SigMO==**0**,MO]; MO[$\boldsymbol{\beta}$_]:=MO/.sol14[[**1**]];

FullSimplify[MO[$\boldsymbol{\beta}$]]

$$\frac{1}{12}R^2w\left(12\text{Cos}[\alpha](\text{Cos}[\alpha]-\text{Cos}[\beta])-6(\text{Cos}[\alpha]-\text{Cos}[\beta])^2\right.$$
$$\left.+\left(\left(9aR^2\text{Cos}[\alpha]-16i\text{Cos}[\alpha]^3+aR^2(7\text{Cos}[3\alpha]+3(\pi-2\alpha)(\text{Sin}[\alpha]-\text{Sin}[3\alpha]))\right)(\text{Sin}[\alpha]-\text{Sin}[\beta])\right)/\right.$$
$$\left.\left((\pi-2\alpha)\left(i+2aR^2-aR^2\text{Cos}[2\alpha]\right)+\left(i-3aR^2\right)\text{Sin}[2\alpha]\right)\right)$$

3.3.4.3 Deflection

The process to compute the deflection in Two-hinged circular arch under uniformly distributed load as well as the numerical values used for the trigonometric variable are similar to that under Self-weight and therefore it is not show here.

3.3.4.4 Summary Of Results

Figure 3.27 show plots for the Two-hinged arch under uniformly distribute load discussed in the above section. The internal axial force and shear force are normalized with respect to the resultant of vertical reaction and thrust at the abutments. The axial compressive force is highest at the abutments and it decreases toward the crown to about 81.5% of the maximum value. The shear force on other hand is comparatively low and it varies between about 5.25% and 2%, respectively from the abutment to the crown. The internal moment is normalized with respect to the product of internal axial force and the rise. The internal moment is zero at the location of the hinges and it is highest at about $\frac{1}{6}$ of span from the abutments. There are two inflection points in the moment

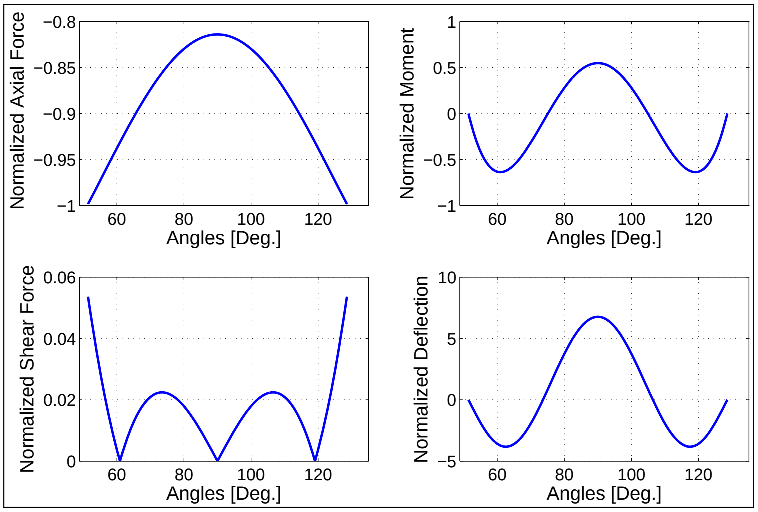

Figure 3.27: Plots for Two-hinged circular arch under UDL

diagram and they correspond with the zero deflection points in the arch. The Deflection is highest at the crown and the graph of deflection follows similar profile as that of the moment diagram. Maximum positive and negative deflection corresponds with the point of maximum positive and negative moment in the arch respectively.

3.3.5 Two-Hinged Circular Arch: Validation

The analytical equations developed above for the Two-hinged circular arch under point load, self-weight and uniformly distributed load are validated in two steps. Firstly, the self weight and uniformly distributed load applied across the arch span are divided in series of 20 point loads. The graphs of internal forces and deflections are plotted using the analytical equations for self weight and uniformly distributed load together with their respective point loads. These graphs are superimposed to check the validity of the analytical solutions. As the self-weight or the uniformly distributed load are equivalent to their respective series of point loads their plots closely match with each other.

Figure 3.28 and Figure 3.29 illustrates the above discussed process used for validating the analytical equations. Secondly, a Sap 2000 model is developed for the Three-hinged circular arch under self-

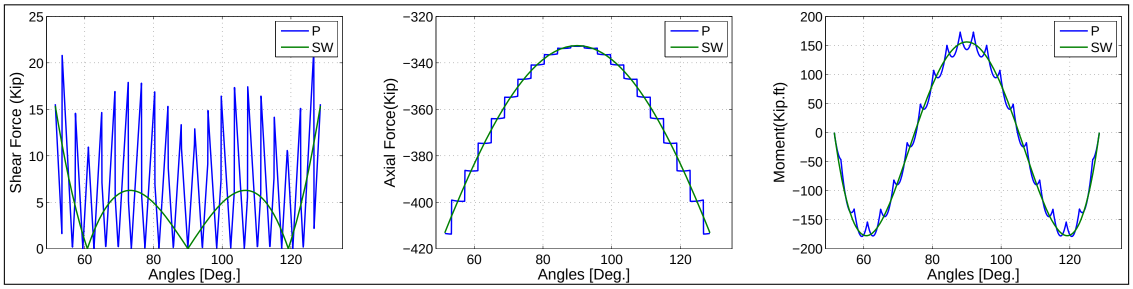

Figure 3.28: Two-hinged circular arch under self-weight vs. series of point load

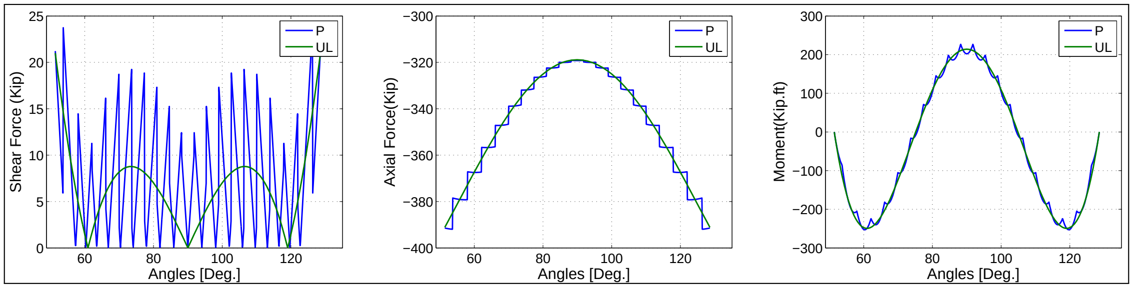

Figure 3.29: Two-hinged circular arch under uniformly distribute load vs. series of point load

weight case. The moment, shear force and axial force diagrams of its analysis are compared with the graphs plotted using the analytical equation. The numerical values on moment diagram in Figure 3.30, axial force diagram in Figure 3.31 and shear force diagram in Figure 3.32 closely matches with their respective values on the graphs Figure3.28.

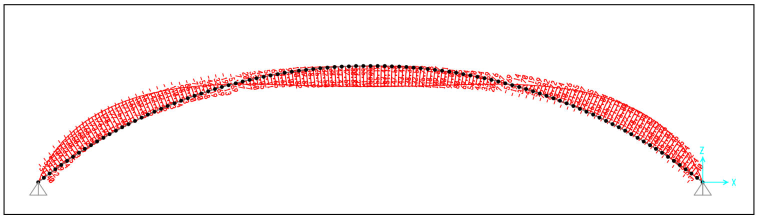

Figure 3.30: SAP 2000 - Moment diagram of Two-hinged circular arch under self-weight

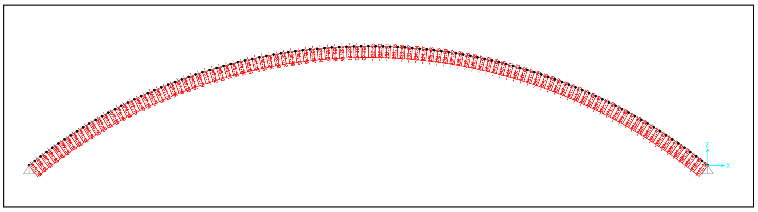

Figure 3.31: SAP 2000 - Axial force diagram of Two-hinged circular arch under self-weight

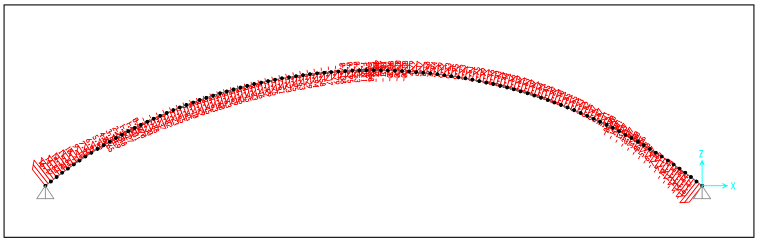

Figure 3.32: SAP 2000 - Shear force diagram of Two-hinged circular arch under self-weight

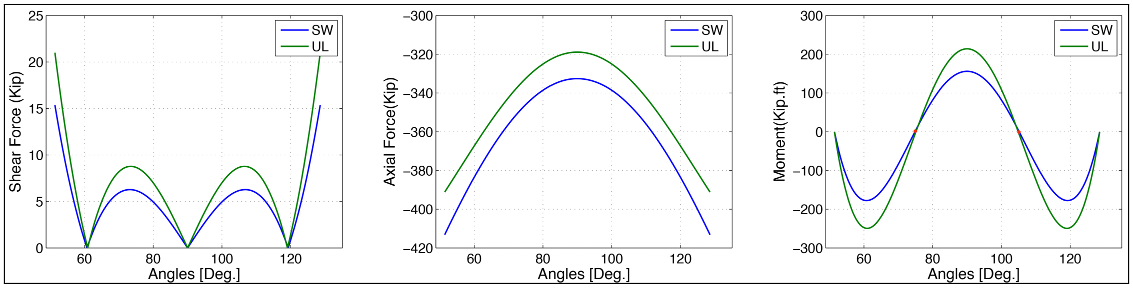

Figure 3.33: Two-hinged circular arch under self-weight vs.UDL

3.3.6 Conclusion

This sections discuss the structural behavior of a Two-hinged arch under point load, Self-weight and uniformly distributed load in terms of internal forces and deflection. Figure 3.33 compares the self- Weight loading condition with the uniformly distributed loading condition under an equal load w=2.275 kip/ft.Compared to the self-weight, a uniformly distributed load causes more internal shear force and moment , and it causes less internal compressive axial force.

Figure 3.34 show plots of an asymmetric loading condition. For this purpose, a unit load is applied

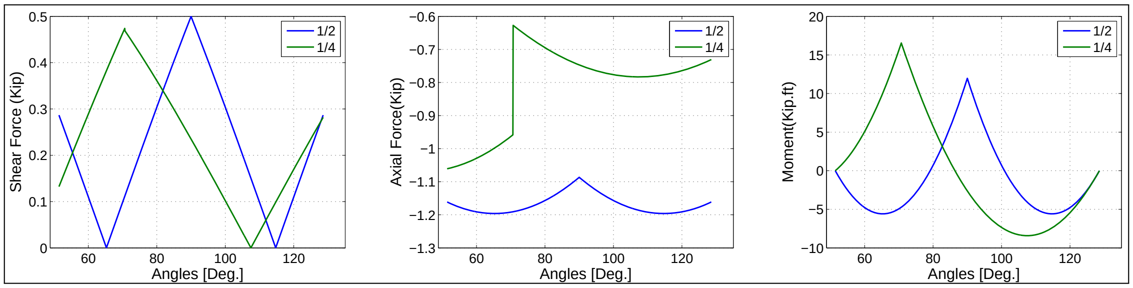

Figure 3.34: Two-hinged circular arch under point load at 1/2 and 1/4 span

at the crown and at the quarter of the span. Under this condition, the maximum moment due to the point load applied at the quarter of the span is about 1.4 times more than that applied at the crown. The maximum axial force due to the point load applied at the crown of the span is about 1.2 times more than that applied at the at the quarter of the span.

3.4 Hingeless Circular Arch

A symmetrical Hingeless circular arch has total six reactions - three at each support. Since the arch rib of a Hingeless arch is continuous between the supports and the point of the supports are immovable, applied load not only produce vertical but also horizontal reactions, commonly know as a thrust. With only three equation of equilibrium to solve the six unknown reactive forces, a Hingeless arch is statically indeterminate to third degree.

3.4.1 Analysis Procedure

To begin with, three redundant reaction of the statically indeterminate Hingeless arch are removed converting it into a statically determinate arch, primary structure. Using the ordinary method of statics, the support reaction and internal forces in the primary structure due to the applied load are computed. Later, assuming that no external force exists on the primary structure, a unit virtual force or moment is applied at the location of the removed redundant forces or moment respectively and the internal forces caused are computed. Compatibility equation for the deformation of an arch under applied load is considered to compute the redundant reaction in the original statically indeterminate Hingeles arch. Once all the support reactions are found, the internal forces in the arch are computed using ordinary method of statics. Further, these internal forces are used to compute the deflection in the arch under the applied load. The analysis process described here is performed in seven steps using Mathematica.The Mathematica files for all steps are included in relevant sections and for simplification only final equations for reactions and internal forces are expanded. For the purpose of analysis, three loading conditions are considered; a point load , self-weight of the arch and applied uniformly distributed load across the arch. The self- weight and the uniformly distributed load are symmetric about the center of the arch where as a point load, when applied anywhere but at the crown is asymmetric about the center of the arch. Hence to illustrate the analysis, same figures are used for the self-weight and the uniformly distributed loading conditions where as different set of figures is used for the point load condition.

3.4.2 Point Load

In this case the elementary applied force is given by

$$dp = P \tag{3.14}$$

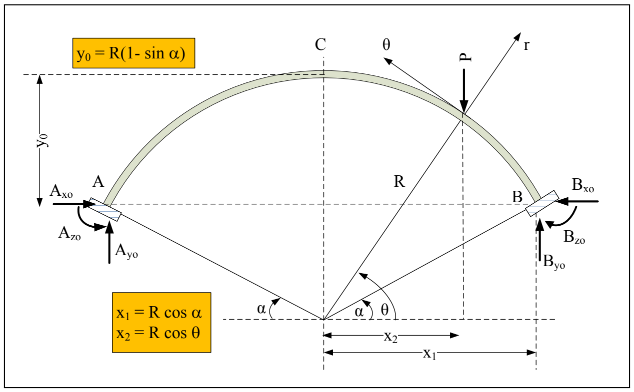

Figure 3.35: Hingeless circular arch under point load

3.4.2.1 Primary Structure: Reactions and Internal Forces

The redundant force Bxo and redundant moments Bzo and Azo in the original Hingeless arch shown in Figure 3.35 are removed converting it into a primary structure.The location of a point load anywhere on the arch causes discontinuity in the internal forces. This discontinuity in the internal forces in shown in Figure 3.3.Hence the expression for the internal forces at any angle β across the arch span is dependent on its relation with respect to the angle θ at which the point load is applied. By taking in consideration following conditions, different sets of equations are developed for the internal forces.

$$\beta < \theta,\ \beta \geq \theta \tag{3.15}$$

Primary structure for Hingeless arch is similar to that of the Two-hinged arch. The free body diagram in Figure 3.18, is used to determine the horizontal, vertical reactions at the supports as well as the internal forces - axial, shear and moment at any angle β across the arch span. Following is the output from Mathematica illustrating the derivation for computing support reaction.

Primary Structure: Reactions

Define the load

```
P=P;
```

Determine vertical reaction at B by taking moment with respect to A (CCW +ve)

```
SigMA=BY2x1 − P(x1 + x2);
```

```
Sol1=Solve[SigMA==0,BY]; BY=BY/.Sol1[[1]]
```

$\frac{1}{2}P(\mathrm{Cos}[\alpha] + \mathrm{Cos}[\theta])\mathrm{Sec}[\alpha]$

Determine vertical reaction at A by taking summation of forces in the y direction

```
Sol2=Solve[BY − P + AY==0,AY]; AY=AY/.Sol2[[1]]
```

$\frac{1}{2}(P - P\mathrm{Cos}[\theta]\mathrm{Sec}[\alpha])$

Determine horizontal reaction at A by taking moment with respect to Z (CCW +ve)

```
BX=0;
```

```
SigMZ=AXy0 − AY2x1 + P(x1 − x2) − BXy0;
```

```
Sol3=Solve[SigMZ==0,AX]; AX=AX/.Sol3[[1]];
```

Check statics by taking moment about O CCW +ve

```
MO=FullSimplify[BXy1 + BYx1 − AXy1 − AYx1 − x2P]
```

```
0
```

Following is the output from Mathematica illustrating the derivation for internal forces - axial, shear and moment at any angle β across the arch span.

Primary Structure: Reactions

Define the load

```
P=P;
```

Determine vertical reaction at B by taking moment with respect to A (CCW +ve)

```
SigMA=BY2x1 − P(x1 + x2);
```

```
Sol1=Solve[SigMA==0,BY]; BY=BY/.Sol1[[1]]
```

$$\frac{1}{2}P(\text{Cos}[\alpha] + \text{Cos}[\theta])\text{Sec}[\alpha]$$

Determine vertical reaction at A by taking summation of forces in the y direction

```
Sol2=Solve[BY − P + AY==0,AY]; AY=AY/.Sol2[[1]]
```

$$\frac{1}{2}(P - P\text{Cos}[\theta]\text{Sec}[\alpha])$$

Determine horizontal reaction at A by taking moment with respect to Z (CCW +ve)

```
BX=0;
```

```
SigMZ=AXy0 − AY2x1 + P(x1 − x2) − BXy0;
```

```
Sol3=Solve[SigMZ==0,AX]; AX=AX/.Sol3[[1]];
```

Check statics by taking moment about O CCW +ve

```
MO=FullSimplify[BXy1 + BYx1 − AXy1 − AYx1 − x2P]
```

```
0
```

3.4.2.2 Primary Structure: Virtual Unit Force

A unit virtual force is applied at the location Bxo in the direction of displacement of abutment B under real load.The free body diagram in Figure 3.19, is used to determine the internal forces at any angle β across the arch span caused due to virtual unit load .Similarly a unit moment is applied at the location of Bzo and Azo in the direction of rotation at the abutments B and A respectively under real load. The free body diagram in Figure 3.36, and Figure 3.37, are used to determine the internal forces at any angle β across the arch span caused due to virtual moment applied at the abutments B and A . Following is the output from Mathematica illustrating the derivation for computing internal forces caused due to virtual forces.

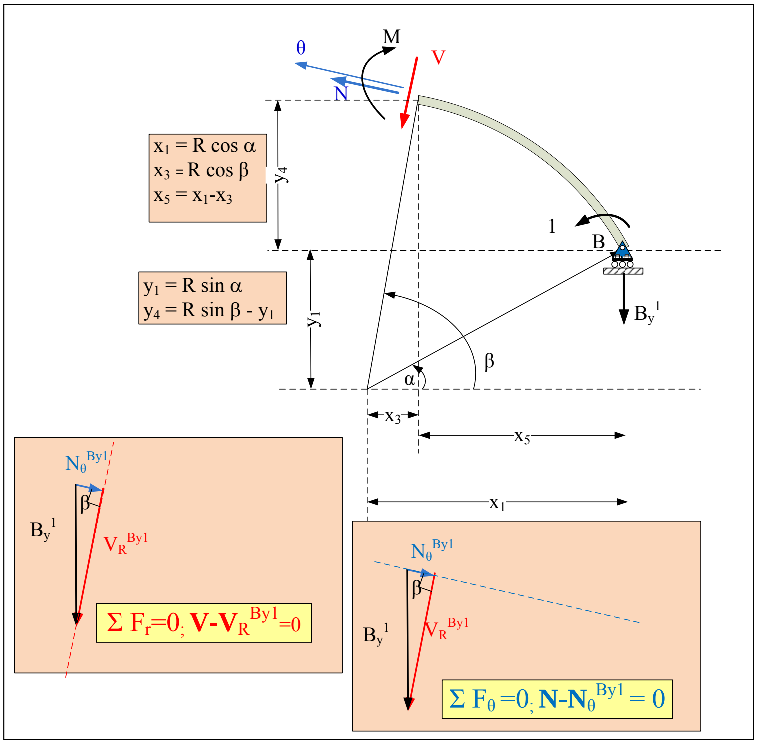

Figure 3.36: Hingeless circular arch with virtual moment at ’B’

Primary Structure: Virtual Forces

Apply virtual horizontal force at B

```
BX1=1;
```

Summation of forces in the radial direction; Shear (+ve outward)

```
SigFδVBX1=FullSimplify[BX1Cos[β] + δVBX1];
```

```
Sol7=Solve[SigFδVBX1==0,δVBX1]; δVBX1[β_]=δVBX1/.Sol7[[1]]
```

```
−Cos[β]
```

Summation of forces in the tangential direction; Normal force (+ve Tension)

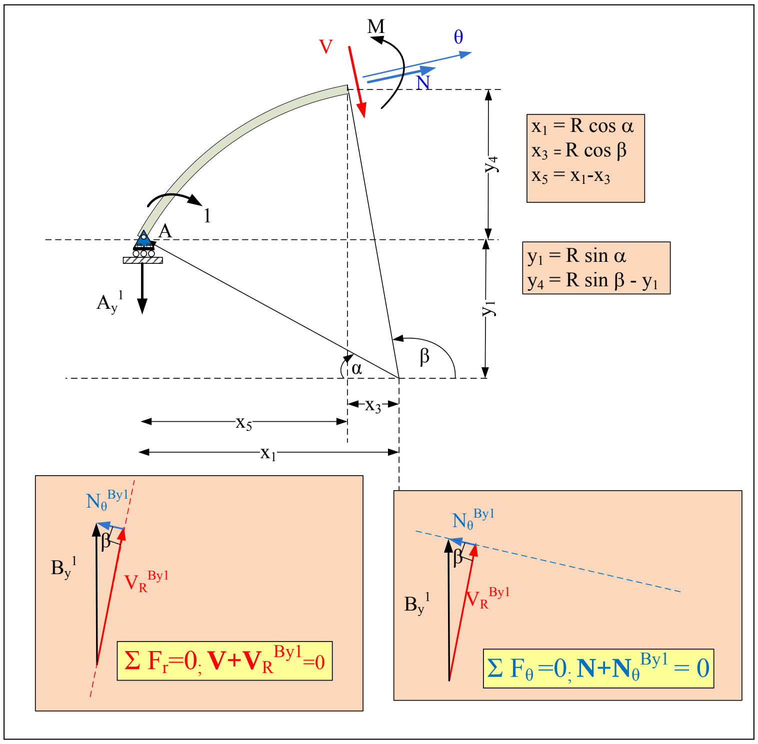

Figure 3.37: Hingeless circular arch with virtual moment at 'A'

```
SigFδNBX1=FullSimplify[−BX1Sin[β] + δNBX1];
```

```
Sol8=Solve[SigFδNBX1==0,δNBX1]; δNBX1[β_]=δNBX1/.Sol8[[1]]
```

```
Sin[β]
```

Summation of moments; Internal moment (CW +ve)

```
SigδMBX1=FullSimplify[−BX1y4 + δMBX1];
```

```
Sol9=Solve[SigδMBX1==0,δMBX1]; δMBX1[β_]=δMBX1/.Sol9[[1]]
```

```
−RSin[α] + RSin[β]
```

Apply virtual moment at B

```
BZ1=1;
```

Determine vertical reaction at B by taking moment about A (CW +ve)

```
SigMABZ1=FullSimplify[2x1BY1 − BZ1];
```

```
Sol10=Solve[SigMABZ1==0,BY1]; BY1=BY1/.Sol10[[1]]
```

$$\frac{\text{Sec}[\alpha]}{2R}$$

Summation of forces in the radial direction; Shear(+ve outward)

```
SigFδVBZ1=FullSimplify[−BY1Sin[β] + δVBZ1];
```

```
Sol11=Solve[SigFδVBZ1==0,δVBZ1]; δVBZ1[β_]=δVBZ1/.Sol11[[1]]
```

$$\frac{\text{Sec}[\alpha]\text{Sin}[\beta]}{2R}$$

Summation of forces in the tangential direction; Normal force (+ve Tension)

```
SigFδNBZ1=FullSimplify[−BY1Cos[β] + δNBZ1];
```

```
Sol12=Solve[SigFδNBZ1==0,δNBZ1]; δNBZ1[β_]=δNBZ1/.Sol12[[1]]
```

$$\frac{\text{Cos}[\beta]\text{Sec}[\alpha]}{2R}$$

Summation of moments; Internal moment (CW +ve)

```
SigδMBZ1=FullSimplify[BY1x5 − BZ1 + δMBZ1];
```

```
Sol13=Solve[SigδMBZ1==0,δMBZ1]; δMBZ1[β_]=δMBZ1/.Sol13[[1]]
```

$$\frac{1}{2}(1 + \text{Cos}[\beta]\text{Sec}[\alpha])$$

Apply virtual moment at A

```
AZ1=1;
```

Determine vertical reaction at B by taking moment about A (CW +ve)

```
SigMAAZ1=FullSimplify[AZ1 − 2x1BY2];
```

```
Sol14=Solve[SigMAAZ1==0,BY2]; BY2=BY2/.Sol14[[1]];
```

Summation of forces in the radial direction; Shear (+ve outward)

```
SigFδVAZ1=FullSimplify[BY2Sin[β] + δVAZ1];
```

```
Sol15=Solve[SigFδVAZ1==0,δVAZ1]; δVAZ1[β_]=δVAZ1/.Sol15[[1]]
```

$$-\frac{\text{Sec}[\alpha]\text{Sin}[\beta]}{2R}$$

Summation of forces in the tangential direction; Normal force (+ve Tension)

```
SigFδNAZ1=FullSimplify[BY2Cos[β] + δNAZ1];
```

```
Sol16=Solve[SigFδNAZ1==0,δNAZ1]; δNAZ1[β_]=δNAZ1/.Sol16[[1]]
```

$$-\frac{\text{Cos}[\beta]\text{Sec}[\alpha]}{2R}$$

Summation of moments; Internal moment (CW +ve)

```
SigδMAZ1=FullSimplify[−BY2x5 + δMAZ1];
```

```
Sol17=Solve[SigδMAZ1==0,δMAZ1]; δMAZ1[β_]=δMAZ1/.Sol17[[1]]
```

$\frac{1}{2}(1-\text{Cos}[\beta]\text{Sec}[\alpha])$

3.4.2.3 Original Structure: Redundant Force

Following Compatibility equation for the deformation of an arch under applied load together with the virtual work method are used to determine the redundant forces Bxo,Bzo and Azo. For this process both flexural and axial components of the compatibility equation as well as the discontinuity in the internal forces are considered.

$$1.\ \Delta_B = \left[\int_{\alpha}^{\theta} \frac{M1\ \delta\text{M1}}{e\ i}\, d\beta + \int_{\theta}^{(\pi-\alpha)} \frac{M2\ \delta\text{M2}}{e\ i}\, d\beta + \int_{\alpha}^{\theta} \frac{N1\ \delta\text{N1}}{a\ e}\, d\beta\ + \int_{\alpha}^{(\pi-\alpha)} \frac{N2\ \delta\text{N2}}{a\ e}\, d\beta\right] \tag{3.16}$$

Where

$M1(\beta < \theta), M2(\beta \geq \theta)$	Internal moment in the beam caused by real load
$\delta M1(\beta < \theta), \delta M2(\beta \geq \theta)$	Internal moment caused due to external virtual unit load
$N1(\beta < \theta), N2(\beta \geq \theta)$	Internal axial force in the beam caused by real load
$\delta N1(\beta < \theta), \delta N2(\beta \geq \theta)$	Internal axial force caused due to external virtual unit load

Following is the output from Mathematica illustrating the derivation for computing the redundant force.

Original Structure: Redundant Forces

Deformation due to real load (Flexural + Axial)

Displacement at B

$$\text{DeltaBX1F=FullSimplify}\left[\int_{\alpha}^{\theta} \frac{\text{M1}[\beta]\delta\text{MBX1}[\beta]}{ei} d\beta + \int_{\theta}^{(\pi-\alpha)} \frac{\text{M2}[\beta]\delta\text{MBX1}[\beta]}{ei} d\beta\right];$$

$$\text{DeltaBX1A=FullSimplify}\left[\int_{\alpha}^{\theta} \frac{\text{NN1}[\beta]\delta\text{NBX1}[\beta]}{ae} d\beta + \int_{\theta}^{(\pi-\alpha)} \frac{\text{NN2}[\beta]\delta\text{NBX1}[\beta]}{ae} d\beta\right];$$

```
DeltaBX1=DeltaBX1F + DeltaBX1A;
```

Rotation at B

DeltaBZ1F=FullSimplify $\left[\int_{\alpha}^{\theta} \frac{\text{M1}[\beta]\delta\text{MBZ1}[\beta]}{ei} \, d\beta + \int_{\theta}^{(\pi-\alpha)} \frac{\text{M2}[\beta]\delta\text{MBZ1}[\beta]}{ei} \, d\beta\right]$;

DeltaBZ1A=FullSimplify $\left[\int_{\alpha}^{\theta} \frac{\text{NN1}[\beta]\delta\text{NBZ1}[\beta]}{ae} \, d\beta + \int_{\theta}^{(\pi-\alpha)} \frac{\text{NN2}[\beta]\delta\text{NBZ1}[\beta]}{ae} \, d\beta\right]$;

DeltaBZ1=DeltaBZ1F + DeltaBZ1A;

Rotation at A

DeltaAZ1F=FullSimplify $\left[\int_{\alpha}^{\theta} \frac{\text{M1}[\beta]\delta\text{MAZ1}[\beta]}{ei} \, d\beta + \int_{\theta}^{(\pi-\alpha)} \frac{\text{M2}[\beta]\delta\text{MAZ1}[\beta]}{ei} \, d\beta\right]$;

DeltaAZ1A=FullSimplify $\left[\int_{\alpha}^{\theta} \frac{\text{NN1}[\beta]\delta\text{NAZ1}[\beta]}{ae} \, d\beta + \int_{\theta}^{(\pi-\alpha)} \frac{\text{NN2}[\beta]\delta\text{NAZ1}[\beta]}{ae} \, d\beta\right]$;

DeltaAZ1=DeltaAZ1F + DeltaAZ1A;

Deformation due to virtual load (Flexural + Axial)

F11F=FullSimplify $\left[\int_{\alpha}^{(\pi-\alpha)} \frac{\delta\text{MBX1}[\beta]\delta\text{MBX1}[\beta]}{ei} \, d\beta\right]$;
F11A=FullSimplify $\left[\int_{\alpha}^{(\pi-\alpha)} \frac{\delta\text{NBX1}[\beta]\delta\text{NBX1}[\beta]}{ae} \, d\beta\right]$;

F11=F11F + F11A;

F12F=FullSimplify $\left[\int_{\alpha}^{(\pi-\alpha)} \frac{\delta\text{MBX1}[\beta]\delta\text{MBZ1}[\beta]}{ei} \, d\beta\right]$;
F12A=FullSimplify $\left[\int_{\alpha}^{(\pi-\alpha)} \frac{\delta\text{NBX1}[\beta]\delta\text{NBZ1}[\beta]}{ae} \, d\beta\right]$;

F12=F12F + F12A;

F13F=FullSimplify $\left[\int_{\alpha}^{(\pi-\alpha)} \frac{\delta\text{MBX1}[\beta]\delta\text{MAZ1}[\beta]}{ei} \, d\beta\right]$;
F13A=FullSimplify $\left[\int_{\alpha}^{(\pi-\alpha)} \frac{\delta\text{NBX1}[\beta]\delta\text{NAZ1}[\beta]}{ae} \, d\beta\right]$;

F13=F13F + F13A;

F22F=FullSimplify $\left[\int_{\alpha}^{(\pi-\alpha)} \frac{\delta\text{MBZ1}[\beta]\delta\text{MBZ1}[\beta]}{ei} \, d\beta\right]$;
F22A=FullSimplify $\left[\int_{\alpha}^{(\pi-\alpha)} \frac{\delta\text{NBZ1}[\beta]\delta\text{NBZ1}[\beta]}{ae} \, d\beta\right]$;

F22=F22F + F22A;

F23F=FullSimplify $\left[\int_{\alpha}^{(\pi-\alpha)} \frac{\delta\text{MBZ1}[\beta]\delta\text{MAZ1}[\beta]}{ei} \, d\beta\right]$;
F23A=FullSimplify $\left[\int_{\alpha}^{(\pi-\alpha)} \frac{\delta\text{NBZ1}[\beta]\delta\text{NAZ1}[\beta]}{ae} \, d\beta\right]$;

F23=F23F + F23A;

$$\text{F33F}=\text{FullSimplify}\left[\int_{\alpha}^{(\pi-\alpha)} \frac{\delta\text{MAZ1}[\beta]\delta\text{MAZ1}[\beta]}{ei} d\beta\right];$$

$$\text{F33A}=\text{FullSimplify}\left[\int_{\alpha}^{(\pi-\alpha)} \frac{\delta\text{NAZ1}[\beta]\delta\text{NAZ1}[\beta]}{ae} d\beta\right];$$

```
F33=F33F + F33A;
```

```
F21=F12; F32=F23; F31=F13;
```

Redundant forces in original structure

```
Solve[{BXOF11+BZOF12+AZOF13==DeltaBX1,BXOF21+BZOF22+AZOF23==DeltaBZ1,BXOF31+
BZOF32 + AZOF33==DeltaAZ1}, {BXO,BZO,AZO}];
```

```
FullSimplify[BXO]
```

$$\frac{P\left(-\left(i+aR^2\right)(\pi-2\alpha)\text{Cos}[2\alpha]+\left(i-aR^2\right)(\pi-2\alpha)\text{Cos}[2\theta]-2aR^2(\pi-2\alpha+2\text{Sin}[2\alpha])+4aR^2\text{Cos}[\alpha]((\pi-2\theta)\text{Cos}[\theta]+2\text{Sin}[\theta])\right)}{2\left(-4aR^2+\left(i+aR^2\right)(\pi-2\alpha)^2-4aR^2\text{Cos}[2\alpha]+\left(i+aR^2\right)(\pi-2\alpha)\text{Sin}[2\alpha]\right)}$$

3.4.2.4 Original Structure: Reactions and Internal Forces

After the redundant force in the original structure Bxo,Bzo and Azo are computed, remaining support reaction and the internal forces in the original structure are determined using the free body diagram in Figure 3.38. Following is the output from Mathematica illustrating the derivation for computing the support reactions.

Original Structure: Reactions

Determine Vertical reaction at B by taking moment with respect to A (CCW +ve)

$$\text{SigMAO}=\text{BYO}\mathbf{2}\text{x1}-\boldsymbol{P}(\text{x1}+\text{x2})+\text{AZO}-\text{BZO};$$

```
Sol21=Solve[SigMAO==0,BYO]; BYO=BYO/.Sol21[[1]];
```

```
FullSimplify[BYO]
```

$$\frac{P\left(-4aR^2\text{Cos}[\theta]\text{Sin}[\alpha]-\left(i+aR^2\right)(2(-\pi+\alpha+\theta)+\text{Sin}[2\alpha])+\left(-i+aR^2\right)\text{Sin}[2\theta]\right)}{2\left(i+aR^2\right)(\pi-2\alpha-\text{Sin}[2\alpha])}$$

Determine vertical reaction at A by taking summation of forces in the y direction

```
Sol22=Solve[BYO - P + AYO==0,AYO]; AYO=AYO/.Sol22[[1]];
```

```
FullSimplify[AYO]
```

$$\frac{P\left(4aR^2\text{Cos}[\theta]\text{Sin}[\alpha]-2\left(i+aR^2\right)(\alpha-\theta+\text{Cos}[\alpha]\text{Sin}[\alpha])+\left(i-aR^2\right)\text{Sin}[2\theta]\right)}{2\left(i+aR^2\right)(\pi-2\alpha-\text{Sin}[2\alpha])}$$

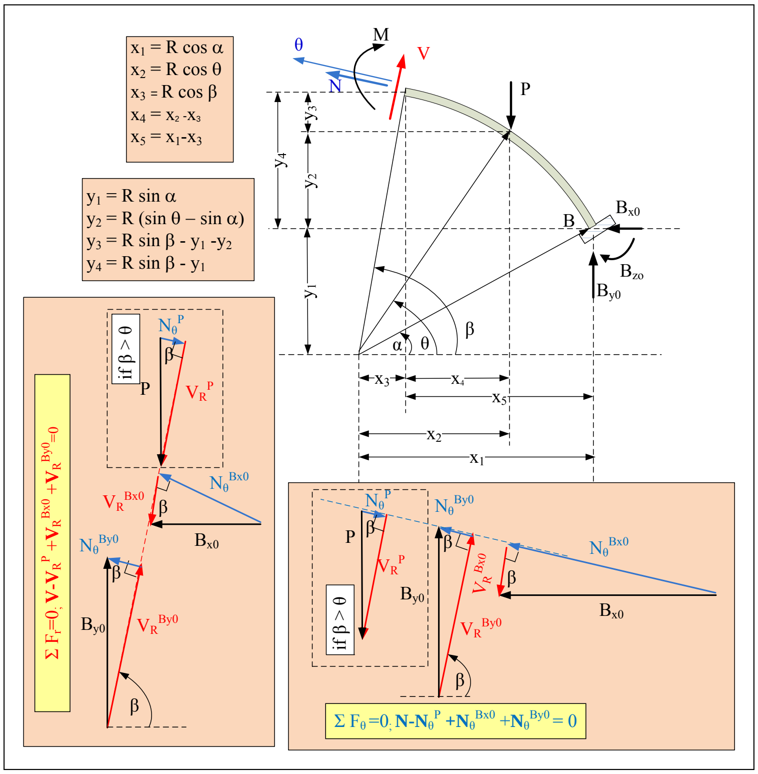

Figure 3.38: FBD of the original Hingeless circular arch under point load

Determine horizontal reaction at A by taking summation of forces in the x direction

```
AXO=BXO;
```

```
Clear[MO];
```

```
MO=FullSimplify[−BZO + BYOx1 + BXOy1 + AZO − AYOx1 − AXOy1 − Px2]
```

```
0
```

Following is the output from Mathematica illustrating the derivation for computing the internal forces.

Original Structure: Internal Forces

For $\beta < \theta$

Summation of forces in the Radial direction ; Shear (+ve outward)

```
SigFVO1= − BXOCos[β] + BYOSin[β] + VO1;
```

```
Sol23=Solve[SigFVO1==0,VO1]; VO1[β_]:=VO1/.Sol23[[1]];
```

```
FullSimplify[VO1[β]]
```

$$\begin{gathered}(P(-2(i+aR^2)\text{Cos}[\beta](-\pi+2\alpha+\text{Sin}[2\alpha])((i+aR^2)(\pi-2\alpha)\text{Cos}[2\alpha]+(\pi-2\alpha)(2aR^2+(-i+aR^2)\text{Cos}[2\theta])+\\ 4aR^2\text{Cos}[\alpha](-\pi\text{Cos}[\theta]+2\theta\text{Cos}[\theta]+2\text{Sin}[\alpha]-2\text{Sin}[\theta]))\\ -2(-4aR^2+(i+aR^2)(\pi-2\alpha)^2-4aR^2\text{Cos}[2\alpha]+(i+aR^2)(\pi-2\alpha)\text{Sin}[2\alpha])\text{Sin}[\beta](4aR^2\text{Cos}[\theta]\text{Sin}[\alpha]+\\ (i+aR^2)(2(-\pi+\alpha+\theta)+\text{Sin}[2\alpha])+(i-aR^2)\text{Sin}[2\theta])))/(4(i+aR^2)(-\pi+2\alpha+\text{Sin}[2\alpha])\\ (-4aR^2+(i+aR^2)(\pi-2\alpha)^2-4aR^2\text{Cos}[2\alpha]+(i+aR^2)(\pi-2\alpha)\text{Sin}[2\alpha]))\end{gathered}$$

Summation of forces in the tangential direction; Normal force (+ve Tension)

```
SigFNO1=BXOSin[β] + BYOCos[β] + NO1;
```

```
Sol24=Solve[SigFNO1==0,NO1]; NO1[β_]:=NO1/.Sol24[[1]];
```

```
FullSimplify[NO1[β]]
```

$$\begin{gathered}(P(2(i+aR^2)(-\pi+2\alpha+\text{Sin}[2\alpha])\text{Sin}[\beta]((i+aR^2)(\pi-2\alpha)\text{Cos}[2\alpha]+(\pi-2\alpha)(2aR^2+(-i+aR^2)\text{Cos}[2\theta])+\\ 4aR^2\text{Cos}[\alpha](-\pi\text{Cos}[\theta]+2\theta\text{Cos}[\theta]+2\text{Sin}[\alpha]-2\text{Sin}[\theta]))\\ -2\text{Cos}[\beta](-4aR^2+(i+aR^2)(\pi-2\alpha)^2-4aR^2\text{Cos}[2\alpha]+(i+aR^2)(\pi-2\alpha)\text{Sin}[2\alpha])(4aR^2\text{Cos}[\theta]\text{Sin}[\alpha]+\\ (i+aR^2)(2(-\pi+\alpha+\theta)+\text{Sin}[2\alpha])+(i-aR^2)\text{Sin}[2\theta])))/(4(i+aR^2)(-\pi+2\alpha+\text{Sin}[2\alpha])(-4aR^2+(i+aR^2)\\ (\pi-2\alpha)^2-4aR^2\text{Cos}[2\alpha]+(i+aR^2)(\pi-2\alpha)\text{Sin}[2\alpha]))\end{gathered}$$

Summation of moments; Internal moment (CW +ve)

```
SigMO1=BXOy4 − BYOx5 + BZO + MO1;
```

```
sol25=Solve[SigMO1==0,MO1]; MO1[β_]:=MO1/.sol25[[1]];
```

```
FullSimplify[MO1[β]]
```

$$\begin{gathered}-(PR((i+aR^2)(\pi-2\alpha-\text{Sin}[2\alpha])((\pi-2\alpha)(2aR^2+(i+aR^2)\text{Cos}[2\alpha]+(-i+aR^2)\text{Cos}[2\theta])+\\ 4aR^2\text{Sin}[2\alpha])\text{Sin}[\beta]\\ -2(i+aR^2)\text{Cos}[\alpha](\pi-2\alpha-\text{Sin}[2\alpha])(i+3aR^2+(-i+aR^2)\text{Cos}[2\theta]+2aR^2\text{Sin}[\beta]((\pi-2\theta)\text{Cos}[\theta]+2\text{Sin}[\theta]))\\ +(i+aR^2)(-\pi+2\alpha+\text{Sin}[2\alpha])(-2\text{Cos}[\theta](-2aR^2+(i+aR^2)(\pi-2\alpha)(\pi-\alpha-\theta)-2aR^2\text{Cos}[2\alpha]+(i+aR^2)\\ (\pi-\alpha-\theta)\text{Sin}[2\alpha])+(i+aR^2)(2(\pi-2\alpha)\text{Sin}[\alpha]-2(\pi-2\alpha+\text{Sin}[2\alpha])\text{Sin}[\theta]))\\ +\text{Cos}[\beta](-4aR^2+(i+aR^2)(\pi-2\alpha)^2-4aR^2\text{Cos}[2\alpha]+(i+aR^2)(\pi-2\alpha)\text{Sin}[2\alpha])(4aR^2\text{Cos}[\theta]\text{Sin}[\alpha]+(i+aR^2)\\ (2(-\pi+\alpha+\theta)+\text{Sin}[2\alpha])+(i-aR^2)\text{Sin}[2\theta])))/(2(i+aR^2)(-\pi+2\alpha+\text{Sin}[2\alpha])(-4aR^2+(i+aR^2)(\pi-2\alpha)^2\\ -4aR^2\text{Cos}[2\alpha]+(i+aR^2)(\pi-2\alpha)\text{Sin}[2\alpha]))\end{gathered}$$

For $\beta > \theta$

Summation of forces in the Radial direction ; Shear (+ve outward)

```
SigFVO2= − BXOCos[β] + BYOSin[β] − PSin[β] + VO2;
```

```
Sol26=Solve[SigFVO2==0,VO2]; VO2[β_]:=VO2/.Sol26[[1]];
```

FullSimplify[VO2[**β**]]

$$-\left(P\left(2\left(i+aR^2\right)\mathrm{Cos}[\beta](-\pi+2\alpha+\mathrm{Sin}[2\alpha])\left(\left(i+aR^2\right)(\pi-2\alpha)\mathrm{Cos}[2\alpha]+(\pi-2\alpha)\left(2aR^2+\left(-i+aR^2\right)\mathrm{Cos}[2\theta]\right)+\right.\right.\right.$$
$$\left.4aR^2\mathrm{Cos}[\alpha](-\pi\mathrm{Cos}[\theta]+2\theta\mathrm{Cos}[\theta]+2\mathrm{Sin}[\alpha]-2\mathrm{Sin}[\theta])\right)$$
$$-4\left(-4aR^2+\left(i+aR^2\right)(\pi-2\alpha)^2-4aR^2\mathrm{Cos}[2\alpha]+\left(i+aR^2\right)(\pi-2\alpha)\mathrm{Sin}[2\alpha]\right)\mathrm{Sin}[\beta]\left(\left(i+aR^2\right)(\alpha-\theta)+\right.$$
$$\left.\left.\left.\left(i+aR^2\right)\mathrm{Cos}[\alpha]\mathrm{Sin}[\alpha]+\mathrm{Cos}[\theta]\left(-i\mathrm{Sin}[\theta]+aR^2(-2\mathrm{Sin}[\alpha]+\mathrm{Sin}[\theta])\right)\right)\right)\right)/\left(4\left(i+aR^2\right)(-\pi+2\alpha+\mathrm{Sin}[2\alpha])\right.$$
$$\left.\left(-4aR^2+\left(i+aR^2\right)(\pi-2\alpha)^2-4aR^2\mathrm{Cos}[2\alpha]+\left(i+aR^2\right)(\pi-2\alpha)\mathrm{Sin}[2\alpha]\right)\right)$$

Summation of forces in the tangential direction; Normal force (+ve Tension)

SigFNO2=BXOSin[β] + BYOCos[β] − *P*Cos[β] + NO2;

Sol27=Solve[SigFNO2==0,NO2]; NO2[β_]:=NO2/.Sol27[[1]];

FullSimplify[NO2[**β**]]

$$-\left(P\left(-2\left(i+aR^2\right)(-\pi+2\alpha+\mathrm{Sin}[2\alpha])\mathrm{Sin}[\beta]\left(\left(i+aR^2\right)(\pi-2\alpha)\mathrm{Cos}[2\alpha]+(\pi-2\alpha)\left(2aR^2+\left(-i+aR^2\right)\mathrm{Cos}[2\theta]\right)+\right.\right.\right.$$
$$\left.4aR^2\mathrm{Cos}[\alpha](-\pi\mathrm{Cos}[\theta]+2\theta\mathrm{Cos}[\theta]+2\mathrm{Sin}[\alpha]-2\mathrm{Sin}[\theta])\right)$$
$$-4\mathrm{Cos}[\beta]\left(-4aR^2+\left(i+aR^2\right)(\pi-2\alpha)^2-4aR^2\mathrm{Cos}[2\alpha]+\left(i+aR^2\right)(\pi-2\alpha)\mathrm{Sin}[2\alpha]\right)\left(\left(i+aR^2\right)(\alpha-\theta)+\right.$$
$$\left.\left.\left.\left(i+aR^2\right)\mathrm{Cos}[\alpha]\mathrm{Sin}[\alpha]+\mathrm{Cos}[\theta]\left(-i\mathrm{Sin}[\theta]+aR^2(-2\mathrm{Sin}[\alpha]+\mathrm{Sin}[\theta])\right)\right)\right)\right)/\left(4\left(i+aR^2\right)(-\pi+2\alpha+\mathrm{Sin}[2\alpha])\right.$$
$$\left.\left(-4aR^2+\left(i+aR^2\right)(\pi-2\alpha)^2-4aR^2\mathrm{Cos}[2\alpha]+\left(i+aR^2\right)(\pi-2\alpha)\mathrm{Sin}[2\alpha]\right)\right)$$

Summation of moments; Internal moment (CW +ve)

SigMO2=BXOy4 − BYOx5 + *P*x4 + BZO + MO2;

sol28=Solve[SigMO2==0,MO2]; MO2[β_]:=MO2/.sol28[[1]];

FullSimplify[MO2[**β**]]

$$-\left(PR\left(\left(i+aR^2\right)(\pi-2\alpha-\mathrm{Sin}[2\alpha])\left((\pi-2\alpha)\left(2aR^2+\left(i+aR^2\right)\mathrm{Cos}[2\alpha]+\left(-i+aR^2\right)\mathrm{Cos}[2\theta]\right)+4aR^2\mathrm{Sin}[2\alpha]\right)\mathrm{Sin}[\beta\right.\right.$$
$$-2\left(i+aR^2\right)\mathrm{Cos}[\alpha](\pi-2\alpha-\mathrm{Sin}[2\alpha])\left(i+3aR^2+\left(-i+aR^2\right)\mathrm{Cos}[2\theta]+2aR^2\mathrm{Sin}[\beta]((\pi-2\theta)\mathrm{Cos}[\theta]+2\mathrm{Sin}[\theta])\right)$$
$$+\left(i+aR^2\right)\left(2\mathrm{Cos}[\theta]\left((\pi-2\alpha)\left(aR^2(2+(\pi-2\alpha)(\alpha-\theta))+i(\pi-2\alpha)(\alpha-\theta)+2aR^2\mathrm{Cos}[2\alpha]\right)-8aR^2\mathrm{Cos}[\alpha]^3\mathrm{Sin}[\alpha]-\right.\right.$$
$$\left.\left.\left(i+aR^2\right)(\alpha-\theta)\mathrm{Sin}[2\alpha]^2\right)+\left(i+aR^2\right)(-\pi+2\alpha+\mathrm{Sin}[2\alpha])(2(\pi-2\alpha)\mathrm{Sin}[\alpha]-2(\pi-2\alpha+\mathrm{Sin}[2\alpha])\mathrm{Sin}[\theta])\right)$$
$$-\mathrm{Cos}[\beta]\left(-4aR^2+\left(i+aR^2\right)(\pi-2\alpha)^2-4aR^2\mathrm{Cos}[2\alpha]+\left(i+aR^2\right)(\pi-2\alpha)\mathrm{Sin}[2\alpha]\right)\left(-4aR^2\mathrm{Cos}[\theta]\mathrm{Sin}[\alpha]+\left(i+aR^2\right)\right.$$
$$\left.\left.\left.(2\alpha-2\theta+\mathrm{Sin}[2\alpha])+\left(-i+aR^2\right)\mathrm{Sin}[2\theta]\right)\right)\right)/\left(2\left(i+aR^2\right)(-\pi+2\alpha+\mathrm{Sin}[2\alpha])\left(-4aR^2+\left(i+aR^2\right)(\pi-2\alpha)^2-\right.\right.$$
$$\left.\left.4aR^2\mathrm{Cos}[2\alpha]+\left(i+aR^2\right)(\pi-2\alpha)\mathrm{Sin}[2\alpha]\right)\right)$$

3.4.2.5 Deflection

Figure 3.21 and the analytical equations developed above are used to compute deflection in the symmetric Hingeless circular arch example discussed in Section 3.2.2.2 (Kinney, 1957, pg

547-558). Following equation of virtual work is used to compute deflection.

$$\delta P.\,\Delta = \left[\int_{\alpha}^{\theta} \frac{M1\ \delta\mathrm{M1}}{e\ i}\, Rd\beta + \int_{\theta}^{(\pi-\alpha)} \frac{M2\ \delta\mathrm{M2}}{e\ i}\, Rd\beta\right] \tag{3.17}$$

Where

δP	External Virtual unit load applied in the direction of Δ
Δ	External displacement caused by the real applied load
$M1(\beta < \theta),\ M2(\beta \geq \theta)$	Internal moment in the beam caused by real point load
$\delta M1(\beta < \theta),\ \delta M2(\beta \geq \theta)$	Internal moment caused due to external virtual unit load

3.4.2.6 Summary Of Results

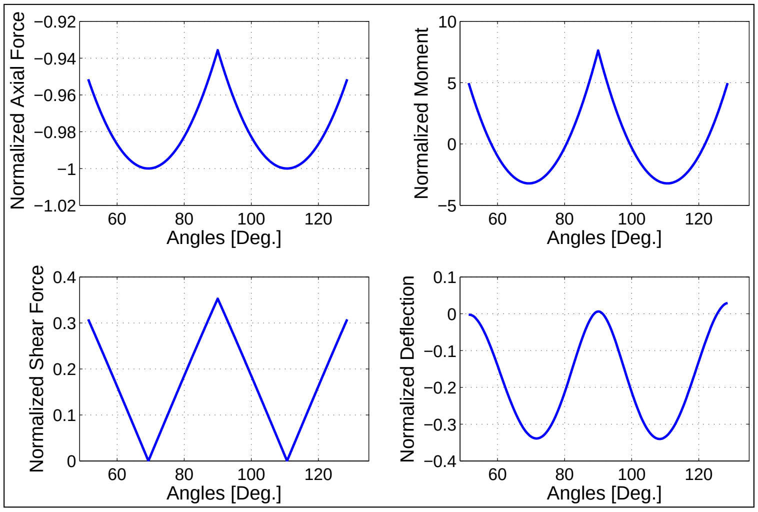

Figure 3.39: Plots for Hingeless circular arch under point load

3.4.2.7 Summary Of Results

Figure 3.39 show plots for a Hingeless arch example discussed in the above section.A point load is applied at the crown of the arch. The internal axial force and shear force are normalized with respect to the resultant of vertical reaction and thrust at the abutments. The internal moment is normalized with respect to the product of internal axial force and the rise. As indicated by the plot, all internal forces are symmetric about the crown of the arch. The axial compressive force is highest at about $\frac{1}{4}$ of the span from both abutments and it decrease to about 93.5% of the maximum value at the crown. The internal moment is maximum at the crown. The shear force on other hand is comparatively lower than the internal axial force and moment. The deflection is zero at the abutments and it maximum at about 1/4 of the span from both abutments.

3.4.3 Self weight

In this case the elementary applied force is given by

$$dP = wds = wRd\theta \tag{3.18}$$

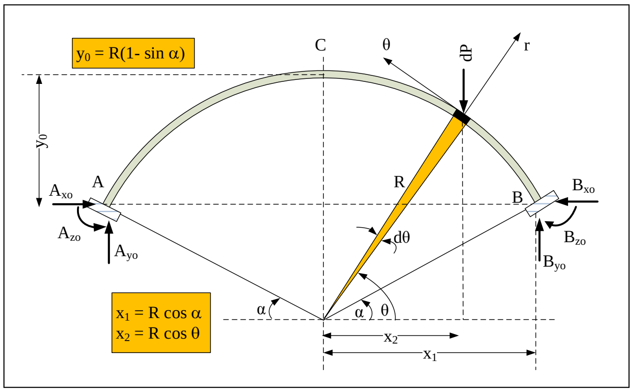

Figure 3.40: Hingeless circular arch under self weight

3.4.3.1 Primary Structure: Reactions and Internal Forces

The redundant force Bxo and redundant moments Bzo and Azo in the original Hingeless arch shown in the Figure 3.40 are removed converting it into a primary structure. Primary structure for Hingeless arch is similar to that of the Two-hinged arch. The free body diagram in Figure 3.24,is used to determine the horizontal, vertical reactions at the supports as well as the internal forces - axial, shear and moment at any angle β across the arch span. Following is the output from Mathematica illustrating the derivation for computing support reaction.

Primary Structure: Reactions

Define the load (omitting the dθ)

$$\mathrm{dP}'\text{=}\boldsymbol{wR};$$

Determine reaction at B by taking moment with respect to A (CCW +ve)

$$\mathrm{SigMA}\text{=}\mathrm{BY}\mathbf{2}\mathrm{x1}-\int_{\boldsymbol{\alpha}}^{\boldsymbol{\pi-\alpha}}(\mathrm{x1}+\mathrm{x2})\mathrm{dP}'\boldsymbol{d\theta};$$

$$\mathrm{Sol1}\text{=}\mathrm{Solve}[\mathrm{SigMA}\text{==}\mathbf{0},\mathrm{BY}];\ \mathrm{BY}\text{=}\mathrm{BY}/.\mathrm{Sol1}[[\mathbf{1}]]$$

$$\frac{1}{2}Rw(\pi-2\alpha)$$

Determine vertical reaction at A by taking summation of forces in the y direction

$$\mathrm{Sol2}\text{=}\mathrm{Solve}\left[\mathrm{BY}-\int_{\boldsymbol{\alpha}}^{\boldsymbol{\pi-\alpha}}\mathrm{dP}'\boldsymbol{d\theta}+\mathrm{AY}\text{==}\mathbf{0},\mathrm{AY}\right];\ \mathrm{AY}\text{=}\mathrm{AY}/.\mathrm{Sol2}[[\mathbf{1}]];$$

Determine horizontal reaction at A by taking moment with respect to Z (CCW +ve)

$$\mathrm{BX}\text{=}\mathbf{0};$$

$$\mathrm{SigMZ}\text{=}\mathrm{AXy0}-\mathrm{AY}\mathbf{2}\mathrm{x1}+\int_{\boldsymbol{\alpha}}^{\boldsymbol{\pi-\alpha}}\mathrm{dP}'(\mathrm{x1}-\mathrm{x2})\boldsymbol{d\theta}-\mathrm{BXy0};$$

$$\mathrm{Sol3}\text{=}\mathrm{Solve}[\mathrm{SigMZ}\text{==}\mathbf{0},\mathrm{AX}];\ \mathrm{AX}\text{=}\mathrm{AX}/.\mathrm{Sol3}[[\mathbf{1}]];$$

Check statics by taking moment about O CCW +ve

$$\mathrm{MO}\text{=}\mathrm{FullSimplify}\left[\mathrm{BXy1}+\mathrm{BYx1}-\mathrm{AXy1}-\mathrm{AYx1}-\int_{\boldsymbol{\alpha}}^{\boldsymbol{\pi-\alpha}}\mathrm{x2dP}'\boldsymbol{d\theta}\right]$$

$$0$$

Following is the output from Mathematica illustrating the derivation for internal forces - axial, shear and moment at any angle β across the arch span.

Primary Structure: Internal Forces

Summation of forces in the radial direction; Shear (+ve outward)

$$\mathrm{SigFV}\text{=}\mathrm{BYSin}[\boldsymbol{\beta}]-\int_{\boldsymbol{\alpha}}^{\boldsymbol{\beta}}\mathrm{dP}'\mathrm{Sin}[\boldsymbol{\beta}]\boldsymbol{d\theta}+\boldsymbol{V};$$

$$\mathrm{Sol4}\text{=}\mathrm{FullSimplify}[\mathrm{Solve}[\mathrm{SigFV}\text{==}\mathbf{0},\boldsymbol{V}]];\ \boldsymbol{V}[\boldsymbol{\beta}\_]\text{=}\boldsymbol{V}/.\mathrm{Sol4}[[\mathbf{1}]]$$

$$-\frac{1}{2}Rw(\pi-2\beta)\mathrm{Sin}[\beta]$$

Summation of forces in the tangential direction; Normal force (+ve Tension)

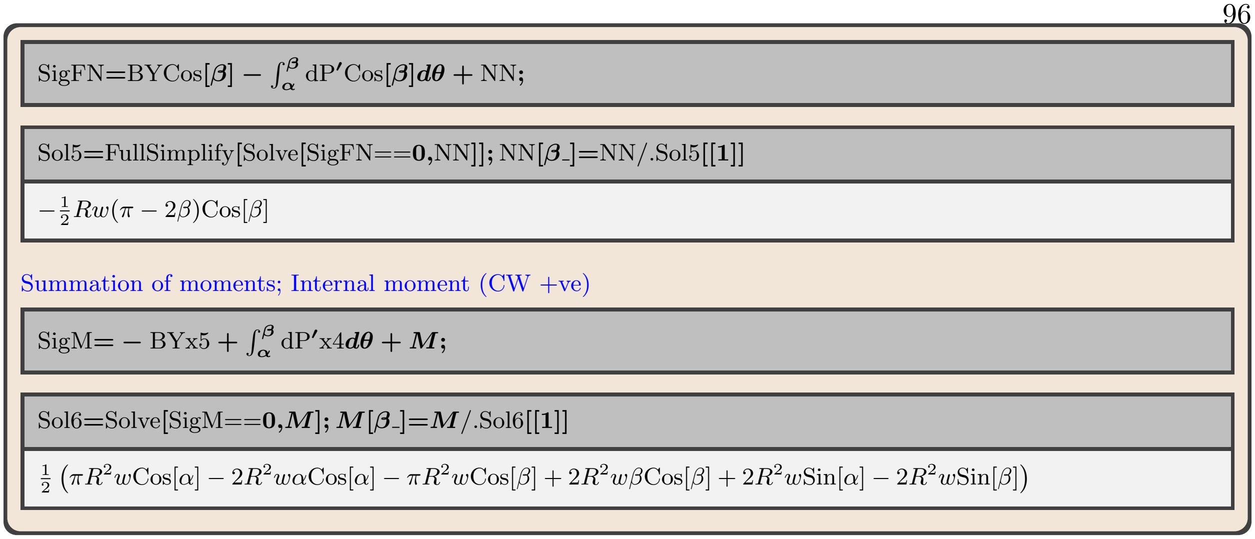

```
SigFN=BYCos[β] − ∫_α^β dP′Cos[β]dθ + NN;
```

```
Sol5=FullSimplify[Solve[SigFN==0,NN]]; NN[β_]=NN/.Sol5[[1]]
```

$-\frac{1}{2}Rw(\pi-2\beta)\text{Cos}[\beta]$

Summation of moments; Internal moment (CW +ve)

```
SigM= − BYx5 + ∫_α^β dP′x4dθ + M;
```

```
Sol6=Solve[SigM==0,M]; M[β_]=M/.Sol6[[1]]
```

$\frac{1}{2}\left(\pi R^2 w\text{Cos}[\alpha]-2R^2 w\alpha\text{Cos}[\alpha]-\pi R^2 w\text{Cos}[\beta]+2R^2 w\beta\text{Cos}[\beta]+2R^2 w\text{Sin}[\alpha]-2R^2 w\text{Sin}[\beta]\right)$

3.4.3.2 Primary Structure: Virtual Unit Force

Figure 3.19, Figure 3.36 and Figure 3.37 and a similar process used for Hingeless circular arch under point load is followed to determine the internal forces at any angle β across the arch span caused due to virtual unit load . The Mathematica output illustrating the derivation for computing internal forces caused due to virtual forces used for the Hingeless arch under point load is also applicable here.

3.4.3.3 Original Structure:Redundant Force

Using the following Compatibility equation for the deformation of an arch under applied load together with the virtual work method are used to determine the redundant forces Bxo,Bzo and Azo. For this process both flexural and axial components of the compatibility equation are considered.

$$1.\ \Delta_B = \left[\int_{\alpha}^{(\pi-\alpha)} \frac{M\ \delta\mathrm{M}}{e\ i}\ d\beta + \int_{\alpha}^{(\pi-\alpha)} \frac{N\ \delta\mathrm{N}}{a\ e}\ d\beta\right] \tag{3.19}$$

Where

M Internal moment in the beam caused by real load

δM Internal moment caused due to external virtual unit load

N Internal axial force in the beam caused by real load

δN Internal axial force caused due to external virtual unit load

Following is the output from Mathematica illustrating the derivation for computing the redundant force

Original Structure: Redundant Force

Deformation due to the real load (Flexural + Axial)

Displacement at B

DeltaBX1F=FullSimplify $\left[\int_{\alpha}^{(\pi-\alpha)} \frac{M[\beta]\delta \mathrm{MBX1}[\beta]}{ei} d\beta\right]$;

DeltaBX1A=FullSimplify $\left[\int_{\alpha}^{(\pi-\alpha)} \frac{\mathrm{NN}[\beta]\delta \mathrm{NBX1}[\beta]}{ae} d\beta\right]$;

DeltaBX1=DeltaBX1F + DeltaBX1A;

Rotation at B

DeltaBZ1F=FullSimplify $\left[\int_{\alpha}^{(\pi-\alpha)} \frac{M[\beta]\delta \mathrm{MBZ1}[\beta]}{ei} d\beta\right]$;

DeltaBZ1A=FullSimplify $\left[\int_{\alpha}^{(\pi-\alpha)} \frac{\mathrm{NN}[\beta]\delta \mathrm{NBZ1}[\beta]}{ae} d\beta\right]$;

DeltaBZ1=DeltaBZ1F + DeltaBZ1A;

Rotation at A

DeltaAZ1F=FullSimplify $\left[\int_{\alpha}^{(\pi-\alpha)} \frac{M[\beta]\delta \mathrm{MAZ1}[\beta]}{ei} d\beta\right]$;

DeltaAZ1A=FullSimplify $\left[\int_{\alpha}^{(\pi-\alpha)} \frac{\mathrm{NN}[\beta]\delta \mathrm{NAZ1}[\beta]}{ae} d\beta\right]$;

DeltaAZ1=DeltaAZ1F + DeltaAZ1A;

Deformation due to virtual force (Flexural + Axial)

F11F=FullSimplify $\left[\int_{\alpha}^{(\pi-\alpha)} \frac{\delta \mathrm{MBX1}[\beta]\delta \mathrm{MBX1}[\beta]}{ei} d\beta\right]$;

F11A=FullSimplify $\left[\int_{\alpha}^{(\pi-\alpha)} \frac{\delta \mathrm{NBX1}[\beta]\delta \mathrm{NBX1}[\beta]}{ae} d\beta\right]$;

F11=F11F + F11A;

F12F=FullSimplify $\left[\int_{\alpha}^{(\pi-\alpha)} \frac{\delta \mathrm{MBX1}[\beta]\delta \mathrm{MBZ1}[\beta]}{ei} d\beta\right]$;

F12A=FullSimplify $\left[\int_{\alpha}^{(\pi-\alpha)} \frac{\delta \mathrm{NBX1}[\beta]\delta \mathrm{NBZ1}[\beta]}{ae} d\beta\right]$;

F12=F12F + F12A;

$$\text{F13F=FullSimplify}\left[\int_{\alpha}^{(\pi-\alpha)} \frac{\delta\text{MBX1}[\beta]\delta\text{MAZ1}[\beta]}{ei} d\beta\right];$$

$$\text{F13A=FullSimplify}\left[\int_{\alpha}^{(\pi-\alpha)} \frac{\delta\text{NBX1}[\beta]\delta\text{NAZ1}[\beta]}{ae} d\beta\right];$$

F13=F13F + F13A;

$$\text{F22F=FullSimplify}\left[\int_{\alpha}^{(\pi-\alpha)} \frac{\delta\text{MBZ1}[\beta]\delta\text{MBZ1}[\beta]}{ei} d\beta\right];$$

$$\text{F22A=FullSimplify}\left[\int_{\alpha}^{(\pi-\alpha)} \frac{\delta\text{NBZ1}[\beta]\delta\text{NBZ1}[\beta]}{ae} d\beta\right];$$

F22=F22F + F22A;

$$\text{F23F=FullSimplify}\left[\int_{\alpha}^{(\pi-\alpha)} \frac{\delta\text{MBZ1}[\beta]\delta\text{MAZ1}[\beta]}{ei} d\beta\right];$$

$$\text{F23A=FullSimplify}\left[\int_{\alpha}^{(\pi-\alpha)} \frac{\delta\text{NBZ1}[\beta]\delta\text{NAZ1}[\beta]}{ae} d\beta\right];$$

F23=F23F + F23A;

$$\text{F33F=FullSimplify}\left[\int_{\alpha}^{(\pi-\alpha)} \frac{\delta\text{MAZ1}[\beta]\delta\text{MAZ1}[\beta]}{ei} d\beta\right];$$

$$\text{F33A=FullSimplify}\left[\int_{\alpha}^{(\pi-\alpha)} \frac{\delta\text{NAZ1}[\beta]\delta\text{NAZ1}[\beta]}{ae} d\beta\right];$$

F33=F33F + F33A;

F21=F12; F32=F23; F31=F13;

Redundant forces in original structure

Solve[{BXOF11+BZOF12+AZOF13==DeltaBX1,BXOF21+BZOF22+AZOF23==DeltaBZ1,BXOF31+BZOF32 + AZOF33==DeltaAZ1}, {BXO,BZO,AZO}];

FullSimplify[BXO]

$$\frac{Rw\left(-2aR^2\left(-8+(\pi-2\alpha)^2\right)-\left(-16aR^2+\left(i+aR^2\right)(\pi-2\alpha)^2\right)\text{Cos}[2\alpha]-\left(i+7aR^2\right)(\pi-2\alpha)\text{Sin}[2\alpha]\right)}{2\left(-4aR^2+\left(i+aR^2\right)(\pi-2\alpha)^2-4aR^2\text{Cos}[2\alpha]+\left(i+aR^2\right)(\pi-2\alpha)\text{Sin}[2\alpha]\right)}$$

3.4.3.4 Original Structure: Reactions and Internal Forces

After the redundant force in the original structure Bxo,Bzo and Azo are computed, remaining support reaction and the internal forces in the original structure are determined using the free body diagram in Figure 3.41.

Following is the output from Mathematica illustrating the derivation for computing the sup-

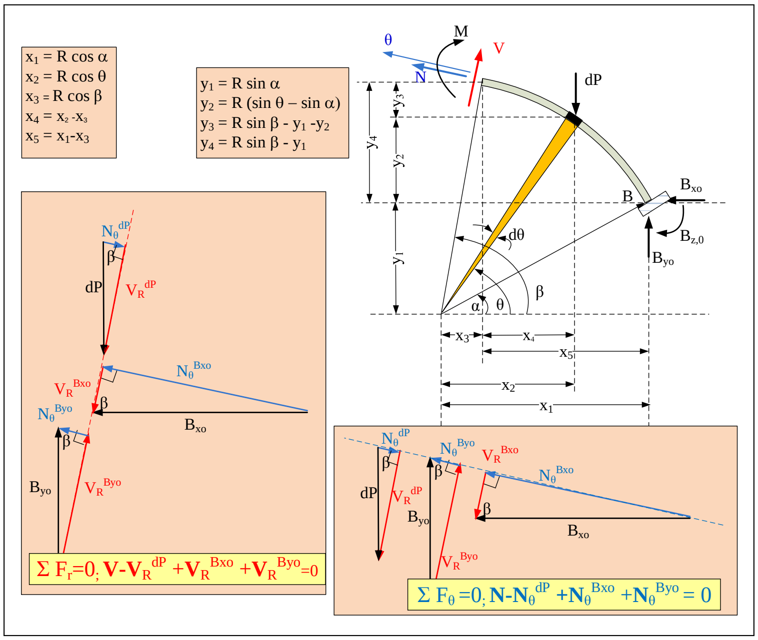

Figure 3.41: Internal forces in Hingeless circular arch

port reactions.

Original Structure: Reactions

Determine vertical reaction at B by taking moment with respect to A (CCW +ve)

SigMAO=BYO**2**x1 − $\int_{\alpha}^{\pi-\alpha}$(x1 + x2)dP′$\boldsymbol{d\theta}$ + AZO − BZO;

Sol18=Solve[SigMAO==**0**,BYO]; BYO=BYO/.Sol18[[**1**]]

$\frac{1}{2}Rw(\pi - 2\alpha)$

Determine vertical reaction at A by taking summation of forces in the y direction

Sol19=Solve $\left[\text{BYO} - \int_{\alpha}^{\pi-\alpha}\text{dP}'\boldsymbol{d\theta} + \text{AYO}==\mathbf{0},\text{AYO}\right]$; AYO=AYO/.Sol19[[**1**]]

$\frac{1}{2}Rw(\pi - 2\alpha)$

Determine horizontal reaction at A by taking summation of forces in the x direction

AXO=BXO;

Clear[MO];

MO=FullSimplify $\left[\text{BZO} + \text{BYOx1} + \text{BXOy1} - \text{AZO} - \text{AYOx1} - \text{AXOy1} - \int_{\alpha}^{\pi-\alpha}\text{dP}'\text{x2}\boldsymbol{d\theta}\right]$

0

Following is the output from Mathematica illustrating the derivation for computing the internal forces.

Original Structure: Internal Forces

Summation of forces in the Radial direction ; Shear (+ve outward)

$$\text{SigFVO} = -\text{BXOCos}[\boldsymbol{\beta}] + \text{BYOSin}[\boldsymbol{\beta}] - \int_{\boldsymbol{\alpha}}^{\boldsymbol{\beta}} \text{dP}'\text{Sin}[\boldsymbol{\beta}]\boldsymbol{d\theta} + \text{VO};$$

$$\text{Sol20=Solve[SigFVO==}\mathbf{0}\text{,VO]; VO}[\boldsymbol{\beta}\_]\text{:=VO/.Sol20}[[\mathbf{1}]];$$

$$\text{FullSimplify[VO}[\boldsymbol{\beta}\_]]$$

$$-\left(Rw\left(\text{Cos}[\beta]\left(2aR^2\left(-8+(\pi-2\alpha)^2\right)+\left(-16aR^2+\left(i+aR^2\right)(\pi-2\alpha)^2\right)\text{Cos}[2\alpha]+\left(i+7aR^2\right)(\pi-2\alpha)\text{Sin}[2\alpha]\right)\right.\right.$$
$$\left.\left.+(\pi-2\beta)\left(-4aR^2+\left(i+aR^2\right)(\pi-2\alpha)^2-4aR^2\text{Cos}[2\alpha]+\left(i+aR^2\right)(\pi-2\alpha)\text{Sin}[2\alpha]\right)\text{Sin}[\beta]\right)\right)/$$
$$\left(2\left(-4aR^2+\left(i+aR^2\right)(\pi-2\alpha)^2-4aR^2\text{Cos}[2\alpha]+\left(i+aR^2\right)(\pi-2\alpha)\text{Sin}[2\alpha]\right)\right)$$

Summation of forces in the tangential direction; Normal force +(ve Tension)

$$\text{SigFNO=BXOSin}[\boldsymbol{\beta}] + \text{BYOCos}[\boldsymbol{\beta}] - \int_{\boldsymbol{\alpha}}^{\boldsymbol{\beta}} \text{dP}'\text{Cos}[\boldsymbol{\beta}]\boldsymbol{d\theta} + \text{NO};$$

$$\text{Sol21=Solve[SigFNO==}\mathbf{0}\text{,NO]; NO}[\boldsymbol{\beta}\_]\text{:=NO/.Sol21}[[\mathbf{1}]];$$

$$\text{FullSimplify[NO}[\boldsymbol{\beta}\_]]$$

$$-\left(Rw\left((\pi-2\beta)\text{Cos}[\beta]\left(-4aR^2+\left(i+aR^2\right)(\pi-2\alpha)^2-4aR^2\text{Cos}[2\alpha]+\left(i+aR^2\right)(\pi-2\alpha)\text{Sin}[2\alpha]\right)\right.\right.$$
$$\left.\left.-\left(2aR^2\left(-8+(\pi-2\alpha)^2\right)+\left(-16aR^2+\left(i+aR^2\right)(\pi-2\alpha)^2\right)\text{Cos}[2\alpha]+\left(i+7aR^2\right)(\pi-2\alpha)\text{Sin}[2\alpha]\right)\text{Sin}[\beta]\right)\right)/$$
$$\left(2\left(-4aR^2+\left(i+aR^2\right)(\pi-2\alpha)^2-4aR^2\text{Cos}[2\alpha]+\left(i+aR^2\right)(\pi-2\alpha)\text{Sin}[2\alpha]\right)\right)$$

Summation of moments; Internal moment (CW +ve)

$$\text{Clear[MO]};$$

$$\text{SigMO=BXOy4} - \text{BYOx5} + \text{BZO} + \int_{\boldsymbol{\alpha}}^{\boldsymbol{\beta}} \text{dP}'\text{x4}\boldsymbol{d\theta} + \text{MO};$$

$$\text{sol22=Solve[SigMO==}\mathbf{0}\text{,MO]; MO}[\boldsymbol{\beta}\_]\text{:=MO/.sol22}[[\mathbf{1}]];$$

$$\text{FullSimplify[MO}[\boldsymbol{\beta}\_]]$$

$$\left(R^2w\left(2\left(3i+aR^2\right)(\pi-2\alpha)\text{Cos}[\alpha]+2\left(aR^2-i\left(-3+(\pi-2\alpha)^2\right)-aR^2(\pi-2\alpha)^2+\left(3i+aR^2\right)\text{Cos}[2\alpha]\right)\text{Sin}[\alpha]\right.\right.$$
$$+(\pi-2\beta)\text{Cos}[\beta]\left(4aR^2-\left(i+aR^2\right)(\pi-2\alpha)^2+4aR^2\text{Cos}[2\alpha]-\left(i+aR^2\right)(\pi-2\alpha)\text{Sin}[2\alpha]\right)$$
$$\left.\left.+\left(-2\left(4aR^2+i(\pi-2\alpha)^2\right)+\left(-8aR^2+\left(i+aR^2\right)(\pi-2\alpha)^2\right)\text{Cos}[2\alpha]-\left(i-5aR^2\right)(\pi-2\alpha)\text{Sin}[2\alpha]\right)\text{Sin}[\beta]\right)\right)/$$
$$\left(2\left(-4aR^2+\left(i+aR^2\right)(\pi-2\alpha)^2-4aR^2\text{Cos}[2\alpha]+\left(i+aR^2\right)(\pi-2\alpha)\text{Sin}[2\alpha]\right)\right)$$

3.4.3.5 Deflection

The analytical equations developed above are used to compute deflection in the Hingeless symmetric circular arch example discussed in Section 3.2.3.3 (Kinney, 1957, pg 547-558).Following equation of virtual work is used to compute deflection.

$$\delta P.\,\Delta = \left[\int_{\alpha}^{\theta} \frac{M\ \delta \mathrm{M1}}{e\ i}\ Rd\beta + \int_{\theta}^{(\pi-\alpha)} \frac{M\ \delta \mathrm{M2}}{e\ i}\ Rd\beta\right] \tag{3.20}$$

Where

δP	External Virtual unit load applied in the direction of Δ
Δ	External displacement caused by the real applied load
M	Internal moment in the beam caused by real load
$\delta M1(\beta < \theta),\ \delta M2(\beta \geq \theta)$	Internal moment caused due to external virtual unit load

3.4.3.6 Summary Of Results

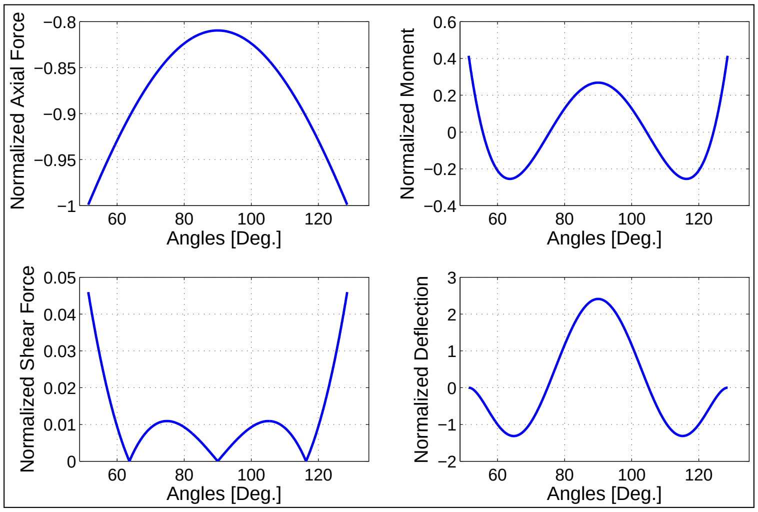

Figure 3.42: Plots for Hingeless circular arch under self-weight

Figure 3.42 show plots for the Hingeless arch under self-weight discussed the section above. The internal axial force and shear force are normalized with respect to the resultant of vertical reaction and thrust at the abutments. The axial compressive force is highest at the abutments and it decreases toward the crown to about 81% of the maximum value. The shear force on other hand is comparatively low and it varies between about 4.75% and 1.0%, respectively from the abutment to the crown. The internal moment is normalized with respect to the product of internal axial force and the rise. The internal moment is highest at the abutments and it is about 60 % of the maximum value at the crown and at about $\frac{1}{6}$ of span from the abutments. There are four inflection points in the moment diagram and they correspond with the zero deflection points in the arch. The Deflection is highest at the crown and the graph of deflection follows similar profile as that of the moment diagram. Positive and negative deflection corresponds with positive and negative moment in the arch respectively.

3.4.4 Uniformly Distributed Load

In this case the elementary applied force is given by

$$dp = wdx = wRSin\theta \tag{3.21}$$

The redundant force Bxo and redundant moments Bzo and Azo in the original Hingeless arch shown in Figure3.40are removed converting it into a primary structure. First three steps including support reaction and internal forces caused due to the real load and internal forces caused due to the virtual load are similar to that for the Hingeless circular arch under self-weight. For simplicity only the steps involving computation of the redundant force, support reactions and the internal forces in the original structure are shown here.

3.4.4.1 Original Structure: Redundant Force

The process used for the Hingeless arch under self weight repeated here.The Compatibility equation for the deformation of an arch under applied load together with the virtual work method are used to determine the redundant force Bxo at the abutment B. For this process both flexural and axial components of the compatibility equation are considered.Following is the output from

Mathematica, illustrating the derivation for computing the redundant force.

Original Structure: Redundant Forces

Deformation due to real load (Flexural + Axial)

Displacement at B

DeltaBX1F=FullSimplify $\left[\int_{\alpha}^{(\pi-\alpha)} \frac{M[\beta]\delta\text{MBX1}[\beta]}{ei} d\beta\right]$;

DeltaBX1A=FullSimplify $\left[\int_{\alpha}^{(\pi-\alpha)} \frac{\text{NN}[\beta]\delta\text{NBX1}[\beta]}{ae} d\beta\right]$;

DeltaBX1=DeltaBX1F + DeltaBX1A;

Rotation at B

DeltaBZ1F=FullSimplify $\left[\int_{\alpha}^{(\pi-\alpha)} \frac{M[\beta]\delta\text{MBZ1}[\beta]}{ei} d\beta\right]$;

DeltaBZ1A=FullSimplify $\left[\int_{\alpha}^{(\pi-\alpha)} \frac{\text{NN}[\beta]\delta\text{NBZ1}[\beta]}{ae} d\beta\right]$;

DeltaBZ1=DeltaBZ1F + DeltaBZ1A;

Rotation at A

DeltaAZ1F=FullSimplify $\left[\int_{\alpha}^{(\pi-\alpha)} \frac{M[\beta]\delta\text{MAZ1}[\beta]}{ei} d\beta\right]$;

DeltaAZ1A=FullSimplify $\left[\int_{\alpha}^{(\pi-\alpha)} \frac{\text{NN}[\beta]\delta\text{NAZ1}[\beta]}{ae} d\beta\right]$;

DeltaAZ1=DeltaAZ1F + DeltaAZ1A;

Deformation due to virtual force (Flexural + Axial)

F11F=FullSimplify $\left[\int_{\alpha}^{(\pi-\alpha)} \frac{\delta\text{MBX1}[\beta]\delta\text{MBX1}[\beta]}{ei} d\beta\right]$;

F11A=FullSimplify $\left[\int_{\alpha}^{(\pi-\alpha)} \frac{\delta\text{NBX1}[\beta]\delta\text{NBX1}[\beta]}{ae} d\beta\right]$;

F11=F11F + F11A;

F12F=FullSimplify $\left[\int_{\alpha}^{(\pi-\alpha)} \frac{\delta\text{MBX1}[\beta]\delta\text{MBZ1}[\beta]}{ei} d\beta\right]$;

F12A=FullSimplify $\left[\int_{\alpha}^{(\pi-\alpha)} \frac{\delta\text{NBX1}[\beta]\delta\text{NBZ1}[\beta]}{ae} d\beta\right]$;

F12=F12F + F12A;

F13F=FullSimplify $\left[\int_{\alpha}^{(\pi-\alpha)} \frac{\delta\text{MBX1}[\beta]\delta\text{MAZ1}[\beta]}{ei} d\beta\right]$;

F13A=FullSimplify $\left[\int_{\alpha}^{(\pi-\alpha)} \frac{\delta\text{NBX1}[\beta]\delta\text{NAZ1}[\beta]}{ae} d\beta\right]$;

F13=F13F + F13A;

$$\text{F22F=FullSimplify}\left[\int_{\alpha}^{(\pi-\alpha)} \frac{\delta\text{MBZ1}[\beta]\delta\text{MBZ1}[\beta]}{ei} d\beta\right];$$

$$\text{F22A=FullSimplify}\left[\int_{\alpha}^{(\pi-\alpha)} \frac{\delta\text{NBZ1}[\beta]\delta\text{NBZ1}[\beta]}{ae} d\beta\right];$$

F22=F22F + F22A;

$$\text{F23F=FullSimplify}\left[\int_{\alpha}^{(\pi-\alpha)} \frac{\delta\text{MBZ1}[\beta]\delta\text{MAZ1}[\beta]}{ei} d\beta\right];$$

$$\text{F23A=FullSimplify}\left[\int_{\alpha}^{(\pi-\alpha)} \frac{\delta\text{NBZ1}[\beta]\delta\text{NAZ1}[\beta]}{ae} d\beta\right];$$

F23=F23F + F23A;

$$\text{F33F=FullSimplify}\left[\int_{\alpha}^{(\pi-\alpha)} \frac{\delta\text{MAZ1}[\beta]\delta\text{MAZ1}[\beta]}{ei} d\beta\right];$$

$$\text{F33A=FullSimplify}\left[\int_{\alpha}^{(\pi-\alpha)} \frac{\delta\text{NAZ1}[\beta]\delta\text{NAZ1}[\beta]}{ae} d\beta\right];$$

F33=F33F + F33A;

F21=F12; F32=F23; F31=F13;

Redundant forces in original structure

Solve[{BXOF11+BZOF12+AZOF13==DeltaBX1,BXOF21+BZOF22+AZOF23==DeltaBZ1,BXOF31+BZOF32 + AZOF33==DeltaAZ1}, {BXO,BZO,AZO}];

FullSimplify[BXO]

$$\frac{Rw\text{Cos}[\alpha]\left(-(\pi-2\alpha)\left(2\left(i-aR^2\right)+\left(2i+aR^2\right)\text{Cos}[2\alpha]\right)-3aR^2\text{Sin}[2\alpha]\right)}{3\left(-4aR^2+\left(i+aR^2\right)(\pi-2\alpha)^2-4aR^2\text{Cos}[2\alpha]+\left(i+aR^2\right)(\pi-2\alpha)\text{Sin}[2\alpha]\right)}$$

3.4.4.2 Original Structure: Reactions and Internal Forces

After the redundant force in the original structure Bxo,Bzo and Azo are computed, remaining support reaction and the internal forces in the original structure are determined using the free body diagram in Figure 3.41. Following is the output from Mathematica illustrating the derivation for computing the support reactions.

Original Strcture: Reactions

Determine vertical reaction at B by taking moment with respect to A (CCW +ve)

$$\text{SigMAO=BYO}\mathbf{2}\text{x1} - \int_{\alpha}^{\pi-\alpha}(\text{x1} + \text{x2})\text{dP}'\boldsymbol{d\theta} + \text{AZO} - \text{BZO};$$

Sol18=Solve[SigMAO==**0**,BYO]**;** BYO=BYO/.Sol18[[**1**]]

$Rw\mathrm{Cos}[\alpha]$

Determine vertical reaction at A by taking summation of forces in the y direction

Sol19=Solve $\left[\mathrm{BYO} - \int_{\alpha}^{\pi-\alpha} \mathrm{dP}'\, d\theta + \mathrm{AYO}{=}{=}\mathbf{0}{,}\mathrm{AYO}\right]$ **;** AYO=AYO/.Sol19[[**1**]]

$Rw\mathrm{Cos}[\alpha]$

Determine horizontal reaction at A by taking summation of forces in the x direction

AXO=BXO**;**

Clear[MO]**;**

MO=FullSimplify $\left[\mathrm{BZO} + \mathrm{BYOx1} + \mathrm{BXOy1} - \mathrm{AZO} - \mathrm{AYOx1} - \mathrm{AXOy1} - \int_{\alpha}^{\pi-\alpha} \mathrm{dP}'\mathrm{x2}\, d\theta\right]$

0

Following is the output from Mathematica, illustrating the derivation for computing the internal forces.

Original Structure: Internal Forces

Summation of forces in the Radial direction ; Shear (+ve outward)

SigFVO= $-$ BXOCos[β] + BYOSin[β] $- \int_{\alpha}^{\beta} \mathrm{dP}'\mathrm{Sin}[\beta]\, d\theta$ + VO**;**

Sol20=Solve[SigFVO==**0**,VO]**;** VO[**β_**]:=VO/.Sol20[[**1**]]**;**

FullSimplify[VO[**β_**]]

$$\begin{aligned}&\left(Rw\left(2\mathrm{Cos}[\alpha]\mathrm{Cos}[\beta]\left(-(\pi-2\alpha)\left(2\left(i-aR^2\right)+\left(2i+aR^2\right)\mathrm{Cos}[2\alpha]\right)-3aR^2\mathrm{Sin}[2\alpha]\right)\right.\right.\\&\quad\left.\left.-3\left(-4aR^2+\left(i+aR^2\right)(\pi-2\alpha)^2-4aR^2\mathrm{Cos}[2\alpha]+\left(i+aR^2\right)(\pi-2\alpha)\mathrm{Sin}[2\alpha]\right)\mathrm{Sin}[2\beta]\right)\right)/\\&\quad\left(6\left(-4aR^2+\left(i+aR^2\right)(\pi-2\alpha)^2-4aR^2\mathrm{Cos}[2\alpha]+\left(i+aR^2\right)(\pi-2\alpha)\mathrm{Sin}[2\alpha]\right)\right)\end{aligned}$$

Summation of forces in the tangential direction; Normal force +(ve Tension)

SigFNO=BXOSin[β] + BYOCos[β] $- \int_{\alpha}^{\beta} \mathrm{dP}'\mathrm{Cos}[\beta]\, d\theta$ + NO**;**

Sol21=Solve[SigFNO==**0**,NO]**;** NO[**β_**]:=NO/.Sol21[[**1**]]**;**

FullSimplify[NO[**β_**]]

$$\begin{aligned}&\left(Rw\left(6\mathrm{Cos}[\beta]^2\left(4aR^2-\left(i+aR^2\right)(\pi-2\alpha)^2+4aR^2\mathrm{Cos}[2\alpha]-\left(i+aR^2\right)(\pi-2\alpha)\mathrm{Sin}[2\alpha]\right)\right.\right.\\&\quad\left.\left.+2\mathrm{Cos}[\alpha]\left((\pi-2\alpha)\left(2\left(i-aR^2\right)+\left(2i+aR^2\right)\mathrm{Cos}[2\alpha]\right)+3aR^2\mathrm{Sin}[2\alpha]\right)\mathrm{Sin}[\beta]\right)\right)/\\&\quad\left(6\left(-4aR^2+\left(i+aR^2\right)(\pi-2\alpha)^2-4aR^2\mathrm{Cos}[2\alpha]+\left(i+aR^2\right)(\pi-2\alpha)\mathrm{Sin}[2\alpha]\right)\right)\end{aligned}$$

Summation of moments; Internal moment (CW +ve)

```
Clear[MO];
```

$$\text{SigMO}=\text{BXOy4}-\text{BYOx5}+\text{BZO}+\int_{\alpha}^{\beta}\text{dP}'\text{x4}\,\boldsymbol{d\theta}+\text{MO};$$

```
sol22=Solve[SigMO==0,MO]; MO[β_]:=MO/.sol22[[1]];
```

```
FullSimplify[MO[β_]]
```

$$\left(R^2 w\left(9\left(-3i+aR^2\right)\text{Cos}[\alpha]^2+3\text{Cos}[2\beta]\left(4aR^2-\left(i+aR^2\right)(\pi-2\alpha)^2+4aR^2\text{Cos}[2\alpha]-\left(i+aR^2\right)(\pi-2\alpha)\text{Sin}[2\alpha]\right)+\text{Cos}[\alpha]\left(-\left(5i+aR^2\right)\text{Cos}[3\alpha]-6\left(i+aR^2\right)(\pi-2\alpha)\text{Sin}[\alpha]+4\left((\pi-2\alpha)\left(2\left(i-aR^2\right)+\left(2i+aR^2\right)\text{Cos}[2\alpha]\right)+3aR^2\text{Sin}[2\alpha]\right)\text{Sin}[\beta]\right)\right)\right)/\left(12\left(-4aR^2+\left(i+aR^2\right)(\pi-2\alpha)^2-4aR^2\text{Cos}[2\alpha]+\left(i+aR^2\right)(\pi-2\alpha)\text{Sin}[2\alpha]\right)\right)$$

3.4.4.3 Deflection

The process to compute the deflection in Hingeless circular arch under uniformly distributed load as well as the numerical values used for the trigonometric variable are similar to that under Self-weight and therefore it is not show here.

3.4.4.4 Summary Of Results

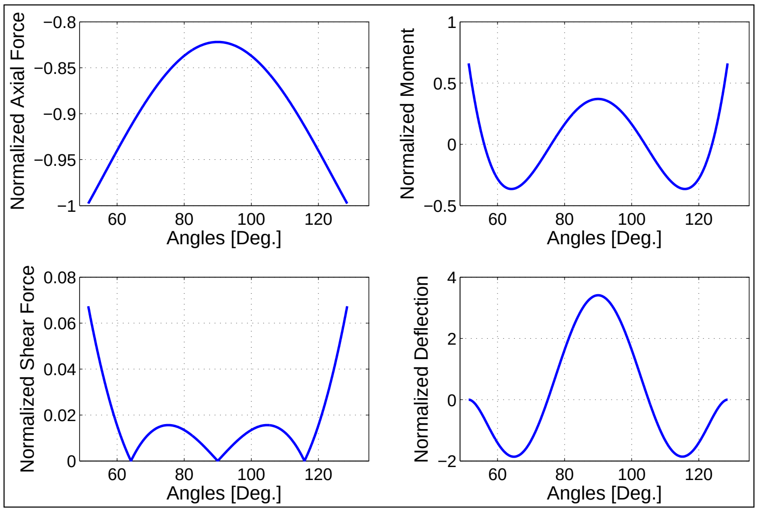

Figure 3.43: Plots for the Hingeless circular arch under UDL

Figure 3.43 show plots for the Hingeless arch under uniformly distributed load discussed in the above section. The internal axial force and shear force are normalized with respect to the resultant of vertical reaction and thrust at the abutments. The axial compressive force is highest at the abutments and it decreases toward the crown to about 82.5% of the maximum value. The shear force on other hand is comparatively low and it varies between about 6.75% and 1.75%, respectively from the abutment to the crown. The internal moment is normalized with respect to the product of internal axial force and the rise. The internal moment is highest at the abutments and it is about 67 % of the maximum value at the crown and at about $\frac{1}{6}$ of span from the abutments. There are four inflection points in the moment diagram and they correspond with the zero deflection points in the arch. The Deflection is highest at the crown and the graph of deflection follows similar profile as that of the moment diagram. Positive and negative deflection corresponds with positive and negative moment in the arch respectively.

3.4.5 Hingeless Circular Arch: Validation

The analytical equations developed above for the Hingeless circular arch under point load, self-weight and uniformly distributed load are validated in two steps. Firstly, the self weight and uniformly distributed load applied across the arch span are divided in series of 20 point loads. The graphs of internal forces and deflections are plotted using the analytical equations for self weight and uniformly distributed load together with their respective point loads. These graphs are superimposed to check the validity of the analytical solutions. As the self-weight or the uniformly distributed load are equivalent to their respective series of point loads their plots closely match with each other.

Figure 3.44 and Figure 3.45 illustrates the above discussed process used for validating the analytical equations. Secondly, a Sap 2000 model is developed for the Hingeless circular arch under self-weight. The moment, shear force and axial force diagrams of its analysis are compared with the graphs plotted using the analytical equation The numerical values on the moment diagram in Figure 3.46, axial force diagram in Figure 3.47 and shear force diagram in Figure 3.48 closely matches with their respective values on the graphs in Figure3.44.

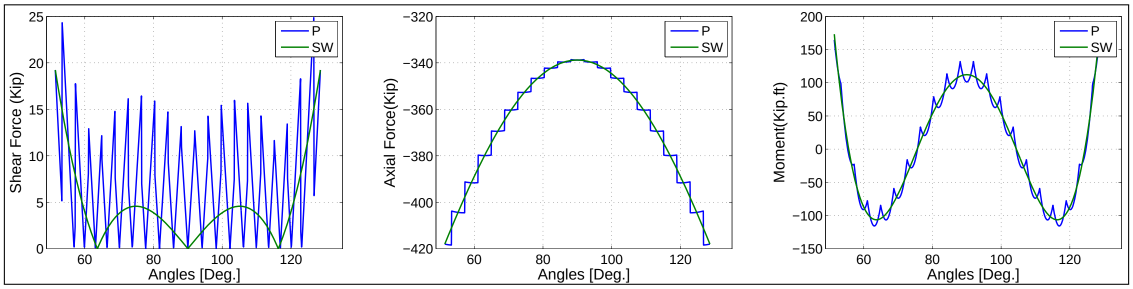

Figure 3.44: Hingeless circular arch under self-weight vs. series of point load

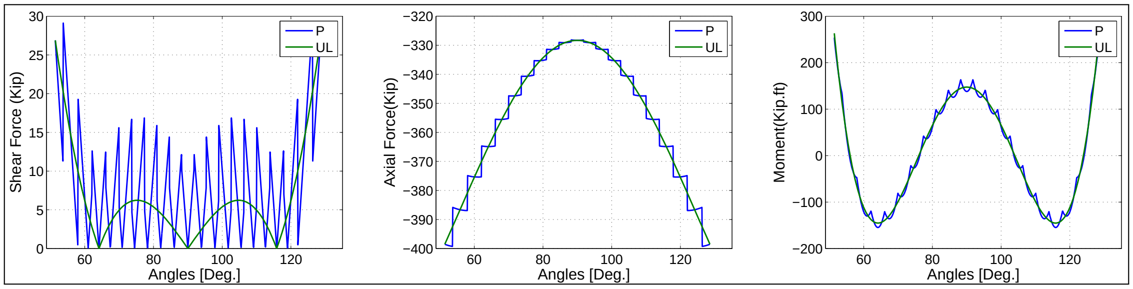

Figure 3.45: Hingeless circular arch under uniformly distribute load vs. series of point load

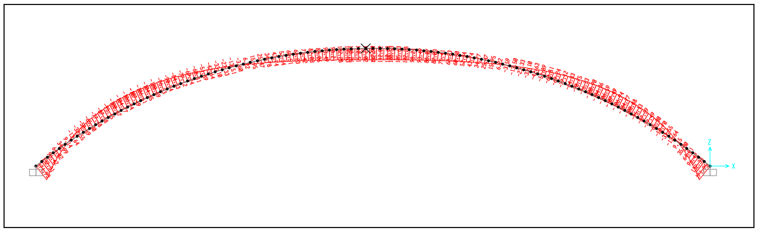

Figure 3.46: SAP 2000 - Moment diagram of Hingeless circular arch under self-weight

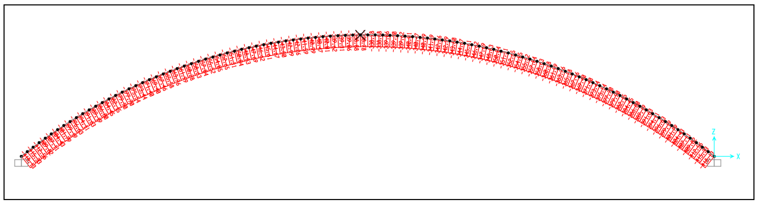

Figure 3.47: SAP 2000 - Axial force diagram of Hingeless circular arch under self-weight

3.4.6 Conclusion

This sections discuss the structural behavior of a Hingeless arch under point load, Self-weight and Uniformly distributed load in terms of internal forces and deflection. Figure 3.49 compares

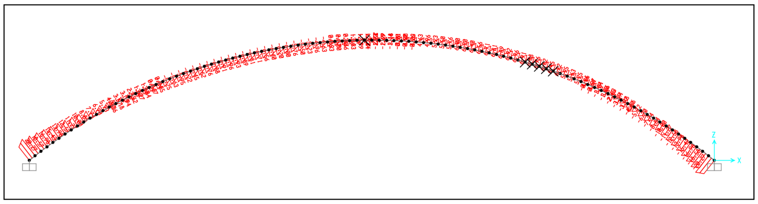

Figure 3.48: SAP 2000 - Shear force diagram of Hingeless circular arch under self-weight

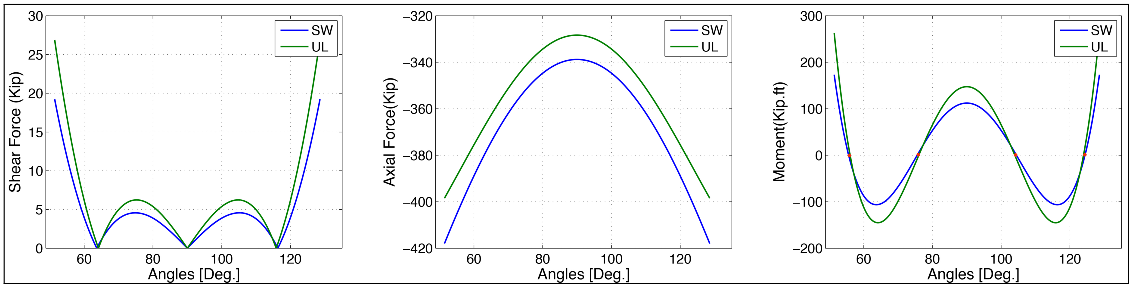

Figure 3.49: Hingeless circular arch under self-weight vs.UDL

the self- Weight loading condition with the uniformly distributed loading condition under an equal load w=2.275 kip/ft.Compared to the self-weight, a uniformly distributed load causes more internal shear force, moment and deflection, and it causes less internal compressive axial force. Figure 3.50 show plots of an asymmetric loading condition.For this purpose, a unit load is applied at the crown and at the quarter of the span. Under this condition, the maximum moment due to the point load applied at the quarter of the span is about 1.2 times more than that applied at the crown. The maximum axial force due to the point load applied at the crown of the span is about 1.3 times

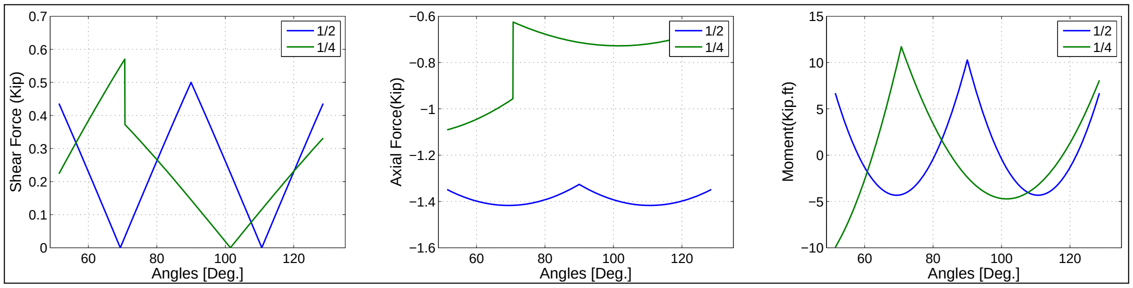

Figure 3.50: Hingeless circular arch under point load at 1/2 and 1/4 span

more than that applied at the at the quarter of the span.

3.5 Conclusion

The focus of this chapter was to develop analytical equations for the support reactions and internal forces in Three-hinged, Two-hinged and Hingeless arch and use these equations to understand structural behavior of each type of the arch. Three-hinged arch being statically determinate only needed ordinary methods of static to derive the analytical equations. On the other hand, for statically indeterminate Two-hinged arch and Hingeless arch, virtual work method together with the compatibility equation for the deformation was used.

Each type of arch was analyzed under three loading conditions point load, self-weight and uniformly distributed load. Under symmetric loading, the primary difference found between the three types of arch is the number of inflection points in their moment diagram and its effect on moment distribution across the arch span. As seen in Figure 3.15 a three-hinge arch has no inflection point and has high negative moment between adjoining hinges. As shown in Figure 3.33 with red dots a Two-hinged arch has two inflections and has high positive moment at the crown. As shown in Figure 3.49 with red dots a Hingeless arch has four inflection points and has high positive moment at the abutments. For all three arches, comparison between the self- weights and uniformly distributed loading condition indicate that the self- weight contributes more toward the internal axial force where as the uniformly distributed load contributes more towards the internal moment. This demonstrates the unique compressive mechanism of an arch to resists its self-weight.

The plots of internal forces for each type of arch indicated that when a point load applied at the crown of an arch causes different pattern of internal forces as compared to self-weight of the arch or uniformly distributed load applied on the entire span of an arch. When a point load is applied at the crown of a Two-hinged or a Hingeless arch it causes maximum axial force at a distance of about $\frac{1}{4}$ to $\frac{1}{6}$ of the span from the abutments and it causes maximum moment at the crown. When a point load is applied at the crown of a Three-hinged arch it causes maximum axial force and moment at a distance of about $\frac{1}{4}$ of the span from the abutments. When the self-weight or uniformly distributed load is applied on a Three-hinged or a Two hinged arch it causes maximum axial force at the abutments and maximum moment at a distance of $\frac{1}{6}$ of the span from the abutments but when same forces are applied on a Hinges arch both maximum axial force and moment occurs at the abutments. Maximum deflection for all the three type arches under self-weight or uniformly distributed load occurs at the crown of the arch. Understating of variation in the internal forces and deflection of the studies arches can be applied toward optimizing their cross section as well as compressive and flexural strength.

For all the type of arches, the analysis also compared internal forces caused due to a point load applied at the crown and at $\frac{1}{4}$ of the span. The result shows that maximum moment occurs when a point load is applied at the $\frac{1}{4}$ of span where as maximum axial force occurs when it is applied at the crown. In general, an asymmetric loading condition in all the three type of arches causes substantially high internal moment compared to a symmetric loading. This relationship of location of a point load with the internal force can be used towards deriving appropriate locations for the piers in case of an open spandrel arch bridge design. From the analysis results, it can be said that a symmetric layout of piers about the center of the arch will provide an efficient design solution.

For the compatibility equations shown in the ‘Original Structure: Redundant Force‘ section of Two-hinges and Hinges arch, both axial and flexural components are considered. It was observed that multiple existing literatures on the arch analysis only use the flexural component of the compatibility equation. While this has negligible effect on the internal forces of Two-hinged arch, it was found that omitting the axial component would cause about 20% error in the internal moment of Hingeless arch.

To validate the analytical solutions, Sap 2000 program was used. Currently there is no readily available arch component and hence multiple segments are used to construct an arch in Sap 2000. The validation process indicted that not having optimum number of segments could cause substantial error in the computation of internal forces. The analytical equations developed here can serve as a preliminary tool to find internal forces in an arch.

Chapter 4

Preliminary Sizing of Circular Arch

4.1 Introduction

The analytical equations of internal forces and support reactions for Three-hinged, Two-hinged and Hingeless circular arch are developed and validated in the previous chapter. In this chapter, these equations are used to compare internal forces and support reaction of a circular arch with that of a parabolic arch. Further they are used for preliminary sizing of the compared circular arch rib. As purpose of this exercise is mainly to check application of the analytical equations, no particular AASHTO or other design specifications are used to determine a preliminary size of the arch rib. For the purpose of comparison as well as preliminary sizing the Hoover Dam Bypass Colorado River Bridge (US 93) (OPAC/HDR/T.Y.LIN2003, 2003, pg 1-392) project is considered. It was constructed with cast-in -place prestress concrete parabolic arch using cantilever segmented construction method.

4.2 Comparison: Parabolic and Circular Arch

4.2.1 Geometry of Parabolic and Circular Arch

To understand the difference between parabolic and circular arch form, their internal forces and support reaction are compared here. The Hoover Dam Bypass Colorado River Bridge (US 93) (OPAC/HDR/T.Y.LIN2003, 2003, pg 1-392) shown in Figure 4.1 has cast-in-place prestreesed concrete twin parabolic arch ribs that are connected by steel strut. Each parabolic arch is Hingless and has span of 1060 ft and rise of 277ft is made of 53 rectangular segments. To simplify the process, only one parabolic arch with its associated loading is compared with a circular arch of same rise, span, rib cross-section and loading.

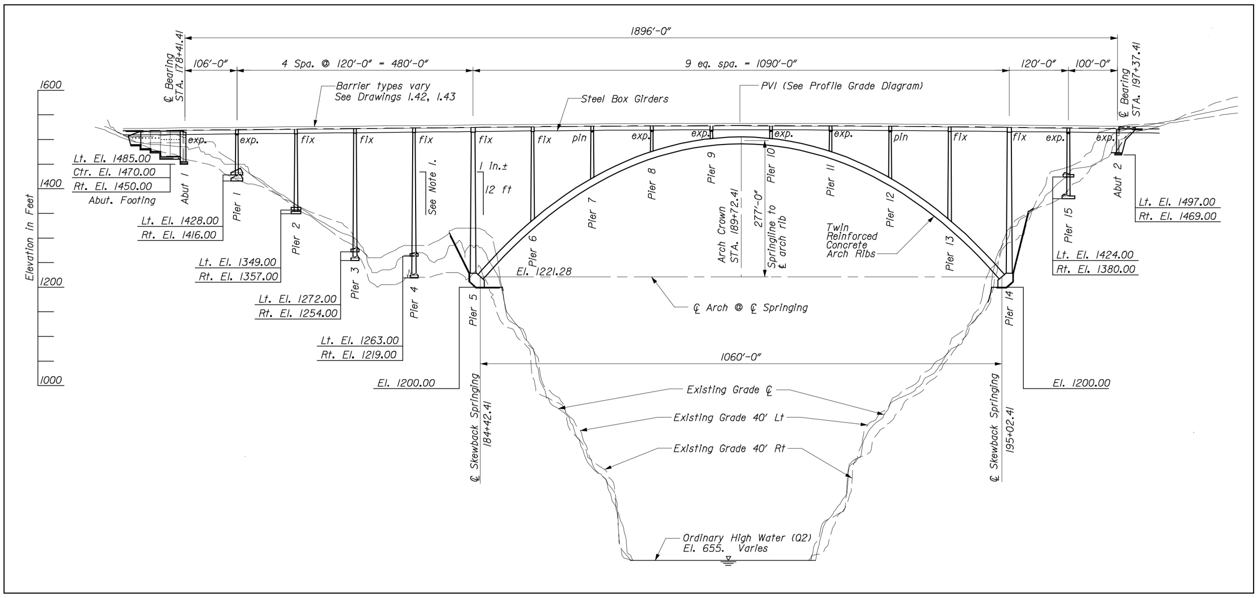

Figure 4.1: Elevation: The Hoover Dam Bypass Colorado River Bridge(US 93)

Figure 4.2 show the geometrical difference between the parabolic bridge arch and the considered circular arch.

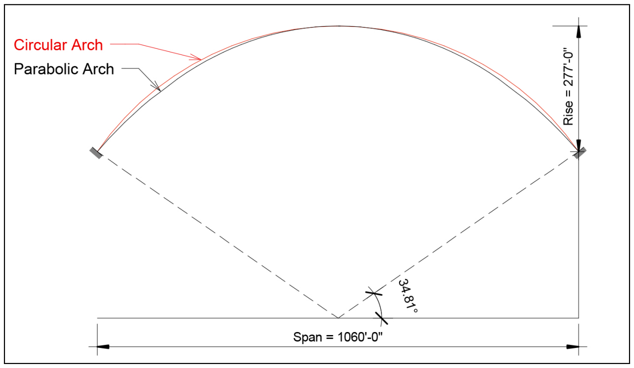

Figure 4.2: Comparison of Parabolic and Circular Arch

4.2.2 Load calculations

In Hoover dam bypass bridge project the live load and dead load of steel girders, concrete deck, stay-in-place forms, concrete bridge railing and steel pedestrian railing are transferred to the parabolic arch through six equally spaced tapering precast concrete piers. The construction document of this project is used for information regarding the applied load (OPAC/HDR/T.Y.LIN2003, 2003, pg267). An excel sheet shown in Figure 4.4 is prepared to compute dead load of tapering piers and the arch. Figure 4.3 show the arch rib cross section of the Hoover dam bypass bridge, which is used to calculate its dead load.The cross sectional area of the rib varies from abutments to the crown. The Area of steel used at the abutment and the crown is about 1.7% and 0.7% respectively of the cross sectional area of concrete.

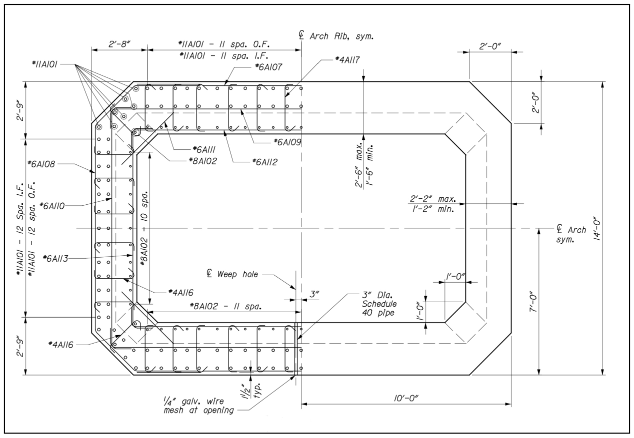

Figure 4.3: Arch Rib Cross Section

The original design of the Hoover dam bypass bridge has used three loading combinations, Strength I, Strength II and Extreme Event I, where Strength I and Strength II are associated with gravity loading and Extreme Event I is associated with lateral loading. As the analytical equation are developed for the gravity loading only, Strength I combination that produces higher gravity loads is considered for this exercise.

Strength I = 1.25 DC + 1.5 DW + 1.75 LL + 1WA+ 1FR+ 1.2 TU+ 1TG + 1 SE

Where

DC	Load of Component and attachments
DW	Load of Wearing surface and utilities
LL	Live Load
TG	Force due to temperature gradient
TU	Force due to uniform temperature
SE	Force due to settlement
WA	wind load
FR	Friction load

The WA, FR, TU, TG and SE components of the load combination are ignored for the load calculation. Figure 4.4 illustrates the load calculations.

4.2.3 Forces in Parabolic and Circular Arch

A SAP model is made using 53 rectangular segments similar to that of the parabolic arch in Hoover Dam bypass bridge, to determine its internal forces and support reactions. To this model, the loads calculated for each pier in Figure 4.4 are applied as point load , where as the dead load of the arch is applied as distributed self-weight. Following Figure 4.5, Figure 4.6, Figure 4.7, show the analysis results of the SAP Model for support reaction, internal moment and axial force respectively.The inflection points in the moment diagram indicate locations of the spandrel piers. Where,

Abutment Thrust = 28301 kips

Vertical Reaction = 30038 kips

Maximum Factored Internal Moment = 3.43 x 10^5 Kip.ft

Maximum Factored Internal Axial Force = 4.12 x 10^4 Kip

Similar to the SAP model , the loads calculated for each pier in Figure 4.4 are considered as

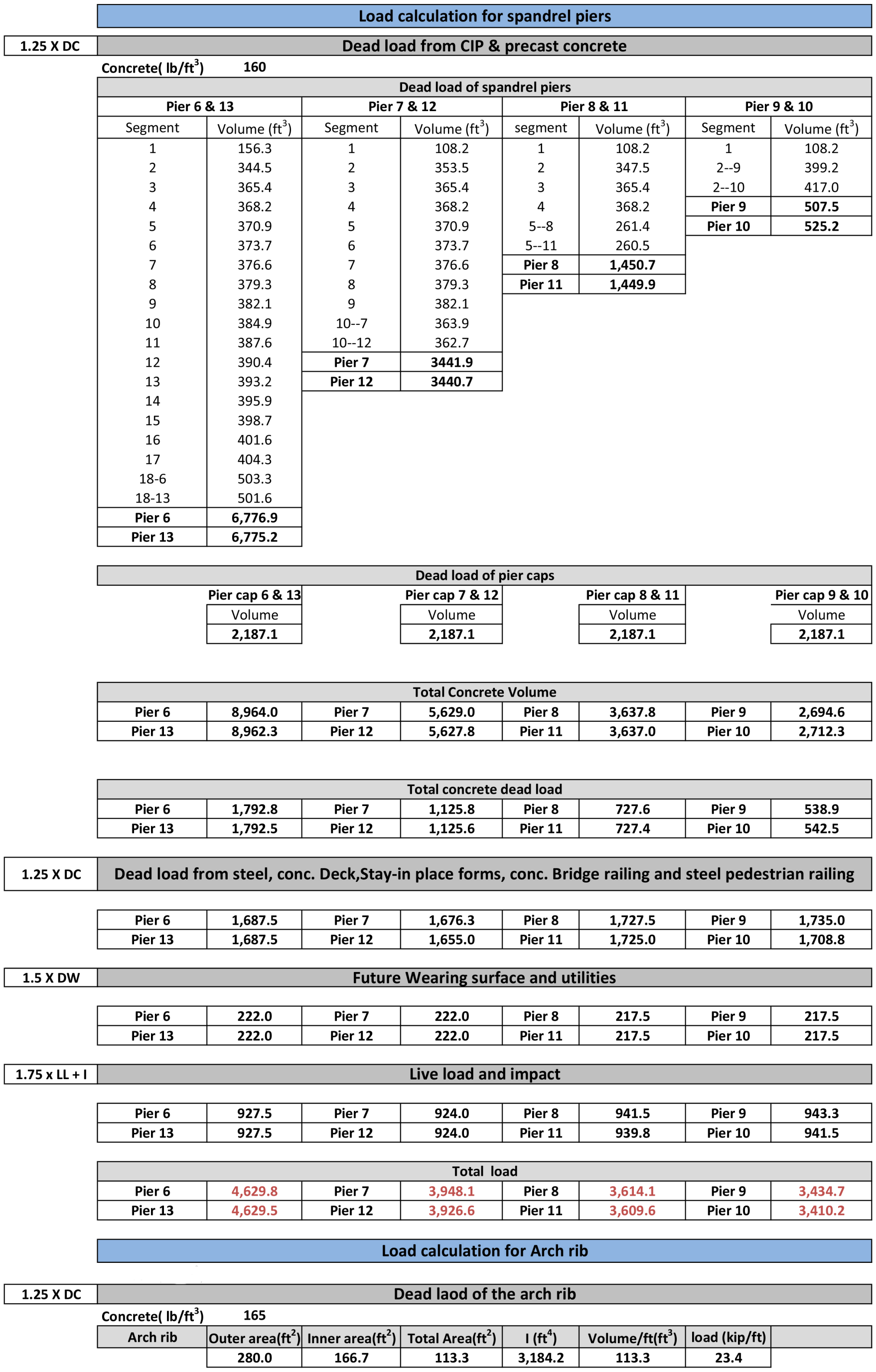

Load calculation for spandrel piers

1.25 X DC — **Dead load from CIP & precast concrete**

Concrete(lb/ft^3) **160**

Dead load of spandrel piers							
Pier 6 & 13		**Pier 7 & 12**		**Pier 8 & 11**		**Pier 9 & 10**	
Segment	Volume (ft^3)	Segment	Volume (ft^3)	segment	Volume (ft^3)	Segment	Volume (ft^3)
1	156.3	1	108.2	1	108.2	1	108.2
2	344.5	2	353.5	2	347.5	2--9	399.2
3	365.4	3	365.4	3	365.4	2--10	417.0
4	368.2	4	368.2	4	368.2	**Pier 9**	**507.5**
5	370.9	5	370.9	5--8	261.4	**Pier 10**	**525.2**
6	373.7	6	373.7	5--11	260.5		
7	376.6	7	376.6	**Pier 8**	**1,450.7**		
8	379.3	8	379.3	**Pier 11**	**1,449.9**		
9	382.1	9	382.1				
10	384.9	10--7	363.9				
11	387.6	10--12	362.7				
12	390.4	**Pier 7**	**3441.9**				
13	393.2	**Pier 12**	**3440.7**				
14	395.9						
15	398.7						
16	401.6						
17	404.3						
18-6	503.3						
18-13	501.6						
Pier 6	**6,776.9**						
Pier 13	**6,775.2**						

Dead load of pier caps			
Pier cap 6 & 13	**Pier cap 7 & 12**	**Pier cap 8 & 11**	**Pier cap 9 & 10**
Volume	Volume	Volume	Volume
2,187.1	**2,187.1**	**2,187.1**	**2,187.1**

Total Concrete Volume							
Pier 6	**8,964.0**	**Pier 7**	**5,629.0**	**Pier 8**	**3,637.8**	**Pier 9**	**2,694.6**
Pier 13	**8,962.3**	**Pier 12**	**5,627.8**	**Pier 11**	**3,637.0**	**Pier 10**	**2,712.3**

Total concrete dead load							
Pier 6	**1,792.8**	**Pier 7**	**1,125.8**	**Pier 8**	**727.6**	**Pier 9**	**538.9**
Pier 13	**1,792.5**	**Pier 12**	**1,125.6**	**Pier 11**	**727.4**	**Pier 10**	**542.5**

1.25 X DC — **Dead load from steel, conc. Deck,Stay-in place forms, conc. Bridge railing and steel pedestrian railing**

Pier 6	**1,687.5**	**Pier 7**	**1,676.3**	**Pier 8**	**1,727.5**	**Pier 9**	**1,735.0**
Pier 13	**1,687.5**	**Pier 12**	**1,655.0**	**Pier 11**	**1,725.0**	**Pier 10**	**1,708.8**

1.5 X DW — **Future Wearing surface and utilities**

Pier 6	**222.0**	**Pier 7**	**222.0**	**Pier 8**	**217.5**	**Pier 9**	**217.5**
Pier 13	**222.0**	**Pier 12**	**222.0**	**Pier 11**	**217.5**	**Pier 10**	**217.5**

1.75 x LL + I — **Live load and impact**

Pier 6	**927.5**	**Pier 7**	**924.0**	**Pier 8**	**941.5**	**Pier 9**	**943.3**
Pier 13	**927.5**	**Pier 12**	**924.0**	**Pier 11**	**939.8**	**Pier 10**	**941.5**

Total load							
Pier 6	**4,629.8**	**Pier 7**	**3,948.1**	**Pier 8**	**3,614.1**	**Pier 9**	**3,434.7**
Pier 13	**4,629.5**	**Pier 12**	**3,926.6**	**Pier 11**	**3,609.6**	**Pier 10**	**3,410.2**

Load calculation for Arch rib

1.25 X DC — **Dead laod of the arch rib**

Concrete(lb/ft^3) **165**

Arch rib	**Outer area(ft^2)**	**Inner area(ft^2)**	**Total Area(ft^2)**	**I (ft^4)**	**Volume/ft(ft^3)**	**load (kip/ft)**
	280.0	**166.7**	**113.3**	**3,184.2**	**113.3**	**23.4**

Figure 4.4: Load Calculations

point load case , where as the dead load of the arch is considered as distributed self-weight case while using the analytical equations of the circular.Following Figure 4.8 show the plots of the two

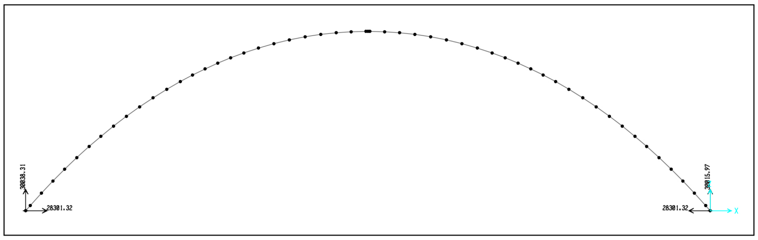

Figure 4.5: Support Reactions in the Parabolic Arch

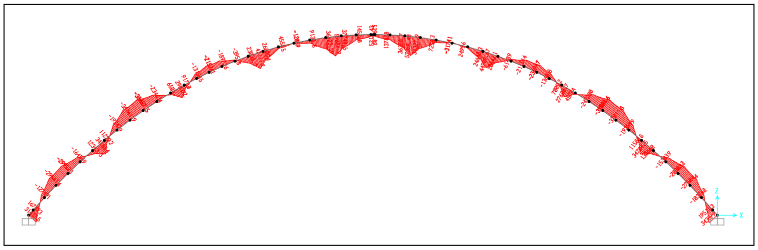

Figure 4.6: Internal Moment in the Parabolic Arch

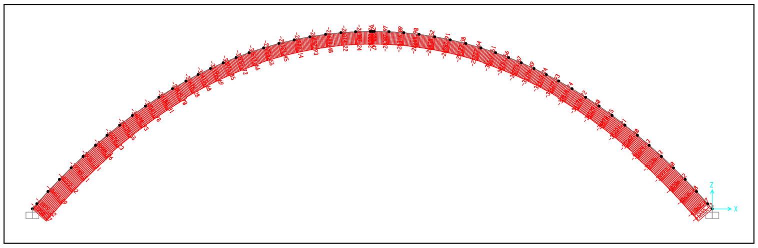

Figure 4.7: Internal Axial Force in the Parabolic Arch

superimposed load cases. Where,

Abutment Thrust = 29328 kips

Vertical Reaction = 30126 kips

Maximum Factored Internal Moment = 3.8 x 10^5 Kip.ft

Maximum Factored Internal Axial Force = 4.15 x 10^4 Kip

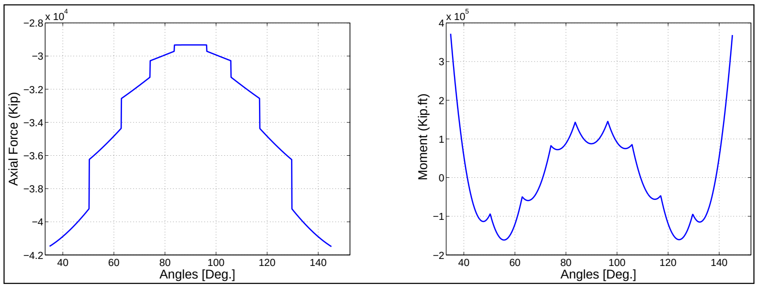

Figure 4.8: Internal Moment and Axial Force in the Circular Arch

4.2.4 Conclusion

The comparison between circular and parabolic arch form showed that a small variation in the curvature of an arch affects its internal forces and support reactions. A parabolic arch and a circular arch of similar Span, rise and cross section are compared in the above-discussed example. The thrust and vertical reaction in the circular arch are about 3% and 0.3% respectively more than that of the parabolic arch. In the circular arch the maximum internal moment is 10.5% and the maximum internal axial force is about 0.65% more than that of the parabolic arch. Overall the parabolic arch has lower internal forces than the circular arch. From this observation it can be said that for an open spandrel bridge a parabolic arch will procure a more efficient design solution.

4.3 Preliminary Sizing of Circular Arch

The example of Hoover Dam Bypass Bridge is further used here to demonstrate preliminary cross section sizing of the circular arch rib. Prestressed concrete has been used in the original design of the Hoover Dam Bypass Bridge -parabolic arch where as a mild steel design is assumed for this preliminary sizing exercise. In real life projects the axial and flexural strength of the arch rib is checked at all locations across the arch span. For simplification, in this preliminary sizing exercise the axial and flexural strength is only checked for two combinations of internal moment and axial force.

For the first design iteration, a hollow core rectangular rib of following cross sectional properties is considered,

Outer dimension = 20ft x 14ft, Inner dimension = 16ft x 10ft, Wall thickness =2ft,

Cross Sectional Area of concrete (Ac) = $120 ft^2$, Moment of Inertia = 3240 ft^4,

Weight /ft. = 120 x 165 = 19.8 kip/ft , Strength I Weight /ft. = 19.8 x 1.25 = 24.75 kip/ft, Area of steel (As) = 213.3 in^2, Concrete Strength = 10,000 Psi and Steel Strength = 60 Ksi

Figure 4.9 show the layout of longitudinal and transverse mild steel rebar used for the first design iteration. The area of the mid steel used is about 1.23% of the cross sectional area of concrete.

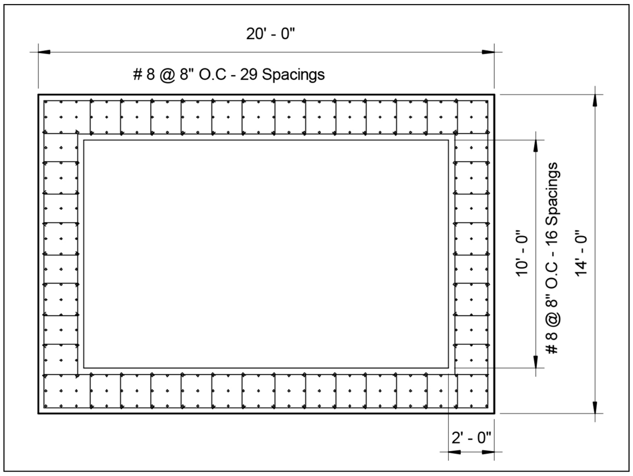

Figure 4.9: Circular Arch Rib - Design Iteration 1

Loads calculated for each pier of the Hoover Dam Bypass Bridge in Figure 4.4 are used as point loads and the dead load of the arch design shown in Figure 4.9 is considered as distributed self-

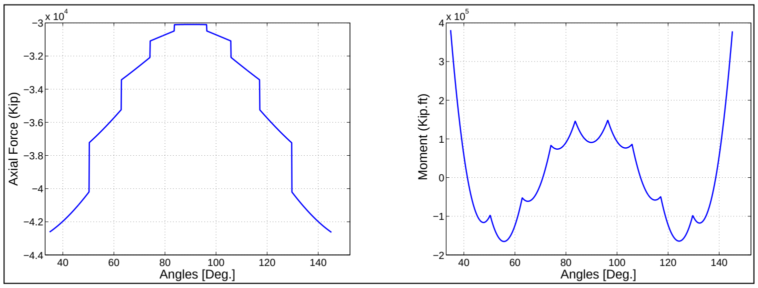

Figure 4.10: Internal and Axial Force in the First Design Iteration

weight. Figure 4.10 show the internal moment and axial force computed for this design using the analytical equations.

This design is checked for two combinations of internal moment and internal axial force are used. Even though these combinations may not occur at the same location, they represent two extreme combinations. Following is the first combination used for the check.

Maximum Factored Internal Moment = 3.81 x 10^5 Kip.ft

Maximum Factored Internal Axial Force = 4.26 x 10^4 Kip.

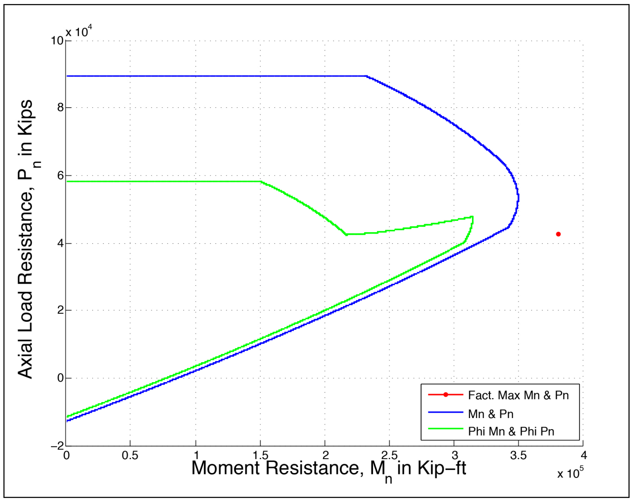

Figure 4.11: Strength Interaction Diagram for 1st Design Iteration (Prusinski, 2015)

A strength interaction diagram Figure 4.11 under combined bending and axial load is constructed for the first design iteration. For this purpose a Matlab code developed in (Prusinski, 2015) is used. A point representing the above mentioned maximum factored internal moment and axial force is plotted on the interaction diagram. As it falls outside the interaction diagram the first design iteration is inadequate for the considered combination of internal moment and internal axial force.

For the second design iteration, a hollow core rectangular rib of following cross sectional properties is considered,

Outer dimension = 20 ft x 16ft , Inner dimension = 15ft x 11ft, Wall thickness = 2.5ft

Cross Sectional Area of concrete (Ac) = 155 ft^2, Moment of Inertia = 5162 ft^4 , Weight /ft. = 155 x 165 = 25.57 kip/ft , Strength I Weight /ft. = 25.57 x 1.25 = 31.97 kip/ft, Area of steel (As) = 360 in^2, Concrete Strength = 10,000 Psi and Steel Strength = 60 Ksi

Figure 4.12 show the layout of longitudinal and transverse mild steel rebar used for the second design iteration. The area of the mid steel used is about 1.61% of the cross sectional area of concrete.

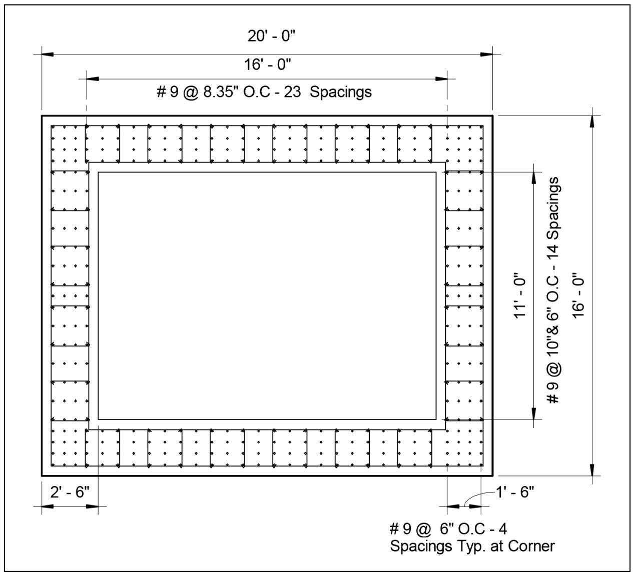

Figure 4.12: Circular Arch Rib - Design Iteration 2

Similar to the first design iteration, loads calculated for each pier of the Hoover Dam Bypass Bridge in Figure 4.4 are used as point loads and the dead load of the arch design shown in Figure 4.12 is considered as distributed self-weight. Figure 4.13 show the Internal moment and axial force

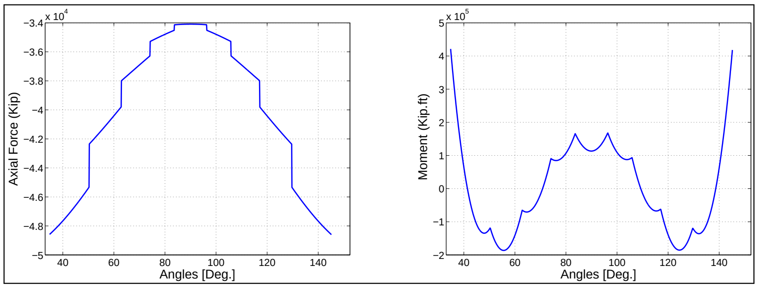

Figure 4.13: Internal and Axial Force in the Second Design Iteration

computed for this design using the analytical equations. The figure also shows that at an angle of 37.57 degree and onwards the internal moment is about half of the maximum value. Therefore the design in optimized for the section of the arch at an angle 37.57 degree and onwards.

This design for the section of the arch between abutment and angle 37.57 degree is checked for two combinations of internal moment and internal axial force. Even though these combinations may not occur at the same location, they represent two extreme combinations. Following is the first combination used for the check.

Maximum Factored Internal Moment = 4.21 x 10^5 Kip.ft

Maximum Factored Internal Axial Force = 4.85 x 10^4 Kip

A strength interaction diagram Figure 4.14 under combined bending and axial load is constructed for the second design iteration. A point representing the above mentioned maximum factored internal moment and axial force is plotted on the interaction diagram. As it falls inside the interaction diagram the second design iteration is adequate for the first combination of internal moment and internal axial force.

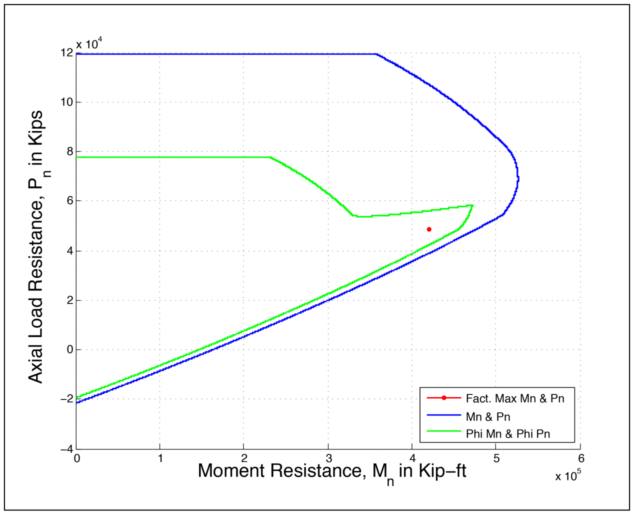

Figure 4.14: Strength Interaction Diagram for 2nd Design Iteration (Prusinski, 2015)

Further the second combination of internal moment and internal axial force is checked against the interaction diagram. Following is the second combination used for the check.

Maximum Factored Internal Moment = 4.21×10^5 Kip.ft

Minimum Factored Internal Axial Force = 4.80×10^4 Kip

Figure 4.15 shows a point representing the above mentioned maximum factored internal moment and minimum factored axial. As it falls inside the interaction diagram the second design iteration is adequate for the second combination of internal moment and internal axial force.

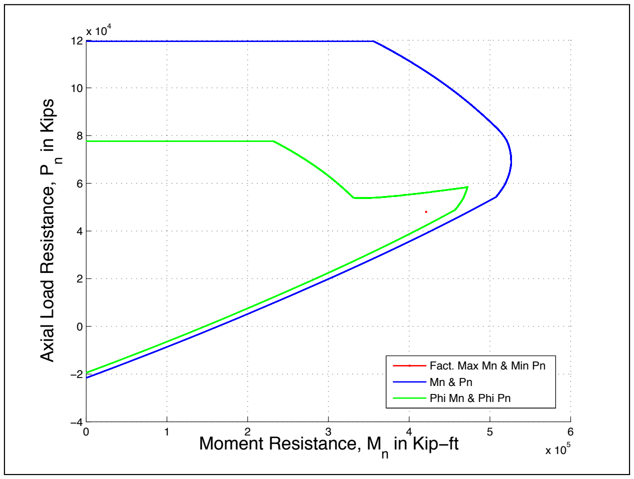

Figure 4.15: Strength Interaction Diagram for 2nd Design Iteration (Prusinski, 2015)

The second design iteration is proved to be satisfactory for both the considered combinations of internal forces. Further checks are required for all locations between the abutment and the angle 37.57 degree to confirm the adequacy of this design. For purpose of this exercise it is assumed that the design iteration is adequate for the considered section of the arch.

The second design iteration is further optimized for the section of the circular arch span where the internal forces are lesser that the maximum values. Figure 4.16 show the optimized version of the second design iteration which can be used for the span of the arch at an angle 37.57 degrees and onwards from both the abutments. All the properties of the cross section are same as that of the second design iteration with exception of the steel are which is reduced to 1.12% of the cross sectional concrete area.

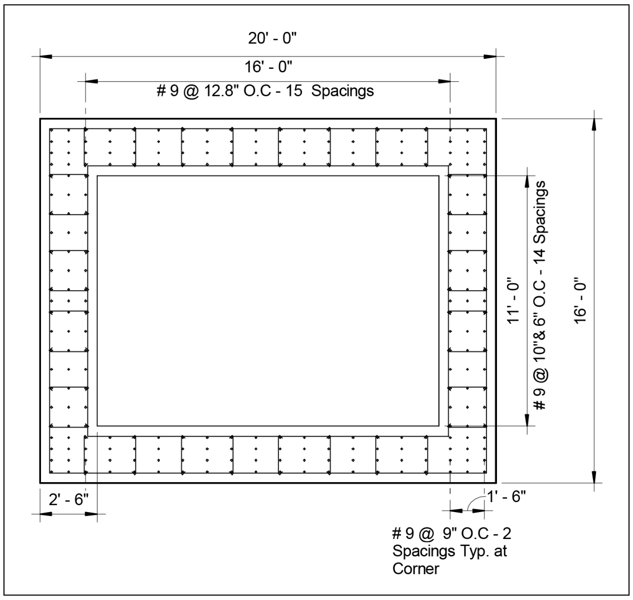

Figure 4.16: Circular Arch Rib - Optimized Design Iteration 2

Once again two combinations of internal moment and internal axial force are used. Even though these combinations may not occur at the same location, they represent two extreme combinations. Following is the first combination used for the check.

Maximum Factored Internal Moment = 2.07 x 10^5 Kip.ft

Maximum Factored Internal Axial Force = 4.8 x 10^4 Kip

A strength interaction diagram Figure 4.17 under combined bending and axial load is constructed for the second design iteration. A point representing the above mentioned maximum factored internal moment and axial force is plotted on the interaction diagram. As it falls inside the interaction diagram the optimized second design iteration is adequate for the first combination of internal moment and internal axial force.

Further the second combination of internal moment and internal axial force is checked against the interaction diagram. Following is the second combination used for the check. Maximum Factored Internal Moment = 2.07 x 10^5 Kip.ft

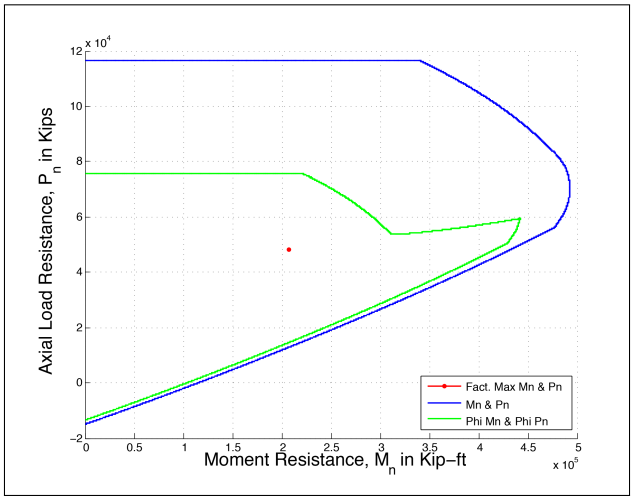

Figure 4.17: Strength Interaction Diagram for Optimized 2nd Design Iteration (Prusinski, 2015)

Minimum Factored Internal Axial Force = 3.414 x 10^4 Kip

Figure 4.18 shows a point representing the above mentioned maximum factored internal moment and minimum factored axial. As it falls inside the interaction diagram the optimized second design iteration is adequate for the second combination of internal moment and internal axial force.

The optimized second design iteration is proved to be satisfactory for both the considered combinations of internal forces. Further checks are required for all locations between the angle 37.57 degrees and onwards from both the abutments. For purpose of this exercise it is assumed that the design iteration is adequate for the considered section of the arch.

Table 4.3 compares the design of the Hoover Dam Bridge - Parabolic arch rib with the preliminary design of the circular arch rib. Even though the internal moment in the circular arch is more than that in the parabolic arch, the area computed for the circular arch is similar to that used in the parabolic arch. It can be said that the additional steel used in the parabolic arch is to compensate for the stresses developed during the cantilevered construction of the arch.

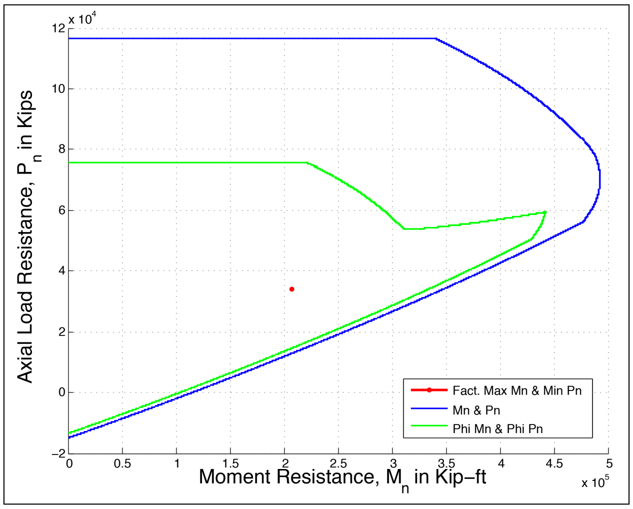

Figure 4.18: Strength Interaction Diagram for Optimized 2nd Design Iteration (Prusinski, 2015)

Type of an Arch	Area of concrete	Area of Steel	ρ
Parabolic Arch	19,972 in^2	340 in^2	1.7
Parabolic Arch-Optimized	12,283 in^2	85 in^2	0.7
Circular Arch-Iteration 1	17,280 in^2	213.3 in^2	1.25
Circular Arch-Iteration 2	22,320 in^2	360 in^2	1.65
Circular Arch-Optimized Iteration 2	22,320in^2	250in^2	1.12

Table 4.1: Comparison of Parabolic and Circular Arch Rib Design

4.4 Conclusion

For the process of preliminary sizing of the circular arch rib cross-section, mainly a strength interaction diagram under combined bending and axial load has been used to check the adequacy of the design. The Plots of internal force for the above discussed Hingless circular arch indicated that the maximum internal moment and axial force occurs at the abutments and it decreases toward the crown. This aspect of a Hingless circular arch can be used toward developing an efficient design. While in the design example discussed above only the area of steel has been reduced at the locations of lesser internal forces, it can be further optimized by reducing the cross sectional area of the rib towards the crown.

The cross section arch of the arch rib was increased in the second design iteration of the above discussed example. It was observed that this change in the self-weight of the arch has contributed more toward the internal axial force than the internal moment of the arch. The comparison between Figure 4.10 and Figure 4.13 shows that the internal moment and axial force in the second design iteration is 10% and 13.85% more respectively than that of the first design iteration.

One of the critical elements in the design of an arch is its deflection across the span. This element has not been taken in consideration in the preliminary sizing exercise discussed in this chapter and hence the design developed here needs further modifications to account for the deflection limits.

Chapter 5

Summary

5.1 Introduction

Analytical equations of internal forces and support reactions for Three-hinged, Two-hinged and Hingeless circular arch are developed and validated in chapter 3. In Chapter 4,these equations are used to compare the stresses in circular and parabolic arch as well as for the preliminary sizing of a circular arch rib. In this chapter the same equations are used to compare the structural behavior of all the three type of arches under similar loading conditions. Rise-to-span ratio is one of the important elements in the design on an arch structure. Its effect on the internal forces of Three-hinged, Two-hinged and Hingelss arch is also discussed in this chapter.

In previous chapters three loading conditions- a point load, self-weight of an arch and uniformly distributed load applied on the entire span of an arch are used for the analysis. Figure 3.11, Figure 3.29, Figure 3.45 in Chapter 3 show that when the uniformly distributed load is divided in series of point load it causes similar stresses in an arch as that due the uniformly distributed load. Hence for simplification only self-weight and uniformly distributed loading conditions are discussed in this chapter.

5.2 Comparative Analysis- Threes- Hinged, Two-Hinged and Hingeless Arch

This section compares the internal forces in Three-hinged, Two hinged and Hingless arch under similar conditional. For this purpose, the example of symmetric circular arch used for the analysis in Chapter 2 is considered here. (Kinney, 1957, pg547-558). Following are the numerical values used for the trigonometric variable,

Arch Rib Width (b) = 2 ft, Arch Rib Depth(d) = 3 ft, Area(a) = 6 ft^2, Moment of Inertia (i) = 4.5 ft^4, Modulus of Elasticity(e) = 3645 Ksi, α= 0.8975 rad., Radius(R) = 160.35 ft., Span = 200 ft, Rise = 35 ft, W=2.275 kip/ft.

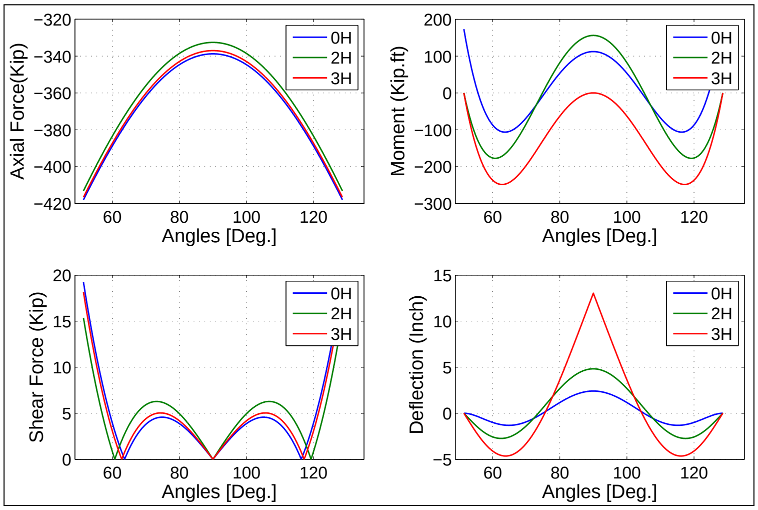

Figure 5.1: Three-hinges,Two-Hinged and Hingeless circular arch under Self-weight

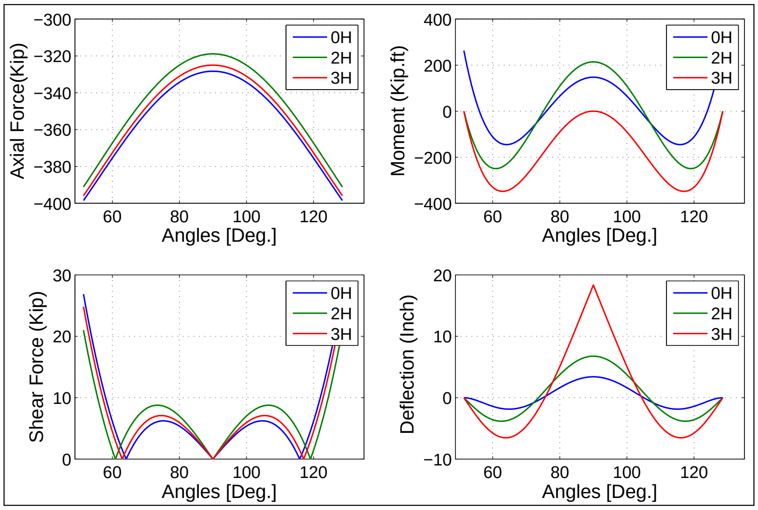

Figure 5.2: Three-hinges,Two-Hinged and Hingeless circular arch under UDL

Figure 5.1 and Figure 5.2 show that self-weight of all the three type of arches contributes more towards the internal axial force and the applied uniformly distributed loads contributes more toward the internal moment. The abutment or support condition has comparative less effect on the internal axial and share force than the internal moment and deflection of an arch structure. The internal moment graph reflects the 'Force Follows Stiffness' property of an arch structure. In a Hingelss arch the abutments can resist the internal moment and hence maximum moment occurs at the abutments. In a Two-hinged arch the abutments cannot resist the moment and hence maximum moment is transferred to the crown of the arch. In a Three-hinged arch both abutments and crown can not resist the moment and hence it occurs in between the hinge supports.

Both Self-weight and uniformly distributed loading conditions cause about the same amount of internal axial force at the abutments of all the three type of arches where as at the crown it causes comparative more axial force in the Two-hinged arch than the Three-hinged or Hingeless arch. The internal shear force at the crown of all the three type of arches is zero and it is largest at the abutment for a Hingeless arch. The largest internal moment occur at the abutments of a Hingelss arch and it is comparable with internal moment at the crown of a Two-hinged arch. In all the three type of arches, the maximum defection occurs at their crown and the defection in the Three-hinged arch is largest among all. Overall the Hingelss arch has the largest internal forces and smallest deflection where as the Three-hinged has smallest internal forces and largest deflection. The Two-hinged arch falls between the Hingeless and Three-hinged arch in terms of internal forces and deflection.

Understanding the effect of support conditions on the internal moment and deflection of an arch can help in developing an efficient design solution. For a project location that allows high movement or deflection in an arch structure, a Three-hinged arch will provide an economical solution where as for a project location with very low tolerance for movement or deflection, a Hingelss arch will provide an adequate solution.

5.3 Rise-to-Span Ratio and Internal Stresses in Arches

The rise-to-span ratio is one of the important elements in the design of an arch structure. While it many times depend on the clearance required under the arch, it also influences the internal forces and support reactions. This section analyzes the effect of rise-to-span ratio on Three-hinged, Two-hinged and Hingeless arches under self-weight and uniformly distributed load. Figure 3.1 shows the trigonometric variables used to define geometry of an arch and the rise-to span ratio depend on angle α used for an arch. This analysis uses following four values of angle α and their associated rise-to span ratios.

$\alpha = 15^\circ \implies$ Rise-to-Ratio $= 0.38$

$\alpha = 30^\circ \implies$ Rise-to-Ratio $= 0.28$

$\alpha = 45^\circ \implies$ Rise-to-Ratio $= 0.20$

$\alpha = 60^\circ \implies$ Rise-to-Ratio $= 0.13$

Both self-weight and uniformly distributed loading conditions are symmetric about the center on an arch and therefore change in the rise-to-span ratio has similar effect on the internal forces and support reactions. For illustration only graphs of all the three type of arches under uniformly distributed loads are shown here. The internal axial force and shear force are normalized with respect to the resultant of vertical reaction and thrust at the abutments. The internal moment is normalized with respect to the product of internal axial force and the rise. Figure 5.3, Figure 5.4 and Figure 5.5 show the effect of rise-to-span ratio on the internal forces of Three-hinged,

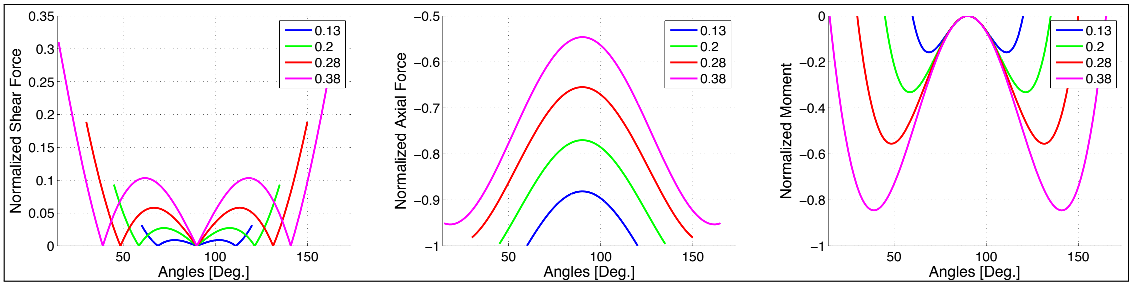

Figure 5.3: Rise to span ratio: Three-hinged circular arch under UDL

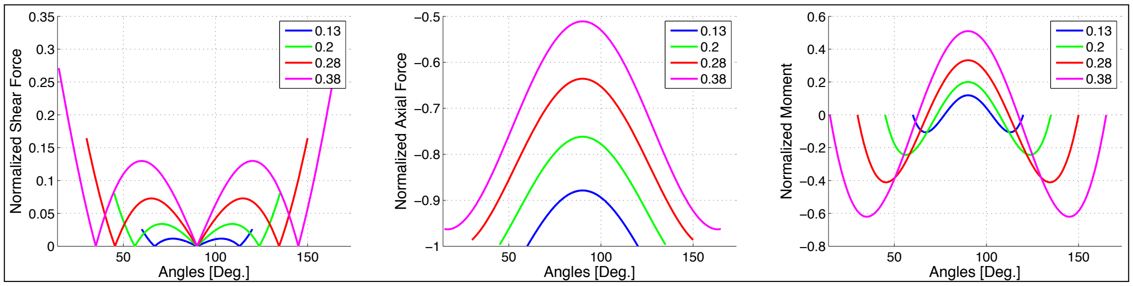

Figure 5.4: Rise to span ratio: Two-hinged circular arch under UDL

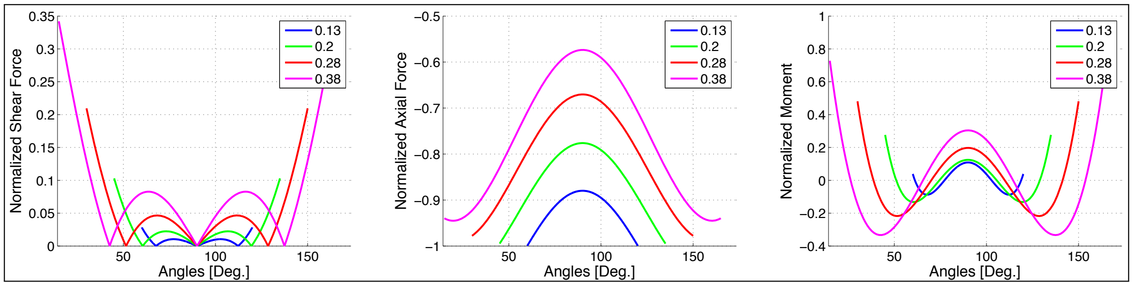

Figure 5.5: Rise to span ratio: Hingeless circular arch under UDL

Two-hinged and Hingelss arch respectively. As the rise-to-span ratio in all the three type of arches increases the internal shear force and moment increases where as the internal axial force decreases. Also as the rise-to-span ratio in all the three type of arches increases the ratio of thrust-to-vertical reaction at the abutments decreases. Based on this observation it can be said that for two arches of similar span, loading and abutment condition, the arch with smaller rise will have more thrust than the arch with bigger rise. Therefore the low-rise arch will need stronger abutment. Among a Three-hinged , a Two-hinged and a Hingeless arch of same rise-to-span ratio and loading condition, the Hingeless arch will have largest thrust where as the Two-hinged arch will have lowest thrust at the abutments.

The rise-to-span ratio has different effect on the internal axial force and moment. Therefore to achieve balance it is important to use an adequate rise-to-span ratio. Based on the above analysis a rise-to-span ratio of 0.2 to 0.3 will be economical for all the three types of circular arches under symmetric loading conditions. Existing literature indicate that where condition permits, a rise-to-span ratio of 0.25 to 0.3 is adequate for all type of arches (Kinney, 1957, pg541).

5.4 Conclusion

This thesis work encompasses analysis of circular arches. In Chapter 2 the development in the circular arch form throughout the history of architecture as well as the influence of elastic theory on the design of modern arches is briefly discussed. In chapter 3 analytical equation for Three-hinged, Two-hinged and hinges arched are developed and validated. Table 5.1 refers to the analytical equations that are used to understand the structural behavior of the arches under different loading conditions. In chapter 4 the analytical equations are used to compare stresses in a parabolic and a circular arch and to derive preliminary design of the circular arch rib. Finally in this chapter the analytical equations are used to compare the structural behavior of the considered three types of arches and the effect of rise-to-span ratio on their internal stresses.

The ancient builders purely relied on their intuitive understanding to develop the empirical rules for the arches that were used to erected great monuments. From 14th century to 18th century many mathematicians and physicist worked on the elastic theory of analysis, which influenced the design of modern arches. The development in the theory of analysis together with the advancement in building material and construction techniques changed the application of arches in contemporary structures.

The analysis of Three-hinged, two-hinged and Hingeless arches indicated that an arch form resists its self-weight by developing compressive stress and the applied load by developing combination of compressive and flexural stresses. Therefore different loading conditions causes different pattern of internal stresses in an arch. In general, an asymmetric loading condition in all the three type of arches causes substantially high internal moment compared to a symmetric loading. Overall it was found that the Hingelss arch has the largest internal stresses and smallest deflection where as the Three-hinged has smallest internal forces and largest deflection. Therefore it can be said that compared to the other type of arches the Hingeless arch is the most rigid. The comparison between circular and parabolic arch form showed that a small variation in the curvature of an arch affects

Type of an Arch	Loading Condition	Reaction	Internal Forces
Three-Hinged Arch	Point Load	Section 3.2.2.1	Section3.2.2.2
Three-Hinged Arch	Self-Weight	Section 3.2.3.1	Section3.2.3.2
Three-Hinged Arch	Uniformly Distributed Load	Section 3.2.4.1	Section3.2.4.2
Two-Hinged Arch	Point Load	Section 3.3.2.4	Section3.3.2.4
Two-Hinged Arch	Self-Weight	Section 3.3.3.4	Section3.3.3.4
Two-Hinged Arch	Uniformly Distributed Load	Section 3.3.3.4	Section3.3.3.4
Hingeless Arch	Point Load	Section 3.4.2.4	Section3.4.2.4
Hingeless Arch	Self-Weight	Section 3.4.3.4	Section3.4.3.4
Hingeless Arch	Uniformly Distributed Load	Section 3.4.4.2	Section 3.4.4.2

Table 5.1: Analytical Equations

its internal stresses and support reactions. Overall the parabolic arch has lower stresses than the circular arch. One of the important elements in the design of an arch structure is its rise-to-span ratio, which many times depend on the site condition. It was found that the rise-to-span ratio has different effect on the internal axial force and moment and to achieve a balance it is important to use an adequate ratio. The analysis indicates that a rise-to-span ratio of 0.2 to 0.3 is economical for all the three types of circular arches under symmetric loading conditions. Understanding the relation between the applied load and the form of an arch on its internal stress is crucial in deriving an economical and efficient design.

This study of the structural behavior of Three-hinged, Two-hinged and Hingless arch using the analysis equations developed here concludes that the internal stress are mainly dependent on three factors. First the pattern in which the forces are applied, their location, intensity and direction, second is the curvature of the arch axis and third is the form of the arch rib that is cross sectional area and the moment of inertia.

5.4.1 Future Work

This thesis work can be further developed by addition of more elements associated with the analysis and design of an arch structure. As indicted in Section 3.2.2.3, complex solution was found for the deflection in Three-hinged arch, which needs further investigation. Similar to the analytical equations derived here for the circular arches, they can also be derived for the parabolic arches. Further the analytical equation can be used to relate the structural behavior of low-rise arches with beams. The cross sectional properties of an arch has effect on its internal stress .The study can be extended to understand how the cross sectional properties affects the deflection in an arch.

Some of the factors that influence the internal stresses of an arch and therefore play important role in its design are buckling in the arch rib, temperature variation and abutment or support settlements. The study of these factors would be a valuable addition to this thesis work.

Bibliography

Acocella, A. (2006). Stone architecture: Ancient and modern construction skills. Milano : Skira ; New York : Distributed in North America by Rizzoli, 2006, first edition edition.

Bertrand, J. (1869). *Communication: Academie des Sciences et les Academiciens de 16666 a 1793.*

Bresse, M. (1859). *Cours de mécanique appliquèe.*

Coulomb, C. (1773). *Essai sur une application de maximis & minimis à quelques problèmes de statique relatifs à l'architecture. mémoires de l'académie Royale des Sciences*, 7:343–382.

de la Hire, P. (1679). *Nouveaux éléments des sections coniques, les lieux géometriques*. Chez Andre Prallard, Paris.

Dym, C. and Williams, H. (2011). Stress and displacement estimates for arches. ASCE Journal of Structural Engineering.

Godoy, L. (2007). Teaching arches in structural analysis courses. Latin American and Caribbean Journal of Engineering Education, 1(2).

Huerta, S. (2006). Structural design in the work of Gaudi. Architectural Science Review, 49:324–339.

Kinney, S. (1957). Indeterminate Structural Analysis. Addison-Wesley Publishing Company, Inc, Reading, Massachusetts, U.S.A.

McCurdy, E. (1939). Leonardo da Vinci's Note–Book. Encyclopedia Britannica.

Navier, C. (1826). *Resumé des leçons données à l'école des ponts et chaussées sur l'application de la mécanique à l'établissement des constructions et des machines*. Dunot, Paris.

OPAC/HDR/T.Y.LIN2003 (2003). Hoover Dam Bypass Colorado River Bridge Drawings. OPAC Consultant Engineers, 315 Bay Street,San Francisco, CA-94133.

Prusinski, K. (2015). Analysis of complex structures. Master's thesis, Department of Civil,Environmental and Architectural Engineering, University of Colorado at Boulder.

Ruddock, T. (2000). Masonry Bridges,Viaducts and Aqueducts, volume Two. Ashgate Publishing Company, 131 Main Street, Burlington, Vermont 05401-5600, USA.

Salvadori, M. and Heller, R. (1986). structural in architecture- The Building of Building. Prentice-Hall,Inc., third edition edition.

Thandavamoothy, T. (2011). Structural Analysis. OXFORD University Press, YMCA Library Building, 1 Jai Singh Road, New Delhi 110001, India, first edition edition.

Timoshenko, S. P. (1953). History of Strength of Materials. McGraw-Hill, New York, U.S.A.

West, H. (1989). Analysis of Structures. John Wiley & Sons, Inc., New York, U.S.A, second edition edition.

Winkler, E. (1880). *Die Lage der Stützlinie im Gewölbe*, volume 13. *Deutsche Bauzeitung*.

Appendix A

Mathematica's 3D Plots

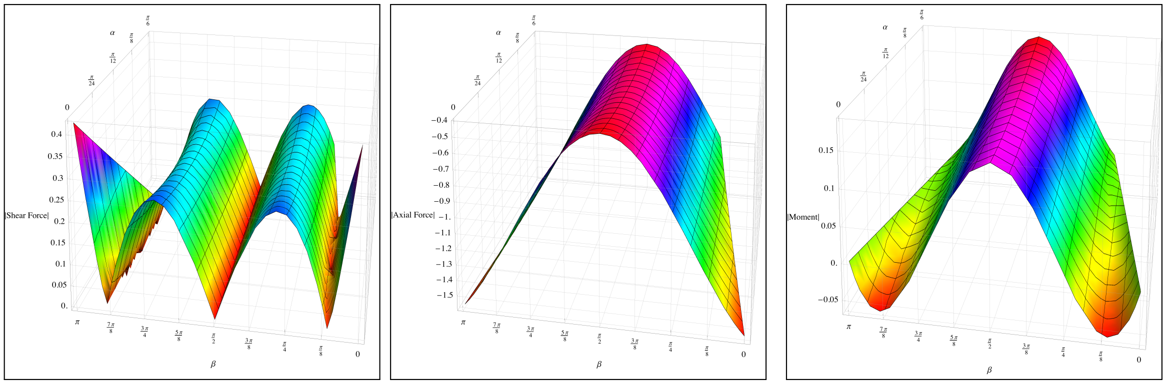

(a) Shear Force Diagram (b) Axial Force Diagram (c) Moment Diagram

Figure A.1: Two-Hinged Arch Under Self-weight

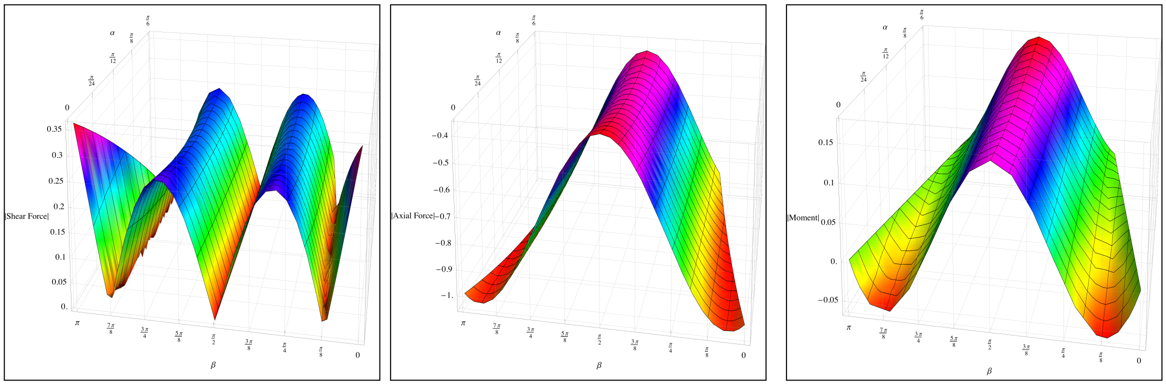

(a) Shear Force Diagram (b) Axial Force Diagram (c) Moment Diagram

Figure A.2: Two-Hinged Arch Under UDL

Figure A.1 and Figure A.2 show example of 3D graphs plotted using the analytical equation developed in Chapter 3. It illustrates the changes in internal forces occurred with the change in angle α. The axial force diagram indicates that maximum force axial force occurs at the abutment and it gradually decreases towards the crown. The moment diagram shows zero moment at the hinges and maximum moment at at the crown. The shear force is largest at the location of zero moment. The 3D plots demonstrates the application of the analytical equation towards understanding the relation between angle α or rise-to span ratio with the internal stresses in arches.

Appendix B

Design Code

Following Matlab code was used to determine the internal forces in the circular arch design.In this code the analytical equation for the point case is used to find the internal forces caused by the precast piers and the self weight case is used to find the internal forces causes from archs self-weight. Internal forces from both the case are combined to compute the total internal forces in the circular arch.

```
cclear
clc
close all
fsb=20; % Larger font for x and y labels
fss=16; % Smaller font for tick label
lw=2;  % line width
scrsz = get(0,'ScreenSize');
figpos=[2 2 scrsz(3) scrsz(4)/2];

%% Properties of the circular arch structure
R=645.54;                          % Radius(ft)
w=25.575*1.25;                     % Uniformly Distributed  Dead Load (kips)
alpha=0.6076;                      % Angle of support from the center
a=155;                             % Area
i=5162.9;                          % Moment of Inertia
theta=[0.8781 1.0971 1.2935 1.4594 1.6821 1.848 2.044 2.263];         % Angle of application of point load
P=[4629.45 3926.56 3609.64 3410.21 3434.66 3614.06 3948.05 4629.79];  % Point Loads
DeltaB=(pi 2*alpha)/1000;
beta=[alpha:DeltaB:pi alpha];      % At any angle across the span

%% 1) When series of point loads are applied by precast concrete piers
%% To compue the thrust
j=1:length(theta);
T1(j)=0;
for j=1:length(theta)
    DeltaP=P(1,j);
      T1(j)= T1(j)+ (1/2)*DeltaP*(( 4)*a*R^2+(( 2)*alpha+pi)^2*
```

```
       (i+a*R^2)+( 4)*a*R^2*cos(2*alpha)+(( 2)*alpha+pi)*...
       (i+a*R^2)*sin(2*alpha))^( 1)*(( 1)*(( 2)*alpha+pi)*...
       (i+a*R^2)*cos(2*alpha)+(( 2)*alpha+pi)*(i+( 1)*a*R^2)*...
       cos(2*theta(j))+( 2)*a*R^2*(( 2)*alpha+pi+2*sin(2*alpha))...
       +4*a*R^2*cos(alpha)*((pi+( 2)*theta(j))*cos(theta(j))+...
       2*sin(theta(j))));
end
T1=sum(T1)
%% To compute the Reaction
j=1:length(theta);
R1(j)=0;
for j=1:length(theta)
    DeltaP=P(1,j);
R1(j) = R1(j) + (1/2)*DeltaP*(i+a*R^2)^( 1)*(( 2)*...
         alpha+pi+( 1)*sin(2*alpha))^( 1)*(( 4)*a*R^2....
         *cos(theta(j))*sin(alpha)+( 1)*(i+a*R^2)*(2*...
         (alpha+( 1)*pi+theta(j))+sin(2*alpha))+(( 1)*...
         i+a*R^2)*sin(2*theta(j)));
end
R1=sum(R1);
%% 1) To compute the Axial, Shear and moment at any angle Beta
 for k=1:length(beta)
       V1(k)=0;M1(k)=0;N1(k)=0;
         for j=1:length(theta)
             DeltaP=P(1,j);
             if beta(k) <= theta(j)
                 V1(k)=V1(k)+(1/4)*DeltaP*(i+a*R^2)^( 1)*(2*alpha+( 1)*...
                     pi+sin(2*alpha))^( 1)*(( 4)*a*R^2+(( 2)*alpha+pi)...
                     ^2*(i+a*R^2)+( 4)*a*R^2*cos(2*alpha)+(( 2)*alpha+pi)*...
                     (i+a*R^2)*sin(2*alpha))^( 1)*(( 2)*(i+a*R^2)*cos...
                     (beta(k))*(2*alpha+( 1)*pi+sin(2*alpha))*((( 2)*...
                     alpha+pi)*(i+a*R^2)*cos(2*alpha)+(( 2)*alpha+pi)*...
                     (2*a*R^2+(( 1)*i+a*R^2)*cos(2*theta(j)))+4*a* ...
                    R^2*cos(alpha)*(( 1)*pi*cos(theta(j))+2*theta(j)*...
                     cos(theta(j))+2*sin(alpha)+( 2)*sin(theta(j))))+...
                     ( 2)*(( 4)*a*R^2+(( 2)*alpha+pi)^2*(i+a*R^2)+( 4)*...
                     a*R^2*cos(2*alpha)+(( 2)*alpha+pi)*(i+a*R^2)*sin(2*...
                     alpha))*sin(beta(k))*(4*a*R^2*cos(theta(j))*sin...
                     (alpha)+(i+a*R^2)*(2*(alpha+( 1)*pi+theta(j))+...
                     sin(2*alpha))+(i+( 1)*a*R^2)*sin(2*theta(j))));
                 N1(k)=N1(k)+(1/4)*DeltaP*(i+a*R^2)^( 1)*(2*alpha+( 1)*...
                     pi+sin(2*alpha))^( 1)*(( 4)*a*R^2+(( 2)*alpha+pi)^2*...
                     (i+a*R^2)+( 4)*a*R^2*cos(2*alpha)+(( 2)*alpha+pi)*...
                     (i+a*R^2)*sin(2*alpha))^( 1)*(2*(i+a*R^2)*(2*alpha+...
                     ( 1)*pi+sin(2*alpha))*sin(beta(k))*((( 2)*alpha+pi)*...
                     (i+a*R^2)*cos(2*alpha)+(( 2)*alpha+pi)*(2*a*R^2+(( 1)*...
                     i+a*R^2)*cos(2*theta(j)))+4*a*R^2*cos(alpha)*(( 1)*pi*...
                     cos(theta(j))+2*theta(j)*cos(theta(j))+2*sin(alpha)+
                     ( 2)*sin(theta(j))))+( 2)*cos(beta(k))*(( 4)*a*R^2+...
                     (( 2)*alpha+pi)^2*(i+a*R^2)+( 4)*a*R^2*cos(2*alpha)+...
                     (( 2)*alpha+pi)*(i+a*R^2)*sin(2*alpha))*(4*a*R^2*cos...
```

```
                (theta(j))*sin(alpha)+(i+a*R^2)*(2*(alpha+( 1)*pi+...
                theta(j))+sin(2*alpha))+(i+( 1)*a*R^2)*sin(2*theta(j))));
            M1(k)=M1(k)+( 1/2)*DeltaP*R*(i+a*R^2)^( 1)*(2*alpha+( 1)*...
                pi+sin(2*alpha))^( 1)*(( 4)*a*R^2+(( 2)*alpha+pi)^2*...
                (i+a*R^2)+( 4)*a*R^2*cos(2*alpha)+(( 2)*alpha+pi)*...
                (i+a*R^2)*sin(2*alpha))^( 1)*((i+a*R^2)*(( 2)*...
                alpha+pi+( 1)*sin(2*alpha))*((( 2)*alpha+pi)*...
                (2*a*R^2+(i+a*R^2)*cos(2*alpha)+(( 1)*i+a*R^2)*...
                cos(2*theta(j)))+4*a*R^2*sin(2*alpha))*sin ...
                (beta(k))+( 2)*(i+a*R^2)*cos(alpha)*(( 2)*alpha+...
                pi+( 1)*sin(2*alpha))*(i+3*a*R^2+(( 1)*i+a*R^2)*...
                cos(2*theta(j))+2*a*R^2*sin(beta(k))*((pi+( 2)*...
                theta(j))*cos(theta(j))+2*sin(theta(j))))+(i+a*...
                R^2)*(2*alpha+( 1)*pi+sin(2*alpha))*(( 2)*cos ...
                (theta(j))*(( 2)*a*R^2+(( 2)*alpha+pi)*(i+a*R^2)*...
                (( 1)*alpha+pi+( 1)*theta(j))+( 2)* a*R^2*cos(2*...
                alpha)+(i+a*R^2)*(( 1)*alpha+pi+( 1)*theta(j))* ...
                sin(2*alpha))+(i+a*R^2)*(2*(( 2)*alpha+pi)*...
                sin(alpha)+( 2)*(( 2)*alpha+pi+sin(2*alpha))*...
                sin(theta(j))))+cos(beta(k))*(( 4)*a*R^2+(( 2)*...
                alpha+pi)^2*(i+a*R^2)+( 4)*a*R^2*cos(2* ...
                alpha)+(( 2)*alpha+pi)*(i+a*R^2)*sin(2*alpha))*...
                (4*a*R^2*cos(theta(j))*sin(alpha)+(i+a*R^2)*...
                (2*(alpha+( 1)*pi+theta(j))+sin(2*alpha))+(i+...
                ( 1)*a*R^2)*sin(2*theta(j))));
        else
            V1(k)=V1(k)+( 1/4)*DeltaP*(i+a*R^2)^( 1)*(2*alpha+( 1)*...
                pi+sin(2*alpha))^( 1)*(( 4)*a*R^2+(( 2)*alpha+pi)^2*...
                (i+a*R^2)+( 4)*a*R^2*cos(2*alpha)+(( 2)*alpha+pi)*...
                (i+a*R^2)*sin(2*alpha))^( 1)*(2*(i+a*R^2)*cos ...
                (beta(k))*(2*alpha+( 1)*pi+sin(2*alpha))*((( 2)*...
                alpha+pi)*(i+a*R^2)*cos(2*alpha)+(( 2)*alpha+pi)*...
                (2*a*R^2+(( 1)*i+a*R^2)*cos(2*theta(j)))+4*a*R^2*cos ...
                (alpha)*(( 1)*pi*cos(theta(j))+2*theta(j)*cos ...
                (theta(j))+2*sin(alpha)+( 2)*sin(theta(j))))+( 4)*...
                (( 4)*a*R^2+(( 2)*alpha+pi)^2*(i+a*R^2)+( 4)*a*R^2*...
                cos(2*alpha)+(( 2)*alpha+pi)*(i+a*R^2)*sin(2*alpha))*...
                sin(beta(k))*((i+a*R^2)*(alpha+( 1)*theta(j))+(i+a*...
                R^2)*cos(alpha)*sin(alpha)+cos(theta(j))*(( 1)*i*...
                sin(theta(j))+a*R^2*(( 2)*sin(alpha)+sin(theta(j))))));
            N1(k)=N1(k)+( 1/4)*DeltaP*(i+a*R^2)^( 1)*(2*alpha+( 1)*...
                pi+sin(2*alpha))^( 1)*(( 4)*a*R^2+(( 2)*alpha+pi)^2*...
                (i+a*R^2)+( 4)*a*R^2*cos(2*alpha)+(( 2)*alpha+pi)*...
                (i+a*R^2)*sin(2*alpha))^( 1)*(( 2)*(i+a*R^2)*(2*...
                alpha+( 1)*pi+sin(2*alpha))*sin(beta(k))*((( 2)*...
                alpha+pi)*(i+a*R^2)*cos(2*alpha)+(( 2)*alpha+pi)*(2*...
                a*R^2+(( 1)*i+a*R^2)*cos(2*theta(j)))+4*a*R^2*cos ...
                (alpha)*(( 1)*pi*cos(theta(j))+2*theta(j)*cos ...
                (theta(j))+2*sin(alpha)+( 2)*sin(theta(j))))+( 4)*...
                cos(beta(k))*(( 4)*a*R^2+(( 2)*alpha+pi)^2*(i+a*R^2)+...
                ( 4)*a*R^2*cos(2*alpha)+(( 2)*alpha+pi)*(i+a*R^2)*...
```

```
                    sin(2*alpha))*((i+a*R^2)*(alpha+( 1)*theta(j))+(i+a*...
                    R^2)*cos(alpha)*sin(alpha)+cos(theta(j))*(( 1)*i*sin...
                    (theta(j))+a*R^2*(( 2)*sin(alpha)+sin(theta(j))))));
                M1(k)= M1(k)+( 1/2)*DeltaP*R*(i+a*R^2)^( 1)*(2*alpha+...
                    ( 1)*pi+sin(2*alpha))^( 1)*(( 4)*a*R^2+(( 2)*alpha+...
                    pi)^2*(i+a*R^2)+( 4)*a*R^2*cos(2*alpha)+(( 2)*...
                    alpha+pi)*(i+a*R^2)*sin(2*alpha))^( 1)*((i+a*R^2)*...
                    (( 2)*alpha+pi+( 1)*sin(2*alpha))*((( 2)*alpha+pi)*...
                    (2*a*R^2+(i+a*R^2)*cos(2*alpha)+(( 1)*i+a*R^2)*cos...
                    (2*theta(j)))+4*a*R^2*sin(2*alpha))*sin(beta(k))+...
                    ( 2)*(i+a*R^2)*cos(alpha)*(( 2)*alpha+pi+( 1)*sin...
                    (2*alpha))*(i+3*a*R^2+(( 1)*i+a*R^2)*cos(2*theta(j))...
                    +2*a*R^2*sin(beta(k))*((pi+( 2)*theta(j))*cos...
                    (theta(j))+2*sin(theta(j))))+(i+a*R^2)*(2*cos...
                    (theta(j))*((( 2)*alpha+pi)*(a*R^2*(2+(( 2)*alpha+...
                    pi)*(alpha+( 1)*theta(j)))+i*(( 2)*alpha+pi)*(alpha+...
                    ( 1)*theta(j))+2*a*R^2*cos(2*alpha))+( 8)*a*R^2*cos...
                    (alpha)^3*sin(alpha)+( 1)*(i+a*R^2)*(alpha+( 1)*...
                    theta(j))*sin(2*alpha)^2)+(i+a*R^2)*(2*alpha+( 1)*...
                    pi+sin(2*alpha))*(2*(( 2)*alpha+pi)*sin(alpha)+( 2)*...
                    (( 2)*alpha+pi+sin(2*alpha))*sin(theta(j))))+( 1)  ...
                    *cos(beta(k))*(( 4)*a*R^2+(( 2)*alpha+pi)^2*(i+a*R^2)...
                    +( 4)  *a*R^2*cos(2*alpha)+(( 2)*alpha+pi)*(i+a*R^2)*...
                    sin(2*alpha))*(( 4)*a*R^2*cos(theta(j))*sin(alpha)+...
                    (i+a*R^2)*(2*alpha+( 2)*theta(j)+sin(2*alpha))+(( 1)*...
                    i+a*R^2)*sin(2*theta(j))));
            end
        end
 end
 %% 2) When Self weight of the concrete arch is applied
 %% To compute the thrust
T2= (1/2)*R*w*(( 4)*a*R^2+(( 2)*alpha+pi)^2*(i+a*R^2)+( 4)  ...
    *a*R^2*cos(2*alpha)+(( 2)*alpha+pi)*(i+a*R^2)*sin(2*  ...
    alpha))^( 1)*(( 2)*a*(( 8)+(( 2)*alpha+pi)^2)*R^2+( 1)*((  ...
     16)*a*R^2+(( 2)*alpha+pi)^2*(i+a*R^2))*cos(2*alpha)+(  ...
     1)*(( 2)*alpha+pi)*(i+7*a*R^2)*sin(2*alpha))
%% To compute the Reaction
R2 = (1/2)*(( 2)*alpha+pi)*R*w;
 %% to compute Axial, Shear and Moment at any angle Beta
V2(k)=0;N2(k)=0;M2(k)=0;
for k=1:length(beta)
    V2(k) = V2(k)+ ( 1/2)*R*w*(( 4)*a*R^2+(( 2)*alpha+pi)^2*(i+a*R^2)+
           ( 4)*a*R^2*cos(2*alpha)+(( 2)*alpha+pi)*(i+a*R^2)*sin(2*  ...
            alpha))^( 1)*(cos(beta(k))*(2*a*(( 8)+(( 2)*alpha+pi)^2)*  ...
            R^2+(( 16)*a*R^2+(( 2)*alpha+pi)^2*(i+a*R^2))*cos(2*  ...
            alpha)+(( 2)*alpha+pi)*(i+7*a*R^2)*sin(2*alpha))+(( 2)*  ...
            beta(k)+pi)*(( 4)*a*R^2+(( 2)*alpha+pi)^2*(i+a*R^2)+( 4)*  ...
            a*R^2*cos(2*alpha)+(( 2)*alpha+pi)*(i+a*R^2)*sin(2*alpha))*...
            sin(beta(k)));
    N2(k) = N2(k)+ ( 1/2)*R*w*(( 4)*a*R^2+(( 2)*alpha+pi)^2*(i+a*R^2)+...
            ( 4)*a*R^2*cos(2*alpha)+(( 2)*alpha+pi)*(i+a*R^2)*sin(2*  ...
```

```
            alpha))^( 1)*((( 2)*beta(k)+pi)*cos(beta(k))*(( 4)*a*R^2+(( 2)*  ...
            alpha+pi)^2*(i+a*R^2)+( 4)*a*R^2*cos(2*alpha)+(( 2)*  ...
            alpha+pi)*(i+a*R^2)*sin(2*alpha))+( 1)*(2*a*(( 8)+(( 2)*  ...
            alpha+pi)^2)*R^2+(( 16)*a*R^2+(( 2)*alpha+pi)^2*(i+a*  ...
            R^2))*cos(2*alpha)+(( 2)*alpha+pi)*(i+7*a*R^2)*sin(2*alpha))*...
            sin(beta(k)));
    M2(k) = M2(k)+ (1/2)*R^2*w*(( 4)*a*R^2+(( 2)*alpha+pi)^2*(i+a*R^2)+...
            ( 4)*a*R^2*cos(2*alpha)+(( 2)*alpha+pi)*(i+a*R^2)*sin(2*  ...
            alpha))^( 1)*(2*(( 2)*alpha+pi)*(3*i+a*R^2)*cos(alpha)+  ...
            2*(( 1)*i*(( 3)+(( 2)*alpha+pi)^2)+a*R^2+( 1)*a*(( 2)*  ...
            alpha+pi)^2*R^2+(3*i+a*R^2)*cos(2*alpha))*sin(alpha)+((  ...
             2)*beta(k)+pi)*cos(beta(k))*(4*a*R^2+( 1)*(( 2)*alpha+pi)^2...
           *(i+a*R^2)+4*a*R^2*cos(2*alpha)+( 1)*(( 2)*alpha+pi)*(i+  ...
             a*R^2)*sin(2*alpha))+(( 2)*(i*(( 2)*alpha+pi)^2+4*a*  ...
             R^2)+(( 8)*a*R^2+(( 2)*alpha+pi)^2*(i+a*R^2))*cos(2*  ...
             alpha)+( 1)*(( 2)*alpha+pi)*(i+( 5)*a*R^2)*sin(2*alpha))*...
             sin(beta(k)));
end
T=T1+T2;  % Total Thrust
R=R1+R2;  % Total Reaction
V=V1+V2;  % Total Shear
N=N1+N2;  % Total Axial
M=M1+M2;  % Total Moment
```